Photostability of the solar cell dye sensitizer N719

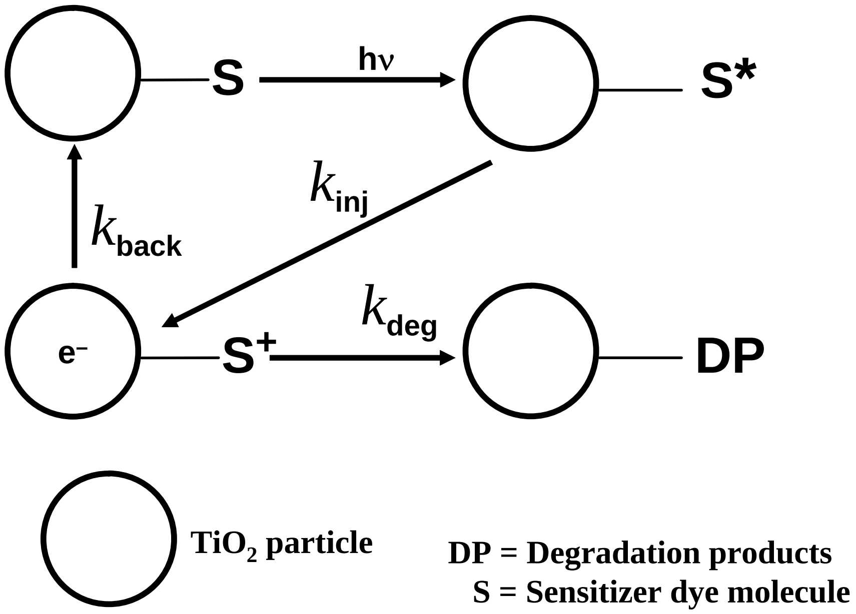

TiO_2 particle

DP = Degradation products
S = Sensitizer dye molecule

Electrochemical synthesis of some arylsulfones and aminobenzoquinones

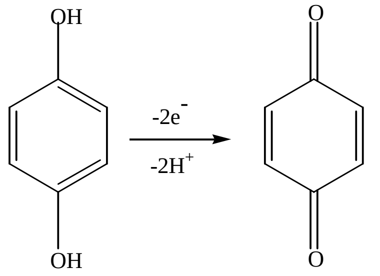

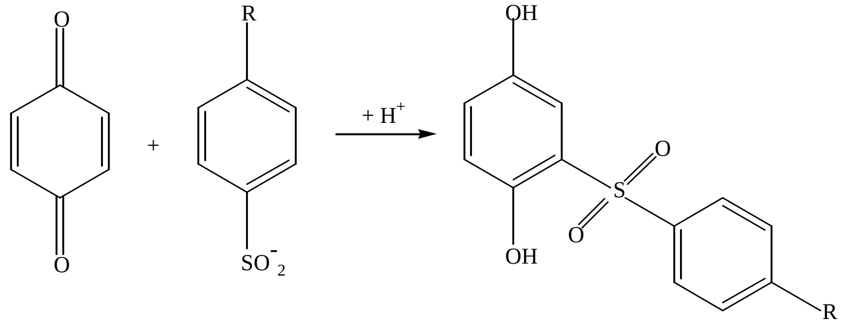

Farahnaz Nour-Mohammadi
Ph.D. Thesis, 2005

Department of Life Sciences and Chemistry
Roskilde University, Denmark

Preface

The work presented in this thesis has been carried out in two different parts. The first part describes the scientific results obtained during my last three-year study (2002-2005) on the field of nanocrystaline dye sensitized titanium dioxide solar cells (nc-DSSC) at the Department of Life Sciences and Chemistry, Roskilde University, Denmark, under the supervision of Associate Professor Torben Lund. This study which is presented in three chapters is focused on the stability of the solar cell sensitizer [Ru(dcbpyH)$_2$(NCS)$_2$] (Bu$_4$N)$_2$ (referred to as **N719**) and the implications of the **N719** dye lifetime in real nc-DSSC. A short introduction to the structure and operating principles of nanocrystaline dye sensitized titanium dioxide solar cells (nc-DSSC) is given in chapter 1. Chapter 2 describes the results of the investigation of the photooxidative degradation of sensitizing dye **N719** under illumination in a simple model system in place of a real nc-DSSC (paper I). This work was conducted in collaboration with MSc student Sau Doan Nguyen. Chapter 3 outlines the preliminary results on the possible substitution reaction between the **N719** dye sensitizer and **4-TBP** under visual illumination (collected as manuscript II for publication).

The second part of the thesis is based on the scientific results on electrochemical synthesis of some arylsulfones and diaminosubstituted benzoquinones, obtained during the last two-year study of my first four-year studies at Faculty of Chemistry, Tabriz University, Tabriz, Iran (1997-2001) under the supervision of Professor S. M. Golabi and co-supervisor, Associate Professor Ali Saadnia. This part describes the results of the study of cyclic voltammetric behaviour of some *o*- and *p*-dihydroxybenzenes in the presence of nucleophiles like sulfinic acids and amines and consequently electrosynthesis of some sulfones and 2,5-diaminosubstituted hydroquinones (Papers III, IV).

Acknowledgements

Undoubtedly the work presented in this thesis would not have been possible without the assistance and contribution of all the people who involved in the development and fulfilment of this project. I appreciate all the people who have been helpful in the development of this thesis: First of all I would like to thank my supervisors at Roskilde and Tabriz Universities.

- I would like to express my deepest gratitude to my supervisor at Roskilde University, Associate Professor Torben Lund for giving me the opportunity to continue my Ph.D. study at the Department of Life Sciences and Chemistry, for his excellent scientific support, for his invaluable comments, for fruitful discussions, for letting me benefit from his scientific insight and for his tireless assistance in giving guidance to me to finish this work.
- Special thanks to Gerrit Boschloo at Uppsala University who gave me the opportunity to visit his laboratory and did the PIA experiments at Uppsala University.
- I am greatly thankful to my supervisor at Tabriz University, Professor S. M. Golabi, for giving me the opportunity to start working at the electroanalytical chemistry laboratory as a Ph.D. student and provided me with nice scientific feedback and invaluable insights. He allowed me to benefit from his invaluable guidance throughout my doctoral studies during my stay at Tabriz University.
- I am sincerely grateful to my co-supervisor Associate Professor Ali Saadnia at Tabriz University due to his valuable assistance in purification of the products, interpreting the IR and ^{1}H NMR data and general discussions on organic chemistry.
- Thanks to my second co-supervisor Associate Professor M. H. Pournaghi-Azar and other Professors at Faculty of Chemistry at Tabriz University who have contribution to my scientific knowledge.

I appreciate all the people who have been helpful in the development of this thesis:

- Peter Christensen for his invaluable assistance.
- Niels Jakob Krake for the synthesis of uncarboxylated analogue of the **N3** dye.
- All the members of analytical chemistry laboratories at Faculty of chemistry at Tabriz University and Department of Life Sciences and Chemistry at Roskilde University who helped me to accomplish this work.
- My colleagues at Tabriz University and friends at Roskilde University for creating a pleasure working atmosphere.

- Research Council of Tabriz University for financial support of part 2 of the project (electrochemistry part).
- I commend my family due to their strong encouragement, patient and their sincere love and kindness which have supported me throughout my life.
- Last but not least thank to my husband who have been an enthusiastic supporter and partner by his efforts to make this work to come to success.

Abstract

The photostability of the sensitizer dye [Ru(dcbpyH)$_2$(NCS)$_2$] (Bu$_4$N)$_2$ (referred to as **N719**) was investigated in a simple model system instead of a complete nanocrystaline dye sensitized titanium dioxide solar cells (nc-DSSC). The applied model system consisted of **N719** dyed titanium dioxide nanoparticles, suspended in a cuvette containing acetonitrile as the solvent which were illuminated with 532/525 nm monochromatic light of different light intensity. Under these experimental conditions and in the absence of any redox couple as a regenerative electron donor, the number of mole of photodegradation products: [RuL$_2$(CN)$_2$], [RuL$_2$(NCS)(CN)] and [RuL$_2$(NCS)(ACN)] increased almost linearly as a function of increasing mole of absorbed photons. The total quantum yields of these degradation products, Φ_{deg} showed light intensity dependence, being higher at low light intensities and smaller at higher intensities. This light intensity dependency of the quantum yield was attributed to the back electron transfer reaction rate between the titanium dioxide conduction band electrons and the oxidized dye cation. Photoinduced absorption spectroscopy (PIA) was used to measure the back electron transfer reaction rate, k_{back} at the same light intensities as used in the model experiments. The PIA measurements showed that k_{back} increased with increasing light intensities. By applying the equation $k_{deg} = \Phi_{deg} \times k_{back}$ to the experimentally obtained total quantum yields and back electron transfer rates it was possible to calculate an average value for the oxidative degradation rate of the **N719** dye attached to the TiO$_2$ nanoparticles, $k_{deg} = 4 \times 10^{-2}$ s^{-1} .

Heating and illumination of the model system in the presence of 4-*tert*-butylpyridine (**4-TBP**), the commonly used additive in nc-DSSC, revealed the possible involvement of the dye in a substitution reaction with **4-TBP** with the formation of the substitution product [Ru(dcbpyH)$_2$(NCS)(4-TBP)]$^-$, Bu$_4$N$^+$. It was also found that the amount of the additive substituted product formed under illumination increases upon adsorption of the dye on TiO$_2$ nanoparticles. Quantum yield measurements of the substitution product under different experimental conditions directed us to conclude that the main part of the substitution product is formed through the oxidized state of the dye, S$^+$. The quantum yield of the substitution reaction initiated from the dye oxidized state was $\phi^+_{sub\ (TiO_2)} = 7.1 \times 10^{-5}$. Based on this value the rate of the photosubstitution reaction was calculated to be $k^+_{sub(TiO_2)} = 0.07$ M^{-1}s^{-1}. The influence of the photosubstitution reaction on the **N719** dye lifetime was discussed based on the $k^+_{sub(TiO_2)}$ value and the literature values of the dye regeneration reaction, k_{reg} between the oxidized dye, S$^+$ and iodide.

Abstrakt

Fotostabiliteten af farvestof sensibilisatoren ([Ru(dcbpyH)$_2$(NCS)$_2$], (Bu$_4$N)$_2$) (benævnt som **N719**) er blevet undersøgt i et simpelt model system i stedet for i en komplet nanokrystaline farvestof sensibiliseret titan dioxid solcelle (nc-DSSC). Det anvendte modelsystem bestod af **N719** indfarvede titandioxid nanopartikler i en suspension i en cuvette med acetonitril som opløsningsmiddel, som blev belyst med 532 eller 525 nm monokromatisk lys med forskellig intensitet. Under disse eksperimentelle betingelser og i fravær af et redox par som regenerativ elektron donor, voksede mængden af fotonedbrydningsprodukterne [RuL$_2$(CN)$_2$], [RuL$_2$(NCS)(CN)] og [RuL$_2$(NCS)(ACN)] næsten lineært som funktion af mol absorberede fotoner. Det samlede kvanteudbyttet af disse nedbrydningsprodukter Φ_{deg} udviste en afhængighed af lysintensiteten således, at kvanteudbyttet var højest ved lav belysningsintensitet og lavere ved højere lysintensiteter. Denne lysintensitetsafhængig af kvanteudbyttet blev sammenknyttet med tilbage elektronoverførselshastigheden fra titandioxid ledningsbånd elektronerne til den oxiderede form af farvestoffet. Fotoinduceret absorptions spektroskopi (PIA) blev anvendt til at måle tilbageelektronoverførselsreaktionshastigheden, k_{back}, ved samme lysintensiteter, som blev anvendt i modeleksperimenterne. PIA eksperimenterne viste, at k_{back} voksede som funktion af lysintensiteten. Ved anvendelse af ligningen $k_{deg} = \Phi_{deg} \times k_{back}$ på de eksperimentelt bestemte kvanteudbytter og PIA bestemte k_{back} værdier var det muligt at bestemme en gennemsnitlig værdi for den oxidative nedbrydningshastighed af **N719** farvestoffet bundet til TiO$_2$ partikler, $k_{deg} = 4\times 10^{-2}$ s^{-1}.

Opvarmning og belysning af modelsystemet i nærværelse af 4-*tert*-butylpyridine (**4-TBP**), et hyppigt anvendt tilsætningsstof i nc-DSSC, afslørede en mulig involvering af farvestoffet i en ligandsubstitutionsreaktion med **4-TBP** under dannelse af substitutionsproduktet [Ru(dcbpyH)2(NCS)(4-TBP)]$^-$, Bu$_4$N$^+$. Det blev også observeret, at mængden af additiv substitueret produkt dannet under belysning øgedes ved adsorption til TiO$_2$ nanokrystalinske partikler. Kvanteudbytte målinger af substitutionsproduktet under forskellige eksperimentelle betingelser ledte til den konklusion, at substitutionsproduktet fortrinsvis dannes gennem den oxiderede form af farvestoffet S$^+$. Kvanteudbyttet blev bestemt til 7 ×10^{-5} og ud fra denne værdi blev hastigheden for fotosubstitionen $k^+_{sub(TiO_2)}$ beregnet til 0.07 M^{-1}s^{-1}. Indflydelsen af fotosubstitutionsreaktionen på levetiden af **N719** i solcellen blev diskuteret på basis af $k^+_{sub(TiO_2)}$ værdien og litteraturværdier for hastigheden af regenereringsreaktionen mellem S$^+$ og iodid.

List of Appendices

I. **Determination of the Light-Induced Degradation Rate of the Solar Cell Sensitizer N719 on TiO_2 Nanocrystaline Particles.** .

F. Nour-Mohammadi, N. D. Sau, G. Boschloo, A. Hagfeldt, T. Lund.

J. Phys. Chem. B, 109, 2005, 22413.

II. **An investigation of the substitution reaction between the sensitizer N719 dye and the solar cell additive 4-*tert*-butylpyridin.**

F. Nour-Mohammadi, T. Lund.

The results have been collected in a manuscript for publication.

III. **Electrochemical synthesis of organic compounds: 1. Addition of sulfinic acids to electrochemically generated *o*- and *p*-benzoquinones.**

F. Nourmohammadi, S. M. Golabi, A. Saadnia.

J. Electroanal Chem., 529, 2002, 12.

IV. **Electrosynthesis of organic compounds: II. Electrooxidative amination of 1,4-dihydroxybenzene using some aliphatic amines.**

S. M. Golabi, F. Nourmohammadi, A. Saadnia.

J. Electroanal Chem., 548, 2003, 41.

Table of contents

Chapter 1 *Nanocrystaline Dye sensitized Titanium Dioxide Solar Cells (nc-DSSC)*

Chapter 2. *Photoinduced Oxidative Degradation of N719 Dye Adsorbed on TiO_2 Nanoparticles*

Chapter 3 *An investigation of the substitution reaction between the sensitizer N719 dye and the solar cell additive 4–tert–butylpyridine*

Electrochemical Synthesis of Some Arylsulfones and 2,5-disubstituted Aminobenzoquinones

Chapter 1

Nanocrystaline Dye Sensitized Titanium Dioxide Solar Cells (nc-DSSC)

1.1. Introduction

The increasing demand of world's energy consumption along with the unfavourable environmental effects coming from the consumption of non-renewable energy sources (fossil fuels such as coal, crude oil, and natural gas) like green house effects; ozone depletion and global warming have stimulated much interest to replace non-renewable energy sources with renewable ones. Renewable energy sources include all sources of energy that are captured from ongoing natural processes such as solar power, wind power, water flow in streams (hydropower), biomass, biodiesel and geothermal heat flow[1]. One major advantage of the renewable energy sources, among others is that they are clean sources of energy and have a much lower environmental impact than the conventional non-renewable energy sources[2] . The main source of all kind of renewable energy sources is the solar energy[1]. There are a variety of technologies that have been developed to take advantage of solar energy. One is photovoltaic (solar cell) systems. A solar cell is a device that converts solar energy directly into electricity. The most common form of solar cells is based on the silicon semiconductor. The semiconductor (silicon) performs two processes simultaneously: absorption of light, and separation of the electric charges, electrons and holes, which are formed as a consequence of light absorption. However, to avoid the recombination of electrons and holes the semiconductor employed must be highly pure and defect-free which imposes high manufacturing cost. A new generation of solar cells, "**dye sensitized solar cells**" has been developed which is an alternative to the conventional silicon based solar cells. The history of this kind of solar cells which is based on dye sensitized enhancement of photovoltaic effect dates back to 19th century [1]. The major drawback of these cells was very low conversion efficiencies (less than 0.5%). It was partly because of the low absorbance of a single monolayer of dye on a plane surface of a semiconductor. The report of O'Regan and Grätzel in 1991 was the major breakthrough in this field which overcame this problem by use of a nanostructured TiO_2 semiconductor [2]. Because of the large surface area and high porosity of nanostructured TiO_2 film, a monolayer of dye adsorbed onto the porous TiO_2 surface is sufficient to collect a large part of the incident light. This property leads to the enhancement of the light harvesting capability of the dye adsorbed onto the film surface and consequently high efficiency of the cell [3]. Ever since nanocrystaline dye sensitised solar cells (nc-DSSC) specially based on nanocrystaline TiO_2 films, have received significant attention because of the low production cost compared to those of silicon solar cells [4c].

---

[1] http://en.wikipedia.org/wiki/Renewable_energy

[2] http://www.nrel.gov/clean_energy/reimportant.html

1.2. Nanocrystaline dye sensitized solar cell (nc-DSSC)

The nc-DSSC is a regenerative photoelectrochemical system which utilizes light energy to drive electrochemical reactions. Light sensitivity is introduced by a suitable sensitizing dye adsorbed onto the semiconductor electrode surface. Redox active photosensitising dye produces a current through the cell which results in the production of electrical energy by the device. There is no net electrochemical reaction under visible light irradiation, but only driving of the electrolyte ions through the cell, so the cell is regenerative.

1.3. nc-DSSC structure

A dye sensitized solar cell consists of two conducting glass electrodes, photosensitizer dye, a wide band gap semiconductor thin film and an electrolyte system. Figure 1.1 is a schematic representation of a dye sensitized solar cell based on a nonoporous titanium dioxide electrode, coated with a sensitizer dye (usually a ruthenium bipyridine dye) and wetted with an iodide/tri-iodide redox electrolyte [5]. This combination (commonly referred to as Grätzel cell) has achieved to the best performance of a dye sensitized solar cell with an overall energy conversion efficiency of ~ 10% [6].

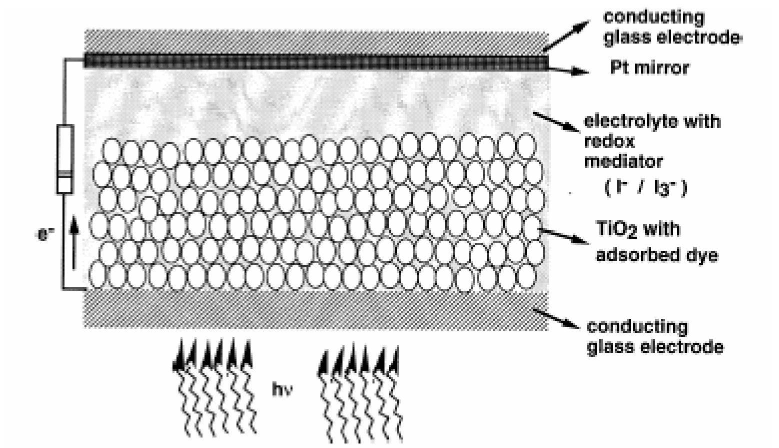

Figure 1.1 Schematic representation of the nc-DSSC structure [5]

1.4. Operating principle of the nc-DSSC

The generally accepted mechanism of energy conversion in regenerative dye sensitized solar cells is as shown in Figure 1.2 [5].

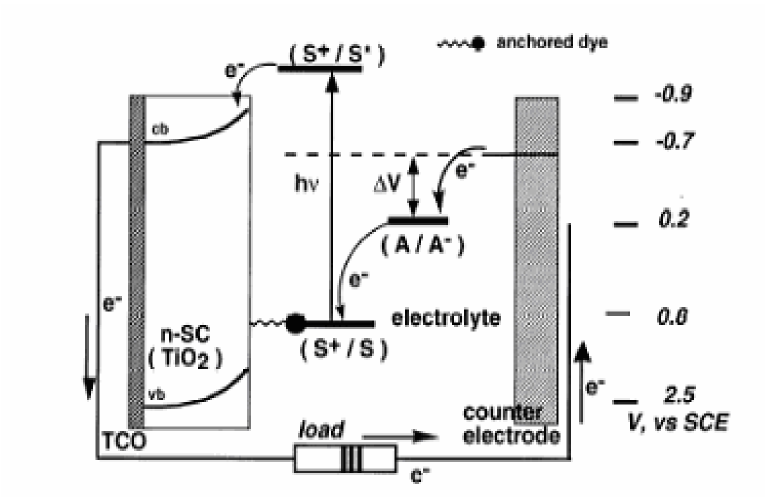

Figure 1.2 Operating principle and energy level diagram of the nc-DSSC [5]

In this model, solar radiation is absorbed by a monolayer of a ruthenium based dye adsorbed onto the surface of a porous nanocrystaline film consisting of electrically connected particles of TiO_2. Upon excitation of the dye by the radiation (step 1), electrons are transferred from the HOMO to the LUMO band of the dye, the latter lying just above the conduction band of the TiO_2. This is followed by electron injection from excited dye molecules into the conduction band of the TiO_2 semiconductor (step 2), which diffuse through the nanocrystaline film to the cathode. The oxidized dye is reduced back to its original state by electron transfer from the iodide ions (I^-) present in the electrolyte leading to the formation of I_3^- (step 3). The iodide ions in turn are regenerated by reduction of tri-iodide ions at the counter electrode facilitated by a layer of platinum which acts as a catalyst (step 4). Electron transfer from I^- ions to the oxidized dye molecules and regeneration of I^- ions from I_3^- ions at the counter electrode link the two transport processes and the circuit is completed through the external load. These operational steps can be summarized as in equations 1.1 – 1.4.

$$TiO_2 \mid S + h\nu \rightarrow TiO_2 \mid S^* \qquad \text{Dye Excitation} \qquad \textbf{(1.1)}$$

$$TiO_2 \mid S^* \rightarrow TiO_2 + e^- \mid S^+ \qquad \text{Electron injection} \qquad \textbf{(1.2)}$$

$$TiO_2 \mid S^+ + I^- \rightarrow TiO_2 \mid S + I^\bullet \qquad \text{Dye regeneration} \qquad \textbf{(1.3)}$$

$$Pt \mid I_3^- + 2e^- \rightarrow Pt \mid 3I^- \qquad \text{Electrolyte reduction} \qquad \textbf{(1.4)}$$

S is representative of a sensitizing dye molecule.

1.5. Advantageous of the nc-DSSC

One major advantage of new generation nc-DSSC in comparison to the conventional silicon based photovoltaic devices is low cost, 0.48–0.64 \$ / W_p for a 10% efficient cell in comparison to 3–8 \$ / W_p for single crystal silicon cells [4c]. Moreover it is claimed that these cells offer high overall photon-to-electric energy conversion efficiency [6] and long term stability [7] during solar cell operation conditions.

1.6. nc-DSSC stability

The stability of the nc-DSSC can be considered from two different points of view: physical stability and chemical stability. Problems encountered in relation to the physical stability, for example solvent evaporation under elevated temperatures have been overcome to a large extent by improving cell fabrication technology. The chemical stability of the nc-DSSC is related to photoelectrochemical and thermal stability of the dye and electrolyte components under solar cell operation conditions.

1.6.1. The role of the sensitizer dye in nc-DSSC stability

Although all various constituting components of the nc-DSSC play their own role on the stability and efficiency of the cell in a direct or indirect way, the most important part which can be considered as a heart of the cell is the light-absorbing dye molecule which is used to sensitize the wide band gap semiconductor electrode. Long term stability of the nc-DSSC in relation to the sensitizing dye molecule requires dye stability under different steps of solar cell operation, i.e. to be stable for long time duration, the dye should be very stable in its ground state (S), excited state (S*) and oxidized state (S^+), so that the probable side reactions occurring from S, S* and S^+ states are suppressed and reactions 1.1–1.3 are the only ones that the dye takes part in.

1.6.2. N3 / N719 dye as the most efficient sensitizer dyes for the nc-DSSC

The ruthenium bipyridine complex cis-$[RuL_2(NCS)_2]$, (L=$dcbpyH_2$=2,2′-bipyridine-4,4′-dicarboxylic acid) (referred to as **N3**) and its half-protonated form cis-$[Ru(dcbpyH)_2(NCS)_2](n\text{-}Bu_4N)_2$ also named **N719** (Figure 1.3) have been reported as particularly efficient photosensitizers in combination with nanocrystaline TiO_2 electrodes with high surface area [6, 8].These complexes have resulted in high light-to-electric energy conversion efficiencies under standard solar conditions.

N3 is an octahedral complex consisting of two bipyridine ligands with 4,4′- substitutions by two carboxylic acid groups, and two mono-dentate thiocyanate ion ligands. In **N719** dye one of the carboxylic acid groups on each bipyridine ligands is in the form of tetra-butylammonium salt.

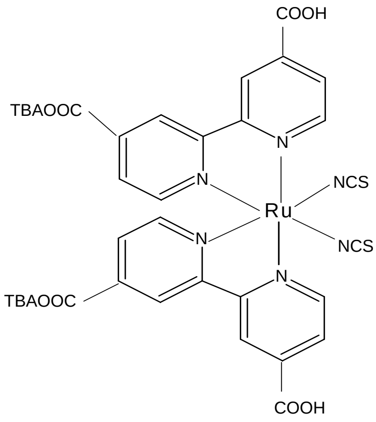

N719

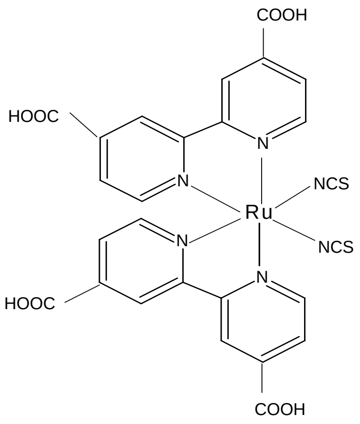

N3

Figure 1.3

The reported stability for **N3** dye is more than 10^8 turnover numbers during cell cycles which are equivalent to more than 20 years of normal solar cell operations [6,7]. This striking photoelectrochemical stability of the dye under solar cell operation condition has brought about this type of cells to a great attention considering their practical applicability.

1.7. Aim of the thesis

In spite of the reported cell lifetime of more than 20 years under standard solar conditions and its verification for at least 10 years outdoor illumination conditions by some research groups [9c], the intrinsic long term stability of the sensitizer dye under solar cell operation conditions have been doubted [10]. Tributsch et al. have claimed that the dye is photoelectrochemically unstable even at very low light intensity and high concentration of iodide, so that proposed long cell lifetime is not achievable [10a]. Considering the vital role of the sensitizer dye in nc-DSSC performance at one hand and disagreement on the proposed cell life time of 20 years with respect to the sensitizer dye stability on the other hand, this part of the dissertation was focused on the investigation of the **N719** dye sensitizer stability with respect to the possible side reactions which may occur during solar cell operation. First the sensitizer oxidative degradation reaction which may compete with the dye regeneration reaction by the redox electrolyte was investigated. This investigation was performed in a simple model system in place of a real nc-DSSC, in order to get an estimation of the oxidative degradation rate of the dye (chapter 2) [I]. Then the **N719** dye stability was evaluated with respect to its reaction with 4-*tert*-butyl pyridine (**4-TBP**) which is commonly used as an additive to improve the cell performance (chapter 3) [II].

Chapter 2

*Photoinduced Oxidative Degradation Of **N719** Dye Adsorbed on TiO_2 Nanoparticles*

2.1. Introduction

Considering the operational steps of the nc-DSSC (equations 1.1–1.4), dye instability may occur from its ground state (S), excited state (S*) and/or oxidized state (S^+). The possible side reactions which the sensitizer dye adsorbed on TiO_2 semiconductor nanoparticles may take part in during the solar cell operation conditions can be summarized as in equations 2.1– 2.3.

$$TiO_2 \mid S \rightarrow \text{Thermal reactions} \quad \textbf{(2.1)}$$

$$TiO_2 \mid S^* \rightarrow \text{Photochemical reactions} \quad \textbf{(2.2)}$$

$$TiO_2 \mid S^+ \rightarrow \text{Photoelectrochemical reactions} \quad \textbf{(2.3)}$$

Thermal substitution reactions of the dye may occur between the dye ground state (S) and solvent molecules, residual water molecules in the solvent and any cell electrolyte components in temperature ranges encountered with nc-DSSC during its operation (equation 2.1). Dye excited state may be involved in ligand exchange reactions with cell constituents such as iodine, additives or solvent molecules (equation 2.2). Dye can also take part in irreversible photoelectrochemical degradation reactions following electron injection into the conduction band of the semiconductor (equation 2.3). Literature data gives an indication of the **N3/N719** dye instability in the excited state [7, 11] and/or oxidized state [7, 12- 14] in solution. Instability of **N3** dye in its oxidized state has been shown by different research groups [12-14]. Cyclic voltammetric investigations of the dye by different voltammetric methods and in different conditions including: solvent, electrode material, dye concentration and added electroinactive surfactants have revealed complex surface based reactions and follow up chemical reactions coupled to the electron transfer process [13]. **N3/N719** dye cation instability has also been shown by identification of the different degradation products following electrochemical oxidation of the dye in different solvents [12, 14]. A half lifetime of ~ 0.2 ms can be estimated for **N3** dye cation in homogeneous acetonitrile solution [12]. Photochemical instability of **N3** dye and some of its analogues compounds has been reported [7]. Illumination of the ethanolic solution of the **N3** dye leads to photochemically induced oxidation of the dye by sulphur atom loss producing dicyano complex [7]. In the presence of strong nucleofiles such as iodide ions the dye may take part in photoinduced ligand substitution reactions yielding iodo complexes [7, 11]. Chemical oxidation of the **N3** dye by using strong oxidants has led to the dicyano complex passing through mixed cyanide/thiocyanate ligand complex as an intermediate [7]. On the other hand it is claimed that adsorption of **N3** dye on TiO_2 semiconductor makes the labile

SCN^- ligand inactive against photochemical and thermal reactions [7] compared to those occurring in solution. This inactivity has been attributed to the fast interfacial electron transfer reactions, i.e. femtosecond time scale electron injection into the semiconductor conduction band [15, 16] and very fast dye cation regeneration reaction by iodide ions [17-19] which intercept effectively with excited state photochemical reactions and oxidized state degradation reactions respectively.

2.2. Aim of the work

By ruling out the probability of dye degradation arising from dye excited state in view of the ultrafast electron injection rate and with reference to literature data on thermal stability of the **N3/N719** dyes both in free state and adsorbed on TiO_2 nanoparticles [20] the most probable degradation pathway would be dye oxidative degradation following electron injection into the TiO_2 semiconductor conduction band. This probability is reinforced by observation of dye degradation products in illuminated nc-DSSC [21] or any model systems closely resembling solar cell conditions [11]. The aim of this part of the dissertation is to estimate the oxidative degradation rate, k_{deg} of the **N719** dye molecules attached directly onto the nanocrystaline TiO_2 particles. Determination of the oxidative degradation rate will allow the estimation of the turnover number of the dye during solar cell operation and consequently the cell lifetime. A simple model system consisting of a stirred colloidal suspension of **N719** dyed TiO_2 nanoparticles in acetonitrile was used instead of a real complete solar cell. The system was illuminated by a monochromatic light in the visible region. The total quantum yield of all degradation products was calculated by monitoring the total amount of degradation products from the peak areas of LC–UV/Vis– MS–chromatograms. Because of the absence of iodide ions as reducing electrolyte, the back electron transfer reaction between the injected electrons and oxidized dye cations (equation 2.4) is considered as the second channel that the oxidized dye molecules can take part in.

$$TiO_2 + e^- \,|\, S^+ \xrightarrow{k_{back}} TiO_2 \,|\, S \quad \text{Back electron transfer reaction} \quad \textbf{(2.4)}$$

The back electron transfer reaction rate was measured by PIA spectroscopy at the same experimental condition used in the model system. The oxidative degradation rate of the dye then was calculated based on k_{back} and quantum yield values. The schematic representation of the described model system and chemical equations representing the reactions taking place under illumination can be represented as in Figure 2.1.

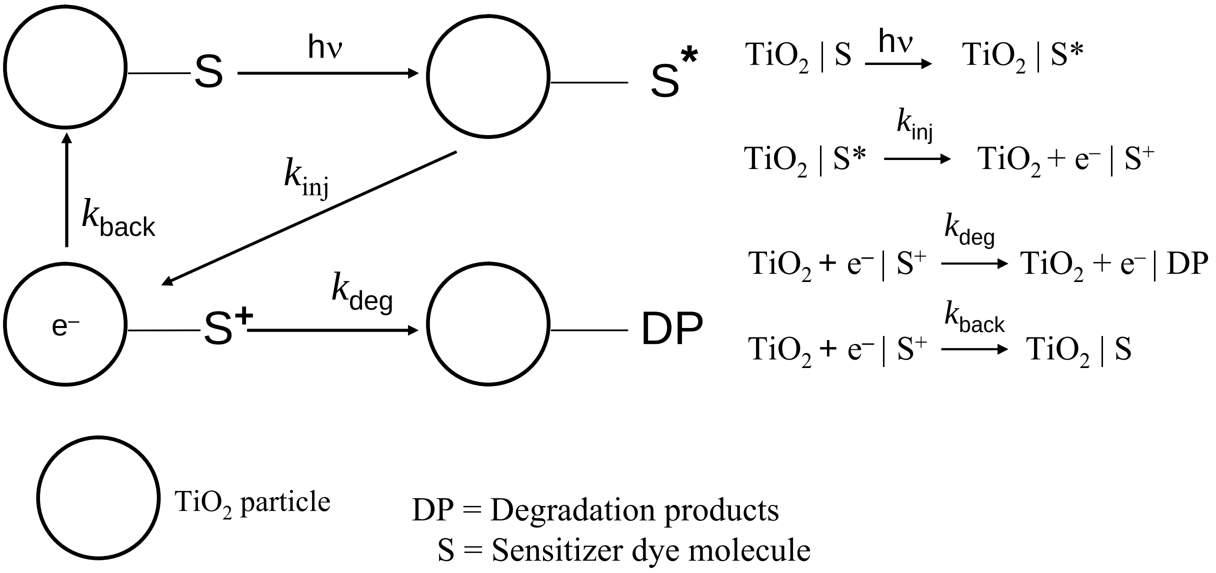

Figure2.1 Schematic representation of the model system used to estimate photooxidative degradation rate of the **N719** dye adsorbed onto TiO_2 nanoparticles under illumination.

2.3. Experimental section

2.3.1. Experimental set-up

All photolysis experiments were performed in a cuvette containing **N719**-dyed TiO_2 nanoparticles suspended in deareated acetonitrile (ACN) solutions. Two different methods were used to prepare these solutions. In method **I** ethanolic solution of Degussa P25 TiO_2 powder were sprayed as thin films on non-conductive glass plates (1.52–2.38 mg TiO_2 /cm^2). After thermal sintering the plates were dyed by soaking in dye solution. The dyed particles were used in photolysis experiments after removing from the plates into the cuvette. In method **II** a known amount of Degussa P25 TiO_2 powder were suspended in **N719** dye solution resulting to dyed particles (0.03 mg/mg TiO_2). These individual particles were used without sintering. The prepared solutions were illuminated by increasing number of photons from different light sources having different light intensities. The two experimental set-up used are shown in Figure 2.2. Both equipments are consisted of a black box with a cuvette holder inside it, a photon counting device and a light source. The light sources were an Oriel 300-W halogen-tungsten lamp, a slide projector equipped with a 250 W halogen lamp and a 532 nm continues wave laser. The two former light sources were used in combination with a 525 ± 5 nm band-pass filters.

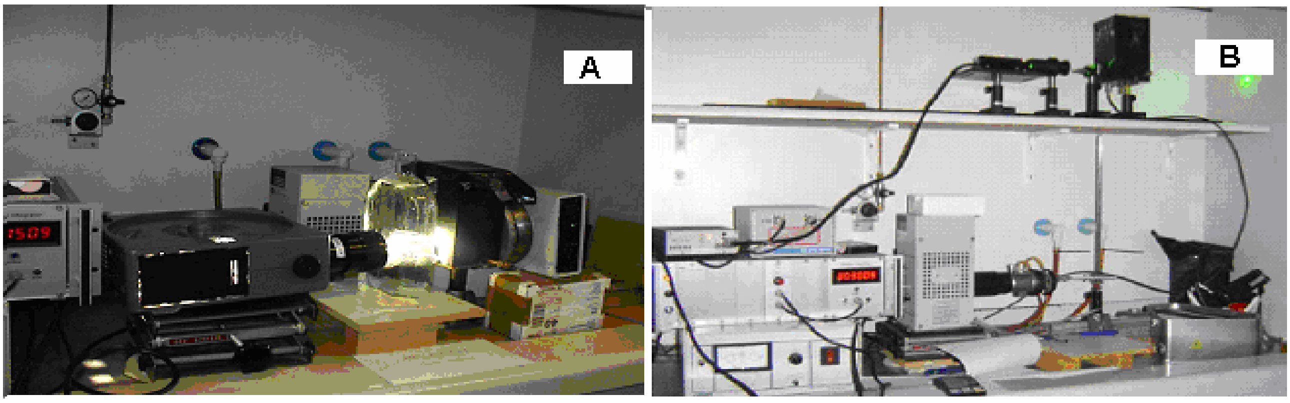

Figure2.2 The two Experimental set-ups used for photolysis experiments. Light sources: (A) Slide projector equipped with a 250 W halogen lamp combined with a 525 ± 5 nm band-pass filter, (B) 532 nm continues wave laser.

Chemical actinometry was used to calibrate the photon counting device. **Aberchrome 540 (AB540)** (Figure 2.3) was used as a chemical actinometer in the visible region. The absorbance of a 3 ml red coloured solution of the compound in toluene (5×10^{-3} M) was measured at 494 nm. The measurement was repeatedly continued following irradiation of the stirred solution of the compound with a monochromatic light at 525/532 nm for different time intervals/counting numbers. The absorbance decrease as a function of counting number recorded on the photon counting device was used to calculate the photon flux of the light sources by equation 2.5 [22].

$$I \times t = (\Delta A \times V \times N_{a}) / (\phi_{b} \times \varepsilon) \tag{2.5}$$

I is photon flux (s^{-1}), ΔA is absorbance difference at 494 nm after light exposure, V is the volume of the irradiated solution, N is 6.023×10^{23} mol^{-1}, ϕ_b is quantum yield at 525/523 nm, ε is the extinction coefficient at 494 nm, t is time (s) and (I × t) is counting number.

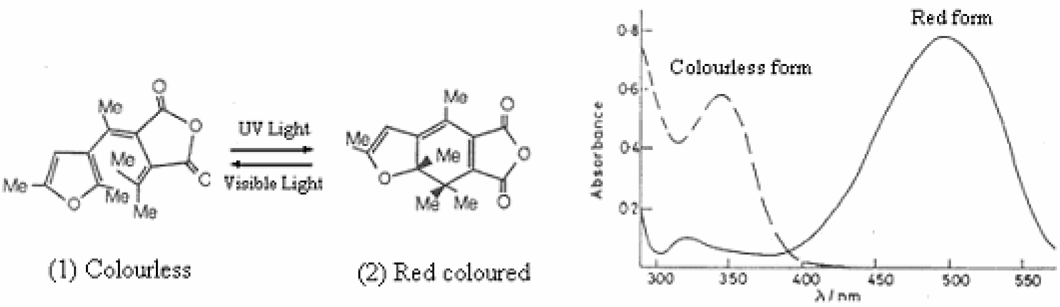

Figure2.3 The ultraviolet and visible spectra of 1×10^{-4} M solution of **Aberchrome 540** (1). (---) in toluene, (—) after quantitative conversion into the coloured form (2) [22].

2.3.2. Analytical methods

The analytical method used for the identification and quantification of the **N719** dye and its degradation products was LC–UV/Vis and LC– ESI–MS. Back electron transfer reaction rates at different light intensities were measured by photoinduced absorption (PIA) spectroscopy.

2.3.2.1. Electrospray ionization-mass spectrometry (ESI-MS)

Electrospray is one of several ionization techniques used in mass spectrometry. Figure 2.4 shows a schematic representation of the ion formation process.

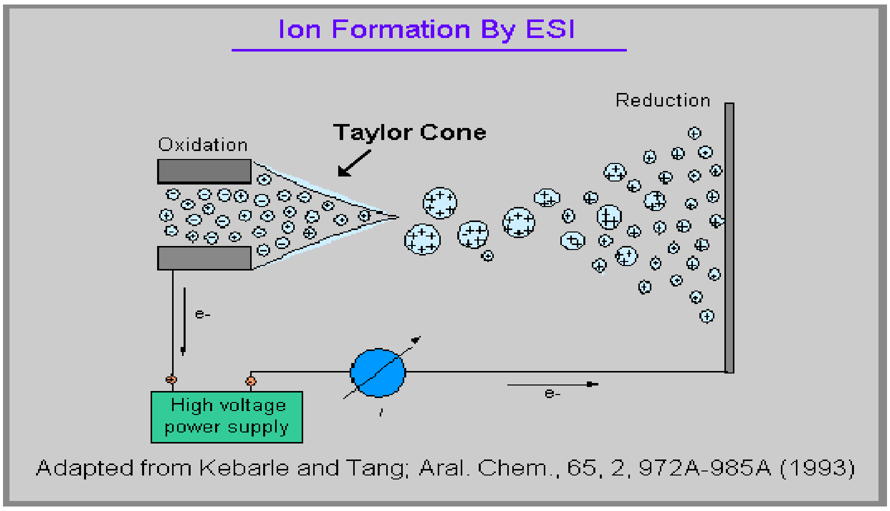

Figure 2.4 Schematic of major processes occurring in electrospray.

Briefly, in this method a solvent which contains the analyte molecules to be studied is passed through an electrically charged needle. During the passage time, the liquid is charged by transfer of electrical charge between the needle and the liquid. The charged liquid at the tip of the needle (the Taylor cone) becomes unstable as it is forced to hold more and more charge. Soon the Taylor cone reaches a critical point at which it can hold no more electrical charge and at the tip of the needle it blows apart and leaves the end of the capillary as a very fine liquid aerosol consisting of highly charged droplets, the process named as nebulization. The droplets which carry negative or positive ions (depending on the sign of the applied potential) pass into a small evaporation chamber. As the droplets pass through the chamber, they rapidly become much smaller through vaporization of solvent which cause the surface area of the droplets gets smaller and smaller. This causes the electrical charge density on the surface increases until a point of instability is reached in which the coulomb repulsion exceeds the surface tension and not only the solvent molecules but also the ions desorb from the surface of the droplets (coulomb explosion). This process is repeated until the analyte ions are free of solvent molecules and then will be directed into the mass analyzer of the mass spectrometer. Electrospray ionization technique has some unique features, for example it is a soft ionization method which overcomes the tendency of macromolecules to fragment. The technique is also very useful for determination of non-volatile molecules. These properties have made the technique very useful and unique for the analysis of large molecules including transition metal complexes [23].

2.3.2.2. Photoinduced absorption spectroscopy (PIA)

Figure 2.5 is schematic representation of the experimental set-up used for PIA measurements. The photoinduced absorption (PIA) apparatus has been described elsewhere [24].

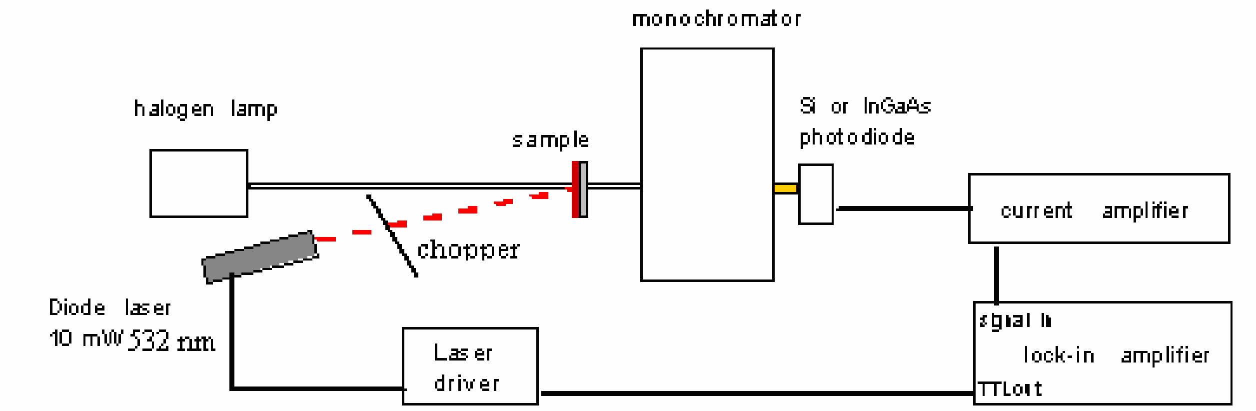

Figure 2.5 Experimental set-up used for photoinduced absorption measurements. The sample is excited by on/off modulated light from the diode laser at frequencies ranging from 1 to 1000 Hz.

2.4. Results and discussion

2.4.1. Degradation products from photolysis of N719-dyed TiO_2 colloidal solutions

A typical LC-MS chromatogram of the extracted solution of illuminated **N719**-dyed TiO_2 nanoparticles is shown in Figure 2.6. The extraction process was carried out by treatment of the illuminated solutions with 0.1 M sodium hydroxide solution, ethanol and concentrated formic acid. Based on the characteristic m/z values from the mass spectra and λ_{max} values of the UV/Vis spectra, peaks **1** and **2** can be assigned to the non-reacted fully protonated **N719** dye and its N/S-bound isomer, and peaks **3, 4** and **5** to [$RuL_2(CN)_2$], [RuL_2(NCS)(CN)] and [RuL_2(NCS)(ACN)] compounds respectively (Figure 2.7).

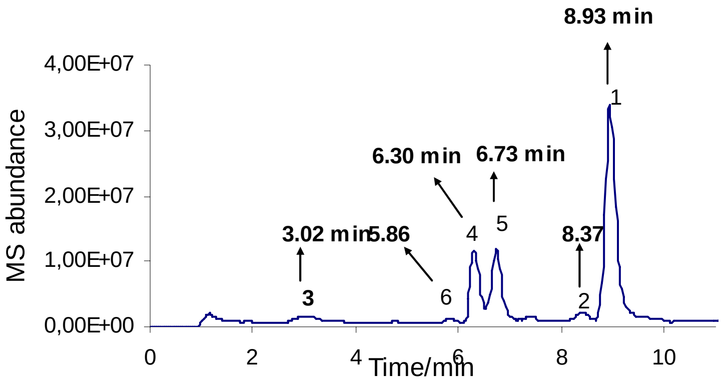

Figure2.6 LC-MS chromatogram of the extracted solution of **N719** dyed TiO_2 nanoparticles in deoxygenated acetonitrile after illumination by a halogen- tungsten lamp. Excitation wavelength: 525 ± 5 nm. Illumination time: 16 hours.

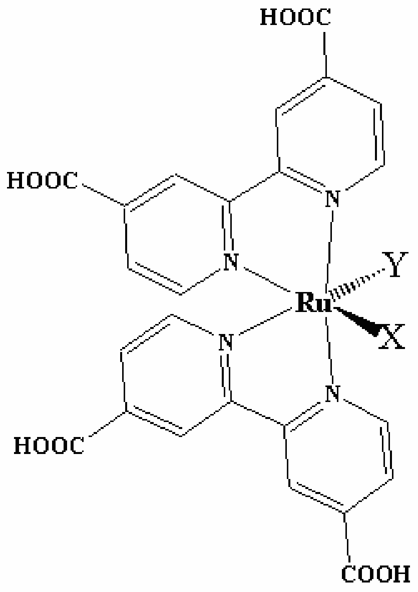

	X	Y
1	**NCS**	**NCS**
2	**SCN**	**NCS**
3	**CN**	**CN**
4	**NCS**	**CN**
5	**NCS**	**CH_3CN**

Figure 2.7 Structure of the fully protonated forms of the **N719** dye and its identified degradation products.

The same product as [RuL_2(NCS)(ACN)] has already been identified and characterized in electrochemically oxidized solutions of **N719** dye in acetonitrile (ACN) [14]. Briefly, compound **4** is the mixed cyanide / thiocyanate ion ligand complex which is an intermediate compound produced from the internal oxidation of thiocyanate ion ligand by the Ru (III) state of the complex [7]. This compound shows an intense ruthenium isotope pattern in the mass spectrum around the ion m/z =

675 (Figure 2.8.a) corresponding to the $[RuL_2(NCS)(CN)+H]^+$ ion. The small ruthenium isotope cluster around the ion m/z = 697 is due to the ion $[RuL_2(NCS)(CN)+Na]^+$.

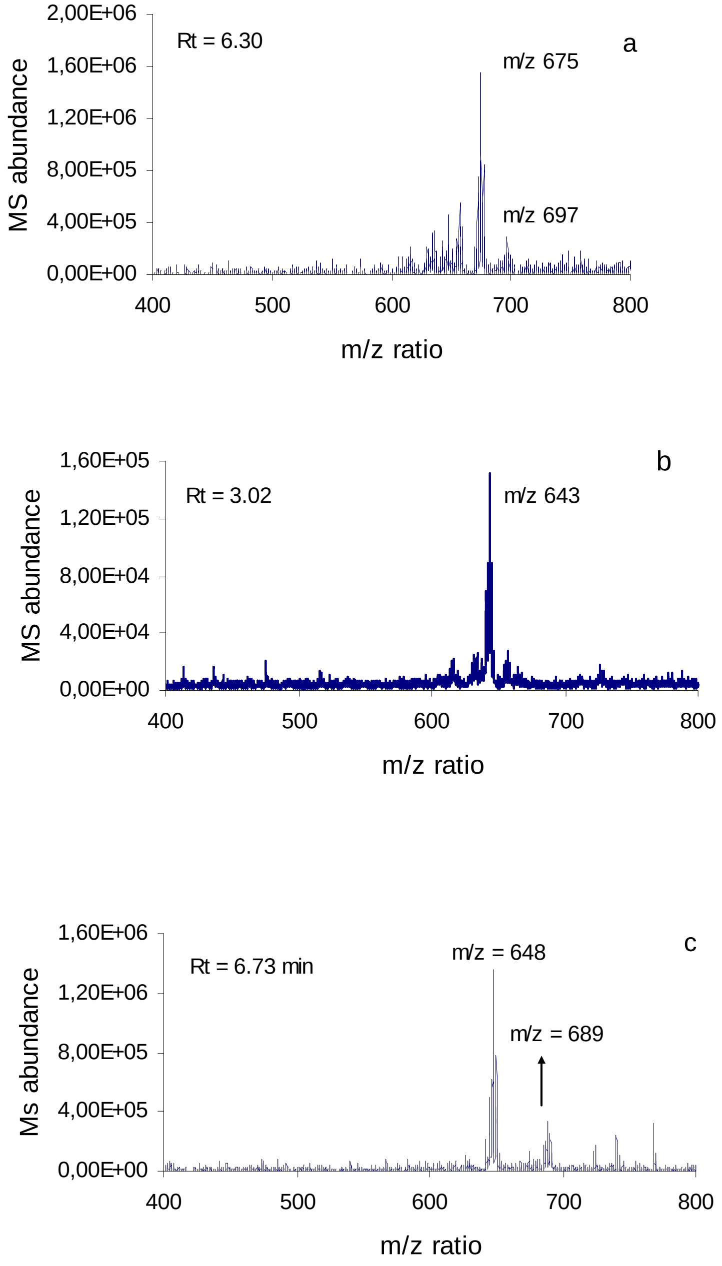

Figure2.8 Mass spectrum of (a) $[RuL_2(NCS)(CN)]$, (b) $[RuL_2(CN)_2]$ and (c) $[RuL_2(NCS)(ACN)]$.

Compound **3** is formed through further oxidation of the intermediate compound **4** yielding the dicyano complex [14] which shows an intense ruthenium isotope pattern around ion m/z = 643 (Figure 2.8.b) corresponding to $[RuL_2(CN)_2{+}H]^+$ ion. Compound **5** is the mono solvent substituted complex which is produced by replacement of one of the SCN^- ligands by the acetonitrile solvent molecule [14]. The mass spectrum of this product (Figure 2.8.c) is characterized by an intense ruthenium isotope pattern around ion m/z = 689 which can be assigned to the $[RuL_2(NCS)(ACN)]^+$ ion. The fragment ion m/z = 648 is formed by the elimination of the solvent molecule (ACN) from the molecular ion. The peak with R_t = 5.86 min (**6**) showing a low intensity ruthenium isotope pattern around ion m/z = 667 and λ_{max} = 512 nm corresponds to the $[RuL_2(NCS)(H_2O){+}H]^+$ ion. The amount of this compound does not increase with increasing number of absorbed photons during photolysis experiments and therefore maybe explained as an impurity of the **N719** dye complex. However, this compound is not observed in the **N719** dye standard solutions. The characteristic m/z values of mass spectra and λ_{max} of UV/Vis spectra for the **N719** dye molecule and its identified degradation products are found in Table 2.1.

Table 2.1.Retention time, characteristic absorption maxima and m/z values of the fully protonated N719 and its oxidative degradation products.

	Complex formula[a]	R_t / min	Characteristic m/z	λ_{max} / nm
1	$[Ru\,L_2(NCS)_2$	8.93	706, 648	525
2	$[RuL_2(NCS)(SCN)]$	8.37	706, 648	521
3	$[RuL_2(CN)_2]$	3.02	643	470
4	$[RuL_2(NCS)(CN)]$	6.30	675, 648	497
5	$RuL_2(NCS)(ACN)$	6.73	689, 648	481

[a] L = 2,2′-bipyridyl-4,4′-dicarboxylic acid. ACN = CH_3CN

The upper layer of the illuminated colloidal solutions after centrifugation and before the extraction step showed no discernable amount of the dye or its degradation products indicating that the dye and all its identified degradation products are attached onto the TiO_2 nanoparticles. The two complexes of the formula $[RuL_2(CN)(ACN)]$ and $[RuL_2(ACN)_2]$, identified by Lund [14] and Cecchet [12] respectively, as electrochemical oxidation products of the **N719** and **N3** dye solutions in acetonitrile were not identified in our results.

2.4.2. Quantum yields of degradation products

The amount of dye degradation products were quantified from the peak areas of each product from LC-MS chromatograms for the samples prepared by method **I** and LC-UV chromatograms for the samples prepared by method **II**. LC-MS peak areas were used to calculate the product moles by using an external calibration curve. It is assumed that the starting **N719** dye complex and all its degradation products have the same response factor in MS detector. In method **II** using LC-UV peak areas, degradation product moles were calculated by dividing the peak area of each product by the total peak areas of compounds **1–5** and multiplying this ratio by the starting mole numbers of the **N719** dye in the cuvette. In these calculations it is again assumed that compounds **1** to **5** all have the same extinction coefficient at their respective visible absorption maxima. Figure 2.9 depicts the evolution of each degradation product moles and sum of them, n_{DP} as a function of mole of absorbed photons, $n_{p,}$ for two different light sources at different light intensities. As is evident from Figure 2.9 the mole number of each degradation product and consequently the total mole of degradation products increase almost linearly with increasing the mole number of absorbed photons. The slope of the plots for each degradation product and also sum of them can be taken as the individual and total quantum yield of all degradation products respectively. The total quantum yields of degradation products for different light intensities ranging from 0.1 to 16.3 mW/cm^2, which can be defined as equation 2.6 are summarized in Table 2.2.

$$\Phi_{deg} = \Sigma n_{DP} / n_p \qquad \textbf{(2.6)}$$

Figure 2.9 also shows the non-zero intercept for the plots of total quantum yield of degradation products. Evaluation of the plots for three individual degradation products reveals that compound **4** is the one that has the most contribution in the observed intercept. This indicates that some non-photochemical degradation of the starting **N719** dye complex has taken place producing compound **4**. In order to clarify the origin of the intercept of the plots for compound **4** we did two analyses with two **N719** dyed-TiO_2 films which have not been exposed to the light. These plates were stored in dark. The adsorbed dye on one of the plates was extracted in dark and the other one under day light in the laboratory. The results of LC-MS analysis of these extracted solutions showed that [$RuL_2(NCS)(CN)$] complex was present before the irradiation of the dyed-TiO_2 films. The origin of this initial dye degradation is not known. However, it might come from the weak degradation of the untreated (dyed, but not illuminated) dye coated TiO_2 films stored under air atmosphere. From lliterature it is known that degradation of the **N3** may occur on dry TiO_2 films in the dark [25]. It has also been shown that air and water [11b] degrade the dye adsorbed onto TiO_2 nanoparticles both in darkness and under visual illumination. The impurity defects in the Degussa P25 nanoparticles may be an alternative possibility for the observed oxidative degradation compound [$RuL_2(NCS)(CN)$].

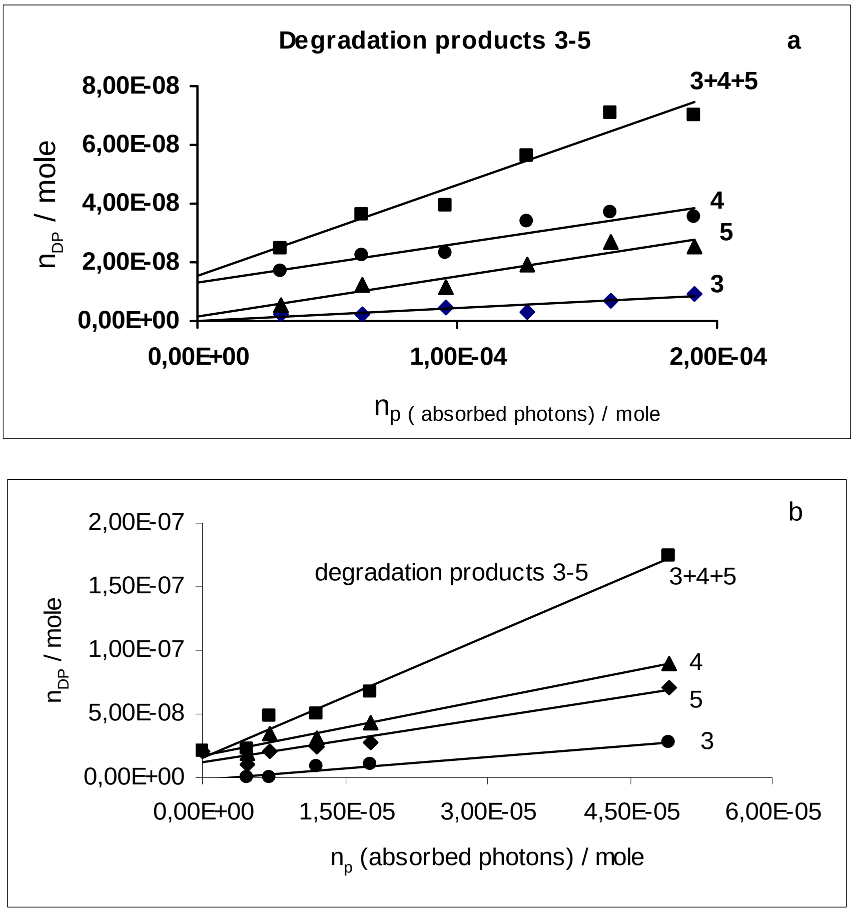

Figure 2.9 Plot of the mole number of each degradation product and sum of them as a function of the mole of absorbed photons. (a) Laser light (I = 9.58 mW/cm^2, excitation wavelength: 532 nm, (b) Halogen-tungsten lamp (I = 0.1mW/cm^2, excitation wavelength: 525 ± 5 nm.

Table 2.2 Qquantum yields, back electron transfer reaction rates, k_{back} and oxidative degradation rates, k_{deg} of N719 dye attached to TiO_2 nanoparticles

Light source	I_0 (mW /cm^2)	τ[a] (s)	k_{back}[b] (s^{-1})	Φ_{deg}	$k^{u}_{\mathrm{deg}} \cdot 10^2$[c] ($s^{-1}$)	k^{c}_{deg} 10^2[d] (s^{-1})
Xenon- Tungsten	0.1	3.22×10^{-2}	31	3.27×10^{-3}	10.0	6.0
Lamp[e,f]	0.54	1.63×10^{-2}	61	1.36×10^{-3}	8.30	4.98
Laser[g,h]	0.93	1.31×10^{-2}	76	7.73×10^{-4}	5.57	3.34
Laser	2.86	1.27×10^{-2}	120	5.51×10^{-4}	6.61	3.97
Laser	4.65	6.82×10^{-3}	147	4.05×10^{-4}	5.95	3.57
Laser	6.79	5.85×10^{-3}	171	3.75×10^{-4}	6.41	3.85
Laser	9.58	5.09×10^{-3}	196	3.10×10^{-4}	6.08	3.64
Laser	16.30	5.85×10^{-3}	243	2.04×10^{-4}	4.98	2.99
Average ± Stdv.					**6.74 ± 1.64**	**4.04 ± 0.98**

[a] Measured using the PIA method, [b] $k_{\mathrm{back}} = 1/\tau$, [c] uncorrected degradation rates, [d] corrected degradation rates, [e] 525 ± 5 nm band-pass filter used, [f] based on method I, [g] $\lambda = 532$ nm, [h] based on method II.

2.4.3. Measuring back electron transfer reaction rate

The results in Table 2.2 show a light intensity dependent degradation rate of the **N719** dye. This dependency is manifested as high total quantum yield at low light intensity and vice versa. As all the photolysis experiments have been performed in the absence of iodide, the two probable channels for the dye cation produced after electron injection is back reaction with the injected electrons and dye degradation from the oxidized state. Therefore, the observed light intensity dependence of the degradation products quantum yields might be due to the variation in the back electron transfer reaction rate under different light intensities. According to the literature data back electron transfer reaction rate, k_{back} is dependent on many parameters including light intensity [24]. In order to get the dye degradation rate it is necessary to know the k_{back} under the same experimental conditions as used for photolysis experiments. Photoinduced absorption spectroscopy (**PIA**) was used at different light intensities between 0.5 – 5 mW/cm^2 on a colloidal solution of **N719** dyed TiO_2 nanoparticles. Figure 2.10 shows the plot of the back electron transfer time, τ_{back} values as a function of the laser light intensity (see Table 2.2). It is seen that τ_{back}, decreases with increasing excitation laser light intensity. The plot can be expressed as equation 2.7.

$$k_{back} = \frac{1}{\tau_{back}} = \frac{1}{0.0127I^{-0.4043}} = 78.74I^{0.4043} \qquad \mathbf{(2.7)}$$

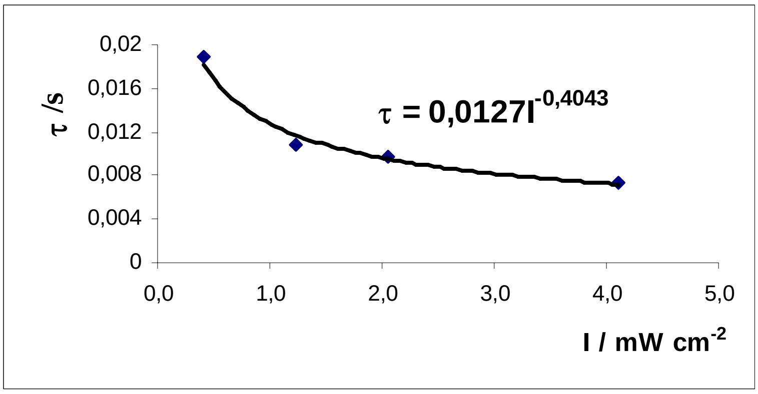

Figure2.10 Back electron transfer time, τ_{back} as a function of laser light intensity, I.

2.4.4. Estimation of the N719 dye oxidative degradation rate

Based on our model system (Figure 2.1) the experimental quantum yields obtained for dye degradation under illumination reflects the competition between oxidized dye degradation reaction (equation 2.3) and back electron transfer reaction of the **N719** dye cation with injected electrons (equation 2.4). Therefore, oxidative degradation rate of dye cation, $k_{\deg}$ may be calculated using equation 2.8 derived from steady state approximation on equations 1.1, 1.2, 2.3 and 2.4.

$$k_{\deg} = \phi_{\deg} \times (k_{\deg} + k_{\text{back}}) \sim \phi_{\deg} \times k_{\deg}\,; \qquad k_{\text{back}} \gg k_{\deg} \qquad \mathbf{(2.8)}$$

Total quantum yield of degradation products was obtained from the slope of the plot of total mole of degradation products versus the total mole of absorbed photons (equation 2.6). Back electron transfer reaction rate was calculated using equation 2.7. From these data and based on equation 2.8 oxidative degradation rate of the **N719** dye was calculated at different light intensities used in our experimental conditions. The results are summarized in Table 2.2. However, due to the absorption by the dyed-TiO_2 nanoparticles, the light intensity is not constant through the light pathway inside the cuvette. Therefore, it is necessary to correct the dye degradation rates which have been obtained at constant laser light intensity I_o, $k_{\deg}^{u}$ (denoted as uncorrected degradation rate constant) for the light intensity change through the cuvette length. Mathematical expression of the corrected rate of degradation (see the appendix in paper **I**) gives a constant value of 0.6 as the correction factor. This value is independent of the illuminating light intensity. Applying this number to the uncorrected degradation rate constants gives the corrected values (denoted as k^c_{deg} (see Table 2.2).

2.4.5. N719 dye turnover number

The turnover number of the dye, N is an estimation of the sensitizer dye stability under solar cell operation. It represents the number of cell cycles a single dye molecule can survive. This number can be calculated via equation 2.9, knowing the dye oxidative degradation rate, k_{deg} and dye regeneration rate by iodide ions, k_{reg}. However an overview of the literature gives various numbers for the **N3** dye regeneration rate by different research groups in a range differing by more than a factor of 100 (see Table 2.3) [17, 18]. This divergence in turn gives different calculated N numbers (see Table 2.3).

$$N = k_{\mathrm{reg}}\,[I^-] / k_{\mathrm{deg}} \qquad \textbf{(2.9)}$$

Table2.3 Literature data of the N3 dye regeneration rates, k_{reg} by iodide ion.

Ref.	Experimental conditions	k_{reg} / M^{-1} S^{-1}	[c]N
18a	CH_3CN, 0.5 M LiI	2.6×10^5	2.5×10^6
18b	Propylene carbonate	1.6×10^5	2.0×10^6
17a	[a] 0.3 M KI in propylene carbonate/ethylene carbonate	2.3×10^7	2.8×10^8
17b	[b] Propylene carbonate, $[I^-]$= 0.1 M, $[Li^+] > 10^{-2}$ M	3.6×10^7	4.5×10^8
17c	MeOH, 0.5 M NaI	7.1×10^7	8.9×10^8

[a] $t_{1/2}$ = 100 ns, $k_3 = \ln 2/(t_{1/2} \times [I^-])$, [b] $1/t_{1/2} = 6 \times 10^6$ s^{-1}, [c]N calculated from equation (2.9), $[I^-]$ = 0.5 M.

2.4.6. N719 dye sensitizer lifetime

By considering the reported 10^8 turnover number for the **N3** dye being equivalent to more than 20 years of DSSC lifetime [6,7], the calculated N numbers based on our model system may be translated to the cell lifetime by equation 2.10.

$$\text{Lifetime of S} = 20 \text{ years} \times N / 10^8 \qquad \textbf{(2.10)}$$

Two different turnover numbers of 5.3×10^8 and 2.6×10^6 was calculated from the mean values of 4.2×10^7 M^{-1} s^{-1} and 2.1×10^5 M^{-1} s^{-1} for the three highest values [17] and the two lowest values [18] of the dye regeneration rate, k_{reg} (see Table 2.3). The **N719** dye sensitizer lifetime was estimated to be more than 20 years and ~ 0.5 years based on the calculated N numbers of 5.3×10^8 and 2.6×10^6 respectively, provided that the oxidative degradation is the only route of dye degradation. We believe that the discrepancy observed for the above calculated N numbers manifested as two different dye lifetime is due to the large divergence for the reported k_{reg} values in the literature.

2.5. Conclusion

2.5.1. Summary

The photooxidative degradation rate of the solar cell dye sensitizer **N719**, k_{deg} was determined based on illumination of a simple model system consisting of colloidal acetonitrile solutions of **N719** dyed TiO_2 nanoparticles with light intensities in the range of 0.1–0.16 mW/cm^2. The quantum yield of the dye degradation products, $[RuL_2(CN)_2]$, $[RuL_2(NCS)(CN)]$ and $[RuL_2(NCS)(ACN)]$, Φ_{deg} were obtained by determining the amount of degradation products as a function of increasing number of absorbed photons of different light intensities. The sum of the quantum yields of degradation products was used to calculate k_{deg} via the equation $k_{deg} = \Phi_{deg} \times k_{back}$. Back electron transfer rates, k_{back} between the oxidized dye cation and the injected electrons were determined as a function of different laser light intensity by the PIA spectroscopy. Based on the obtained total quantum yields and k_{back} values the average value of $k_{deg} = 4 \times 10^{-2}$ s^{-1} was obtained. The stability of **N719** dye during solar cell operation was discussed based on both this number and literature values of the regeneration reaction rate between $[Ru^{(III)} L_2(NCS)_2]$ and iodide ion. Two different turnover numbers of $N = 5.3 \times 10^8$ and $N = 2.6 \times 10^6$ were obtained based on the mean values of the three highest and two lowest k_{reg} values. These numbers were translated to more than 20 years and ~ 0.5 years of the **N719** dye lifetime respectively.

2.5.2. Relevance to nc-DSSC

In a functioning nc-DSSC the dye degradation will result in dye instability and consequently low dye lifetime if the dye regeneration rate by the iodide ions is not sufficient. The results presented in this work were not obtained from a complete real nc-DSSC. In particular they were obtained in the absence of iodide ions. It is also known that the kinetics of dye regeneration by iodide ions is dependent on the electrolyte composition [17b, 19a]. In our calculations of **N719** dye lifetime it is assumed that the model system used in our investigations represents the more complex real nc-DSSC reasonably well. The closeness of the predicted lifetime (in case of using high values of dye regeneration rate by iodide) to the reported nc-DSSC stability equivalent to at least 10 years of normal solar cell operation in the literature [9c] supports this assumption. Furthermore the same dye degradation products have been observed in both our model system and real light exposed nc-DSSC [21]. However, given the clear dependence of the dye regeneration kinetics upon electrolyte composition, a rigorous comparison between these data and a complete nc-DSSC containing redox active electrolyte iodide ions is not possible. Nevertheless, based on our findings the model system used in our investigations represents the more complex real nc-DSSC in a qualitative way reasonably well. Besides, the k_{deg} values obtained in this way may be used to rank the relative stability of various solar cell dyes in an approximately simple and fast way. Obviously in order to predict the sensitizer dye stability and lifetime in a real nc-DSSC, measurement of dye regeneration rate, k_{reg} under the experimental conditions as used in our model system is needed.

Chapter 3

An Investigation of the Substitution Reaction Between the Solar Cell Dye ***N719*** *and* ***4-tert-butyl pyridine***

3.1. Introduction

Since the 1991 breakthrough paper of O'Regan and Grätzel in which an overall solar to electric energy conversion efficiency ~ 7 % was achieved [2], various investigations have been made to improve the solar cell performance by addition of various compounds to the cell. Some investigations have focused on the redox electrolyte solution with the aim of enhancement of the open circuit photovoltage, V_{oc} via suppressing the recombination reaction between the injected electrons and oxidized moiety of the redox electrolyte which occurs at the nanostructured TiO_2/redox electrolyte interface [9, 26-35]. One way to suppress this reaction is by chemically treating of the TiO_2 semiconductor surface by some basic compounds (commonly referred to as an additive) like nitrogen containing heterocycles. Various compounds have been examined and promising results have been reported [27-35]. The most popular additive which has been used by many research groups is 4-*tert*-butylpyridine (**4-TBP**) [6, 7, 9a, 28]. An accepted view is that absorbed **4-TBP** suppresses the reduction reaction between I_3^- ions and the semiconductor conduction band electrons at the semiconductor/electrolyte interface by passivating the recombination centres on the electrode surface [35]. Hagfeldt et al. have proposed an alternative interpretation [11a]. Based on their suggestion the additive **4-TBP** takes part in a complex formation reaction with I_3^- ions which affects cell performance by two different mechanisms. The first one improves the open circuit photovoltage by increasing electron concentration in the semiconductor conduction band via decreasing I_3^- ion concentration in the electrolyte solution. The second one suppresses the loss of the thiocyanate ion ligand from the dye by affecting the complex formation reaction between the thiocyanate ion ligands with tri-iodide ions which in turn improves the cell performance by affecting dye stability.

3.2. Aim of the work

It is well known that the ruthenium bipyridyl complexes of the type $[Ru(bpy)_2XY]$ where X and Y represent monodentate ligands, are prone to substitution by stronger nucleophiles via photochemical [36] or thermal reactions [37]. It is therefore likely that the substitution reaction occurs between the SCN^- ion ligand of the **N719** dye and **4-TBP** additive (which normally is present at a high concentration of ~ 0.5 M) during the nc-DSSC operation condition. Observation of **4-TBP** substituted **N719** dye molecules from the LC–UV/Vis–MS analysis of dye extracts of some light exposed real nc-DSSC [21] intensified this suspicion. To our knowledge nobody has previously investigated this possibility. In view of the key role of the sensitizer dye stability for long-term operation of nc-DSSC, we prompted to investigate the possibility and kinetics of this substitution reaction. This will allow us to estimate the effect of this side reaction on dye stability which in turn will influence nc-DSSC lifetime. We investigated the effect of heat and visible light illumination on the homogeneous **N719/4–TBP** and heterogeneous **N719**–TiO_2/**4–TBP** solutions. However, this work is mainly focused on photolysis experiments evaluating the effect of visible light on the occurrence and extent of this side reaction. Some preliminary results of heat treatment of homogeneous **N719/4–TBP** solutions are also presented. Heating experiments were performed on homogeneous **N719/4–TBP** solutions whereas photolysis experiments were carried out on both homogeneous **N719/4–TBP** and heterogeneous **N719**–TiO_2/**4–TBP** solutions in order to identify the sensitizer dye state which is involved in the substitution reaction.

3.3. Experimental section

3.3.1. Heat and light treatment of N719 dye and 4-TBP solution mixtures

Heating experiments of homogeneous solutions of **N719** dye and **4-TBP** were performed in test tubes capped with air tight membranes which were also protected from the light during the heating period to avoid the photoexcitation reactions. Photolysis experiments were carried out in cuvettes containing deareated acetonitrile/dimethylformamide solutions of **N719/N719–**TiO_2 and **4-TBP**, capped with airtight membranes. The light sources used were halogen-tungsten- lamp (0.1mW/cm^2) combined with a 525 ± 5 nm bad-pass filter and 532 nm continuous wave laser (7.33 mW/cm^2). Light sources were calibrated by using **Aberchrome 540 (AB540)** actinometer (see section 2.3.1).

3.3.2. Electrochemical oxidation of dye/additive solutions

Electrochemical oxidation of the **N719** dye and its uncarboxylated analogue $[\mathrm{RuL'_2(NCS)_2}]$ (L' = 2,2′-bipyridine) in deareated acetonitrile solutions containing 0.02 M $LiCF_3SO_3$ as the supporting electrolyte were carried out at a constant potential of 0.8 V /Ag / (0.02 M $LiCF_3SO_3$) in a three compartment cell. Platinum net was used as the anode and a carbon rod as the cathode. Identification of the products obtained from all thermal and photolysis experiments were made by using LC–UV/Vis–MS and ^{1}H NMR spectroscopy. Peak area of the LC- UV/Vis chromatograms were used to calculate the amount of the additive substituted dye complex and other dye degradation products formed, as described by method (II) (see section 2.3.1). The number of absorbed photons was obtained by using a photon counting device.

3.3.3. Synthesis of $[RuL'_2(NCS)_2]$ (L'=2,2´-bipyridine)

The cis-Ru(bpy)$_2$Cl$_2$.2H$_2$O (1.56 g) was dissolved in 70 ml DMF and transferred into a three-neck flask. Then KSCN (6.3 g) dissolved in 8 ml water was added to the solution. The reaction mixture was heated to reflux under Nitrogen atmosphere while magnetic stirring was maintained. During this time the reaction mixture was protected from the light by covering it with aluminium foil. After three hours the reaction was stopped. Then, the reaction mixture which was still warm was slowly added into 75 ml absolute ethanol and allowed to stand in ice bath overnight. After this time the red crystalline product was isolated by filtration. The solid product was washed twice with 50 ml ethanol 30% and then three times with 40 ml diethylether. The product yield was 81% of theoretical yield and practically pure.

3.4. Results and discussion

3.4.1. Thermal behaviour of the N719 dye complex in the presence of 4-TBP additive

Figure 3.1a and 3.1b depicts the LC-MS chromatograms of solutions containing **N719** dye and **4-TBP** additive in dimethylformamide and acetonitrile respectively, after heating for about 9 hours.

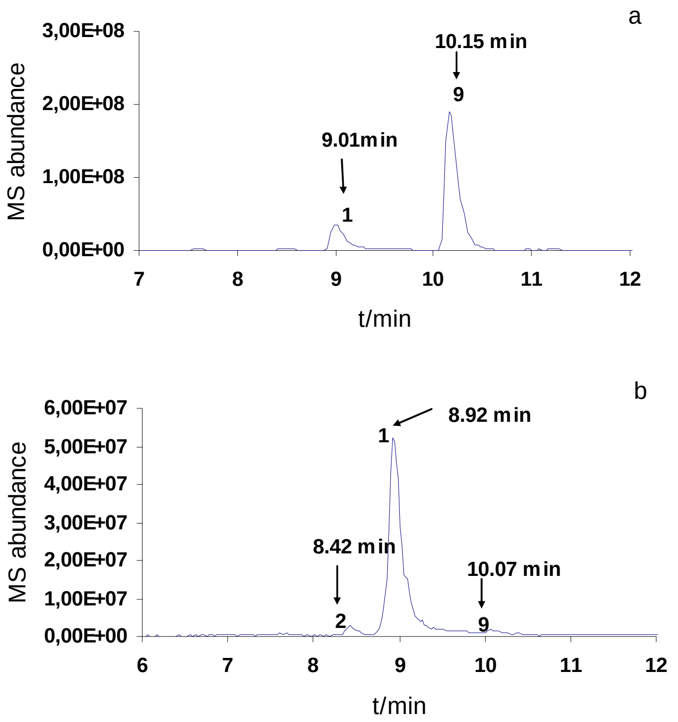

Figure 3.1 LC-MS chromatograms of 10 ml (a) DMF and (b) ACN solutions of **N719** dye (2 mg ~ 0.002 mmole) and 4-**TBP (**~ 25 µl ~ 0. 2 mmole) after removing oxygen with argon gas flow and heating for ~9 hours in dark at about 120 °C and 40 °C respectively.

The peaks eluting at $R_t = 8.92$ min (9.01 min in DMF) and $R_t = 8.42$ min have the UV/Vis and MS characteristics which are related to the fully protonated form of the starting dye complex $[RuL_2(NCS)_2]$ and its N/S bound isomer [14]. The peak with retention time 10.15 min which is dominant in DMF but is in a very small amount in ACN ($R_t = 10.07$ min) has an intense ruthenium isotope pattern in the mass spectrum (Figure3.2a) around the ion m/z = 783 and a peak maximum at $\lambda = 509$ nm (Figure3.2b). This ion corresponds to the M^+ ion $[RuL_2(NCS)(4\text{-TBP})]^+$.

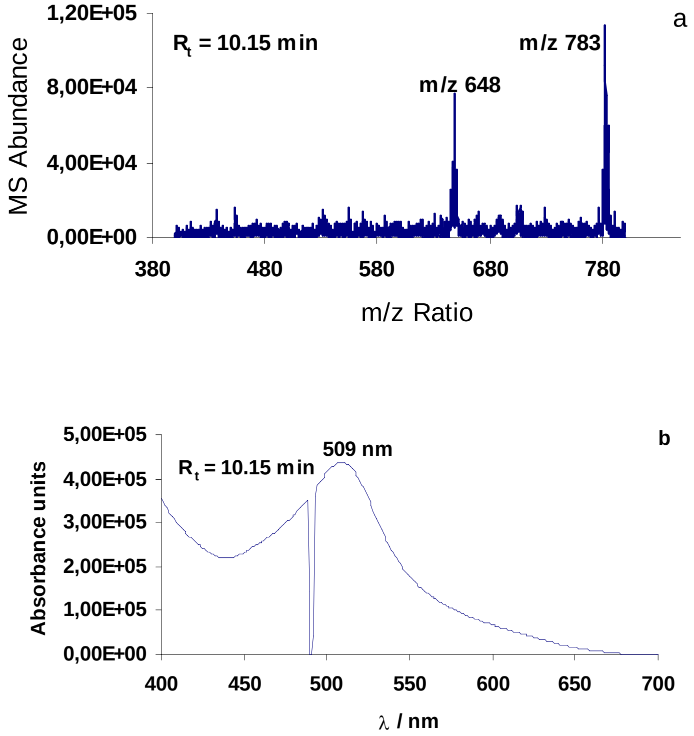

Figure3.2 (a) Mass spectrum and (b) UV/Vis spectrum of the $[RuL_2(NCS)(4\text{-TBP})]$.

Further evidence of the structure (see Figure 3.3) was obtained from the ^1H NMR spectrum of the compound which was synthesized in a large scale by heating 5 ml DMF solution containing ~ 25 mg (~ 0.021 mmole) and ~ 320 μl (~ 2.14 mmole) **4-TBP** additive. The LC-MS chromatogram of an aliquot of the heated solution mixture indicated the occurrence of the reaction by appearance of the peak with the expected MS and UV/Vis characteristics relating to the $[RuL_2(NCS)(4\text{-TBP})]$ compound. The raw product was purified by chromatography and the ^1H NMR spectrum is shown in Figure 3.4. The characteristic chemical shifts of the compound are found in Table 3.1.

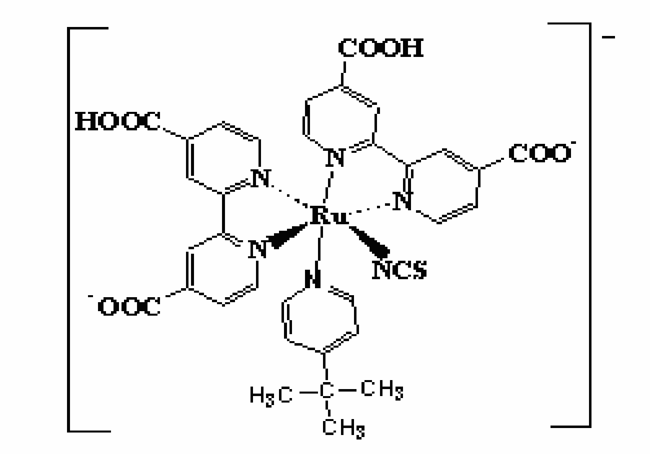

Figure3.3 Structural formula of **4-TBP** substituted **N719** dye product, $[Ru\ (HdcbpyH)_2(NCS)(4\text{-}TBP)]^-$.

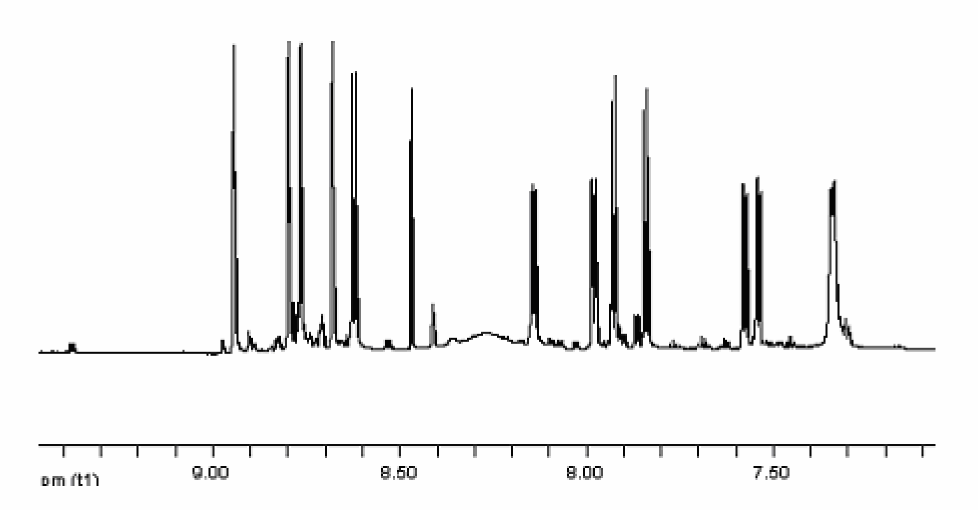

Figure3.4 ^{1}H-NMR spectrum of the $[Ru(dcbpyH)_2(NCS)(4\text{-}TBP)]^-$ complex (aromatic region).

Table 3.1 ^{1}H NMR chemical shifts (Aromatic region) for the 4-TBP substituted N719 dye complex in D_2O-NaOD

H	1	2	3	4	5	6	7	8	9	10	11	12	13	14
δ (ppm)	9.54	8.94	8.80	8.76	8.68	8.60	8.13	7.98	7.93	7.84	7.58	7.54	7.34	7.33

The cis isomer of the **N3** complex in a D_2O + NaOD solution shows six peaks in the aromatic region corresponding to two different pyridine ring protons in which two are trans to each other and the remaining two are trans to the NCS ligands [38]. By replacing one of the thiocyanate ion ligands by **4-TBP** molecule the symmetry of the dye complex is lost leading to the 12 non-equivalent aromatic protons (see Figure 3.4). The four H3 and H3´ protons of the two bipyridine rings can be identified from their small doublet splitting, $^4J \approx 1$ Hz and the eight H5, H6, H5´and H6´ protons by their doublet splitting $^3J = 6\text{-}7$ Hz. Another two aromatic signals at 7.34 and 7.33 ppm are due to the four aromatic protons on the pyridine ring. The signal due to the *tert*-butyl group is appeared at 1.5 ppm.

3.4.2. Photochemical behaviour of N719 dye/colloidal N719-TiO$_2$ solutions in the presence of 4-TBP additive

3.4.2.1. Photolysis in DMF

Figure 3.5a shows the LC-MS chromatogram of a mixture of **N719** dye and **4-TBP** in DMF solution after visible light illumination.

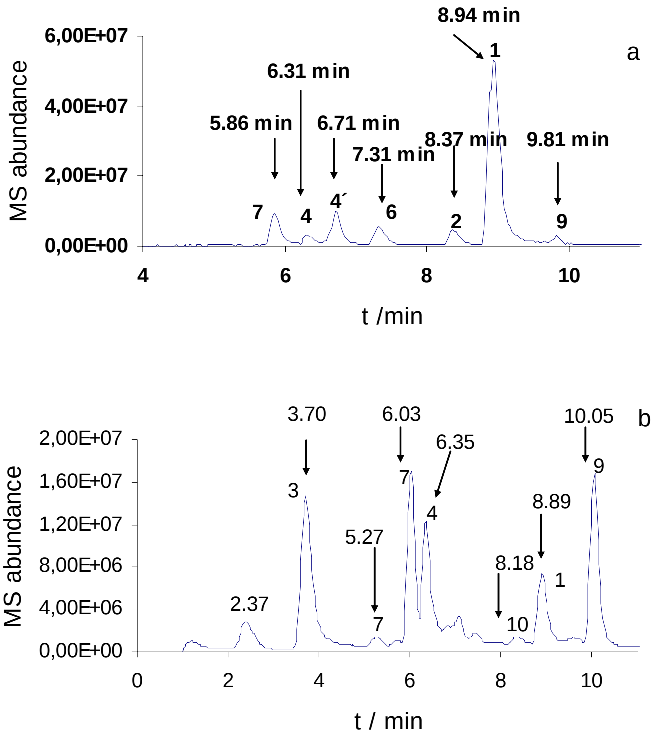

Figure3.5 LC-MS chromatograms of 3 ml illuminated DMF solutions of (a) **N719** dye (~ 2 mg, 0.002 mmole) and **4-TBP** (~ 25 µl, 0.2mmole), (b) **N719** dyed TiO$_2$ nanoparticles and **4-TBP** (~ 25 µl, 0.2mmole) after extraction. Light source: halogen-tungsten lamp combined with 435 nm cut-off filter . illumination time ~ 6 hours.

It is seen that the amount of **4-TBP** substituted product **9** in Figure 3.5a (peak eluting at R_t = 9.81 min) is relatively small in comparison to the other degradation products which are formed under visible light illumination (see Table 3.2).

Table 3.2 N719 dye and its identified degradation products moles from photolysis of a DMF solution containing N719 dye and 4-TBP additive.

	Complex Formula	^{a} mole	^{b} mole
1	$[RuL_2(NCS)_2]$	3.28×10^{-7}	6.98×10^{-8}
2	$[RuL_2(NCS)(SCN)]$	2.91×10^{-8}	–
3	$[RuL_2(CN)_2]$	–	1.76×10^{-7}
4	$[RuL_2(NCS)(CN)]$	3.10×10^{-8}	1.17×10^{-7}
6	$[RuL_2(NCS)(DMF)]$	5.23×10^{-8}	–
7	$[RuL_2(CN)(DMF)]$	5.62×10^{-8}	9.90×10^{-8}
9	$[RuL_2(NCS)(4\text{-}TBP)]$	1.83×10^{-8}	1.16×10^{-7}
10	$[RuL_2(CN)(4\text{-}TBP)]$	–	4.35×10^{-8}

^{a} homogeneous **N719/4-TBP** solution, ^{b} heterogeneous **N719**–TiO_2/**4-TBP** solution.

The peaks eluting at 7.31 and 5.86 minutes correspond to the complexes $[RuL_2(NCS)(DMF)]$ and $[RuL_2(CN)(DMF)]$ respectively which are the same as the products obtained by electrochemical oxidation of the **N719** dye in DMF solution [14]. Compound **4′** eluting at R_t = 6.71 corresponds to the sodium adduct of the compound **4**, $[RuL_2(NCS)(CN) + Na]^+$. Figure 3.5b illustrates the LC-MS chromatogram of the extracted solution of **N719** dye molecules adsorbed on TiO_2 nanoparticles and suspended in DMF solution containing **4-TBP** after visible light illumination. As it can bee seen from Figure 3.5b, the amount of the $[RuL_2(NCS)(4\text{-}TBP)]$ compound **9** (peak eluting at 10.05 min) increases upon adsorption onto TiO_2 nanoparticles (see Table 3.2).

3.4.2.2. Photolysis in ACN

Illumination of the homogeneous **N719/4-TBP** solution in acetonitrile also gives the expected **4-TBP** substituted dye complex (Figure 3.6a, peak with R_t = 9.80 min). Illumination of the dye molecules adsorbed on titanium dioxide nanoparticles and in the presence of **4-TBP** in acetonitrile Figure (3.6b) produces also some other degradation products besides the **4-TBP** substituted dye complex (peak with R_t =10 min). A general increase is observed in the amount of all products upon adsorption of the **N719** dye molecules onto TiO_2 nanopartcles. (see Table 3.3).

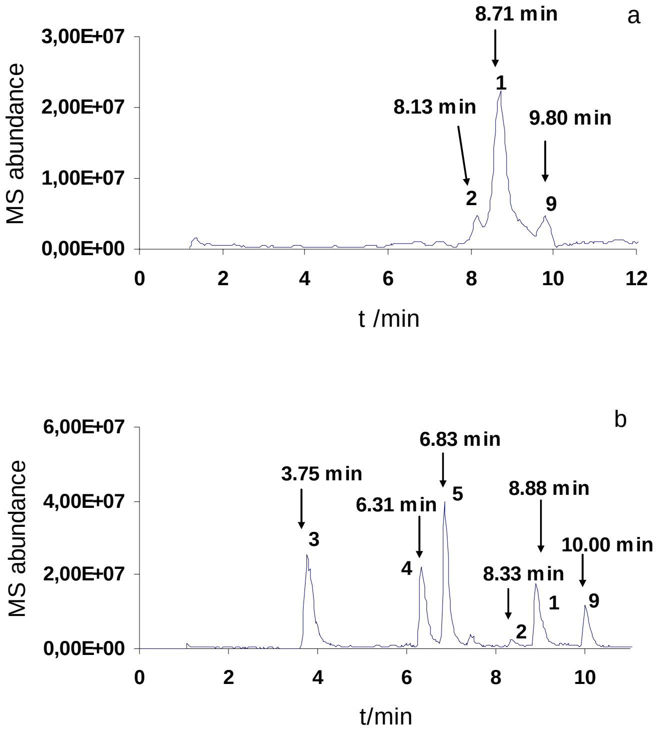

Figure3.6 LC-MS chromatograms of 3 ml deareated acetonitrile solution of (a) **N719** dye (~ 0.8 mg, 0.0007 mmole) and **4-TBP** (~25 µl, 0.2 mmole), (b) **N719** dyed TiO_2 nanoparticles and **4-TBP** (0.06 M) after 24 h and 6 hours illumination respectively. Light source: halogen-tungsten lamp combined with 435 nm cut-off filter.

Table 3.3 N719 dye and its identified degradation products moles from photolysis of an ACN solution containing N719 dye and 4-TBP additive.

	Complex formula	[a] mole	[b] mole
1	$[Ru\,L_2(NCS)_2$	2.98×10^{-7}	1.09×10^{-7}
2	$[RuL_2(NCS)(SCN)]$	3.90×10^{-8}	2.27×10^{-8}
3	$[RuL_2(CN)_2]$	–	3.14×10^{-7}
4	$[RuL_2(NCS)(CN)]$	–	1.56×10^{-7}
5	$[RuL_2(NCS)(ACN)$	–	1.70×10^{-7}
9	$[RuL_2(NCS)(4\text{-}TBP)]$	4.86×10^{-8}	6.98×10^{-8}

[a] homogeneous **N719**/**4-TBP** solution, [b] heterogeneous **N719**–TiO_2/**4-TBP** solution.

The results of the above investigations clearly indicate that the thiocyanate ion ligand of the **N719** dye complex can be substituted by **4-TBP** molecule. Furthermore, all three ground state, S (thermal substitution), excited state, S* (photochemical substitution) and oxidized state, S^+

(photooxidative substitution) of the sensitizer dye can be involved in this reaction (equations 3.1 – 3.3).

$$\mathrm{TiO_2 \mid S + 4\text{–}TBP} \overset{\Delta}{\rightarrow} \mathrm{TiO_2 \mid S\text{–}TBP} \qquad \mathbf{(3.1)}$$

$$\mathrm{TiO_2 \mid S^{*} + 4\text{–}TBP} \overset{h\nu}{\rightarrow} \mathrm{TiO_2 \mid S\text{–}TBP} \qquad \mathbf{(3.2)}$$

$$\mathrm{TiO_2 \mid S^{+} + 4\text{–}TBP} \rightarrow \mathrm{TiO_2 \mid S\text{–}TBP} \qquad \mathbf{(3.3)}$$

Observation of the additive substituted product mainly in solar cells which had been exposed to light at room temperature [21] directed us to focus on photolysis experiments. The investigations were carried out based on our model system used to calculate photooxidative degradation rate of the **N719** dye (see section 2.2) which besides contains **4-TBP** additive. In this case the possible reactions involving **N719** dye sensitizer can be summarized as in Scheme 3.

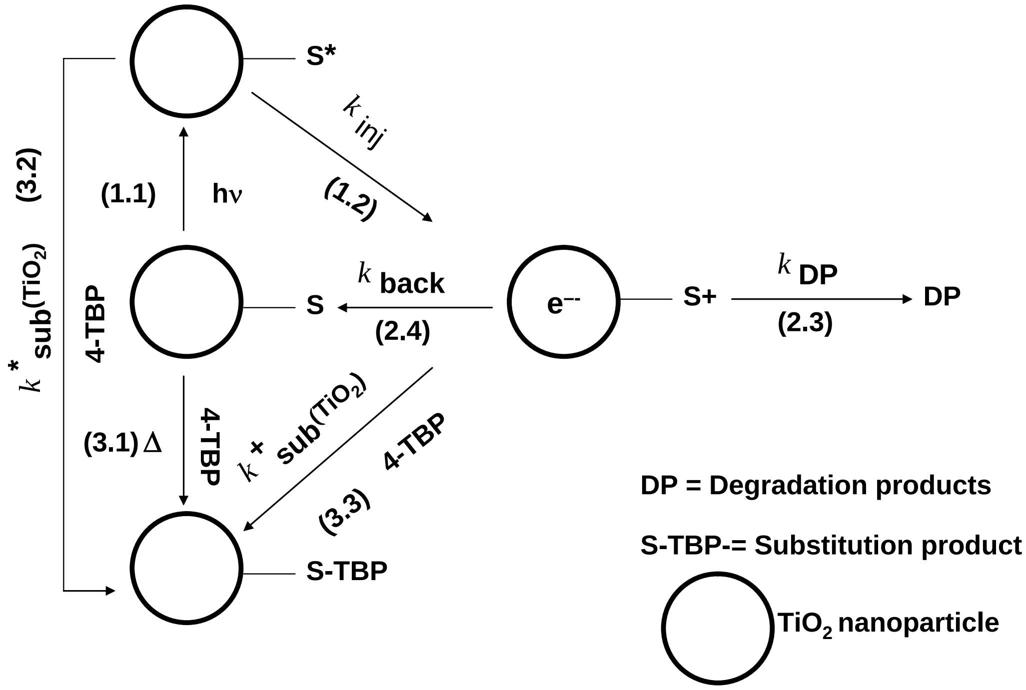

Scheme 3

3.4.3. Quantum yield determination of the photosubstitution reaction of N719 dye with 4-TBP in acetonitrile.

Quantum yield measurements were performed in order to estimate the substitution reaction rates originating from the dye excited and oxidized states. As acetonitrile based solvents have been accepted as the suitable solvents for nc-DSSC [4e], the quantum yield measurements were therefore performed in acetonitrile, unless otherwise stated. These measurements were performed by illuminating acetonitrile solutions of the **N719** dye and **N719** dyed TiO_2 nanoparticles in the presence of **4-TBP** by a 532 nm continues wave laser. Photolysis of the mixture of the **N719** dye and **4-TBP** in homogeneous acetonitrile solutions gave no measurable amount of the substituted product, even after a very long period of illumination (> 24 h). Based on the limit of detection of the substitution product, the quantum yield for this product formation in acetonitrile may be estimated as $\phi^*_{sub} < 10^{-6}$. If we assume that the substitution reaction quantum yield in homogeneous acetonitrile solution is the same as the reaction quantum yield in colloidal **N719** dyed TiO_2 solution, $\phi^*_{sub} \sim \phi^*_{sub}(TiO_2)$, we can then conclude that dye excited state, S* has little or no chance to take part in ligand exchange reaction with **4-TBP**. This is in agreement with the ultrafast electron injection rate [15, 16] from the dye excited state into the TiO_2 conduction band. To have an estimation of the quantum yield of the product formation from the excited state in homogeneouse solution a similar quantum yield measurement as in acetonitrile solution was performed in DMF solution of **N719** dye and **4-TBP** additive. The calculated quantum yield was, $\phi^*_{sub} = 1.6 \times 10^{-5}$ (see Table 3.4). Figure 3.7a and 3.7b shows the LC-UV/Vis and LC-MS chromatograms of a dye extract from illuminated colloidal solution of **N719** dyed TiO_2 nanoparticles in acetonitrile solution containing **4-TBP** (~ 0.7 M). The measured quantum yield of **4-TBP** substituted **N719** dye product (R_t = 9.96), $\phi^+_{sub}(TiO_2) = 7.1\times10^{-5}$ is relatively high from that observed in homogeneous dye / additive solution (see Table 3.4). The quantum yield calculations were made by considering the difference in MS and UV/Vis response factors for the substitution product relative to the **N719** dye molecule. This observation confirms the assumption that in case of the dye molecules attached onto the TiO_2 nanoparticles the substitution reaction occurs from the dye oxidized state rather than dye excited state. The calculated quantum yield for other dye degradation products (peaks eluting at 4.12 and 6.43 minutes and denoted as DP), ϕ_{deg} are also found in Table 3.4.

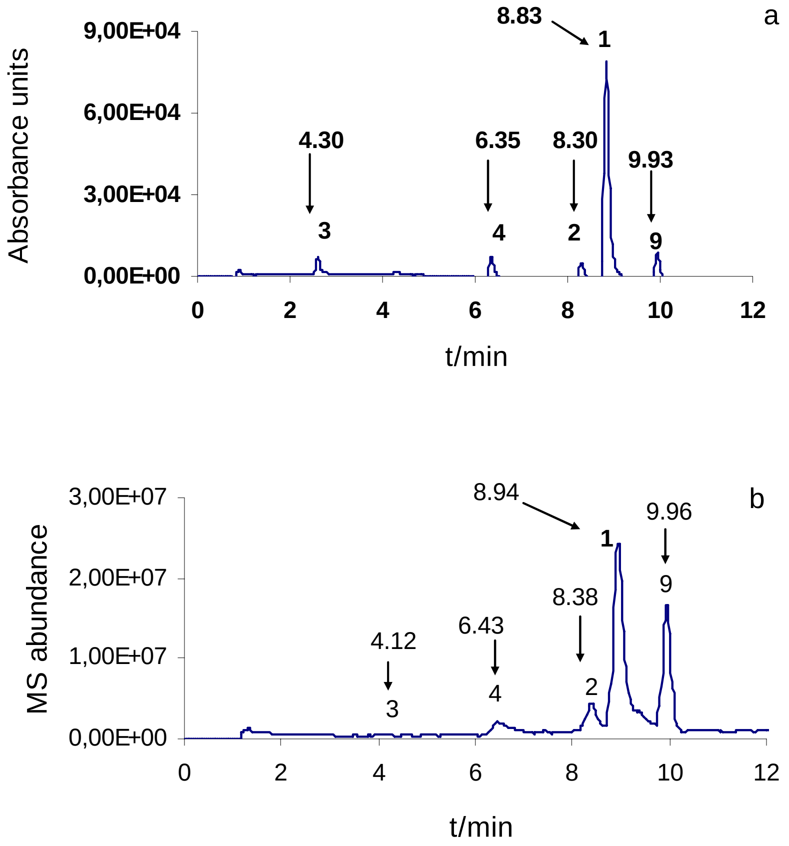

Figure 3.7 (a) LC-UV/Vis, (b) LC-MS chromatograms of the dye extract obtained from illumination of 3 ml deareated colloidal aetonitrile solution containg ~ 12 mg **N719** dyed nanocrystaline TiO_2 particles and **4-TBP (**~ 320 μl, 2.14 mmole).

Table 3.4 Quantum yields of N719 dye substitution reaction with 4-TBP obtained from photolysis of homogeneous N7194 / TBP and heterogeneous N719-TiO_2 / 4-TBP solutions in ACN (^{a} DMF).

Solution illuminated	Side reaction	Quantum yield
Homogeneous N719 + 4 -TBP solution	S* + 4 -TBP → S-TBP	$\phi^*_{sub} < 10^{-6}$ $^a\phi^*_{sub} = 1.6 \times 10^{-5}$
Heterogeneous N719-TiO2 + 4 -TBP solution	TiO2 | S^+ + 4 -TBP → TiO2 | S-TBP	$\phi^+_{sub}(TiO2) = 7.1 \times 10^{-5}$
Heterogeneous N719-TiO2 + 4 -TBP solution	TiO2 | S^+ → TiO2 | DP	$\phi^+_{DP}(TiO2) = 6.2 \times 10^{-5}$

a) Measured in DMF

3.4.4. Photosubstitution reaction rate determination.

The kinetics of the substitution reaction can influence nc-DSSC performance via competing with either electron injection (equation 1.2) or dye regeneration (equation 1.3). Quantum yields obtained from the photolysis experiments, $\phi^{*}_{\mathrm{sub\ and}}$ ϕ^{+}_{sub} $(\mathrm{TiO_2})$ were used to calculate the photosubstitution reaction rates, $k^{*}_{\mathrm{sub}}(\mathrm{TiO_2})$ and $k^{+}_{\mathrm{sub}}(\mathrm{TiO_2})$ initiated from dye excited state and oxidized states respectively. The photosubstitution reaction rate in homogeneous dye/additive solution, k^{*}_{sub} could be calculated from equation 3.4, where τ represents the excited state lifetime of the dye.

$$\Phi^{*}_{\mathrm{sub}} = k^{*}_{\mathrm{sub}} \times [\textbf{4-TBP}] \times \tau \qquad \textbf{(3.4)}$$

Taking $\tau = 10^{-8}$ s the substitution reaction rate from the **N719**–$\mathrm{TiO_2}$ excited state (in DMF), $k^{*}_{\mathrm{sub}}(\mathrm{TiO_2}) = 2.3 \times 10^{3}$ is obtained (see Table 3.5). This is ~ 10^{10}-10^{11} times slower than the ultrafast electron injection rate from dye excited state into the $\mathrm{TiO_2}$ conduction band. Assuming that the photosubstitution reaction rate from dye excited state in heterogeneous solution of **N719**–$\mathrm{TiO_2}$ / **4-TBP** is approximately the same as that in homogeneous dye/additive solution, direct reaction of S^{*} with **4-TBP** can therefore not affect dye stability during solar cell operation. The rate of the substitution reaction initiated from dye oxidized state, $k^{+}_{\mathrm{sub}}(\mathrm{TiO_2})$, can be calculated from equations 3.5 and 3.6. These equations can be derived from the application of the steady state approximation on equations 1.1, 1.2, 2.3, 2.4, 3.3. Φ_{deg} and k_{deg} represent the total quantum yield of the dye photooxidative degradation products and the corresponding degradation rate respectively (see chapter 1). The correction factor, f_{c} accounts for the light intensity decrease during its passage through the cuvette length (see the appendix in paper **I**).

$$k^{+}_{\mathrm{sub}}(\mathrm{TiO_2}) \approx f_{\mathrm{c}} \times \Phi^{+}_{\mathrm{sub}}(\mathrm{TiO_2}) \times k_{\mathrm{back}} / [\text{4-TBP}], \quad f_{\mathrm{c}} = 0.60 \qquad (3.5)$$

$$k^{+}_{\mathrm{sub}}(\mathrm{TiO_2}) = k_{\mathrm{deg}} \times (\Phi^{+}_{\mathrm{sub}}(\mathrm{TiO_2}) / \Phi_{\mathrm{deg}}) / [\text{4-TBP}] \qquad (3.6)$$

As all the experiments were performed in the absence of iodide ions, the back electron transfer reaction of the dye cation with the injected electrons present in $\mathrm{TiO_2}$ conduction band should be considered. The back reaction rate of, $k_{\mathrm{back}} = 176\ \mathrm{S^{-1}}$ was calculated for the laser light intensity of 7.33 $\mathrm{mW/cm^2}$ using equation (2.7) obtained from the PIA measurements (see section 2.4.3). We assumed that k_{back} is independent of the presence of **4–TBP**. Substitution of $\Phi^{+}_{\mathrm{sub}}(\mathrm{TiO_2}) = 7.1 \times 10^{-5}$,

k_{back} = 176 s^{-1}, [**4-TBP**] = 0.7 M^{-1} and f_c = 0.60 into equation 3.5 gives $k^{+}_{\text{sub}(TiO_2)}$ = 0.011 $M^{-1}s^{-1}$ (see Table 3.5). Alternatively the substitution reaction rate of $k^{+}_{\text{sub}(TiO_2)}$ = 0.07 $M^{-1}S^{-1}$ was calculated by substitution of k_{deg} = 0.04 M^{-1} s^{-1}, $\Phi_{\text{deg}} = 6.2\times 10^{-5}$, $\Phi^{+}_{\text{sub}(TiO_2)} = 7.1\times 10^{-5}$ and [**4-TBP**] = 0.7 M^{-1} into equation 3.6 (see Table 3.5). The difference observed for $k^{+}_{\text{sub}(TiO_2)}$ values obtained from equations 3.5 and 3.6 may be explained by the fact that the back electron transfer rate, k_{back} which is obtained in the absence of **4-TBP** is too low. The effect of **4-TBP** on k_{back} has not yet been investigated. However it is known that **4-TBP** affects the conduction band level of the TiO_2 semiconductor. This in turn may also affect the back electron transfer rate. If this suspicion is true, then the $k^{+}_{\text{sub}(TiO_2)}$ = 0.07 $M^{-1}s^{-1}$ obtained from equation 3.6 is the more reliable value.

Table 3.5 Calculated substitution reaction rate, turnover number and lifetime of N719 dye from data of photolysis of homogeneous N719/4-TBP and heterogeneous N719-TiO_2/4–TBP solutions in ACN ([a] DMF).

Side reaction	solvent	Rate constant (k / M^{-1} s^{-1})	Turnover number (N)	Lifetime of dye (years)
S^{*} + 4-TBP → S-4TBP	ACN	$k^{*}_{\text{sub}} < 10^{-2}$		
	DMF	$k^{*}_{\text{sub}} = 2.3\times 10^{3}$	9.8×10^{9}	>1000
TiO_2 | S^{+} + 4–TBP → TiO_2 | S–TBP	ACN	$k^{+}_{\text{sub}}(TiO_2) = 0.07$[a]	4.3×10^{8} ($k_{\text{reg}} = 4.3\times 10^{7}$)[c]	~ 86
			2.1×10^{6} ($k_{\text{reg}} = 2.1\times 10^{5}$)[d]	~ 0.4
TiO_2 | S^{+} → DP	ACN	$k_{\text{deg}} = 0.04$[b]	[b] 5.3×10^{8} ($k_{\text{reg}} = 4.2\times 10^{7}$)[c]	> 20
			[b] 2.6×10^{6} ($k_{\text{reg}} = 2.1\times 10^{5}$)[d]	~ 0.5

(a) Calculations using equation 3.6, (b) see chapter 2, (c) $\boldsymbol{k_{\text{reg}}}$ based on the mean value of three highest values of dye regeneration rates, (d) $\boldsymbol{k_{\text{reg}}}$ based on the mean value of two lowestdye regeneration rates.

3.4.5. Effect of 4-TBP additive on dye stability

The **N719** dye stability during solar cell operation due to the photochemically induced side reactions of **N719** dye with **4-TBP** initiated from the S* or S^+ states (equations 3.2 and 3.3) can be estimated by calculating the dye turnover numbers, N using equations 3.7 and 3.8.

$$N_S^* = k_{inj} / (k^*_{sub} \times [\text{4-TBP}]) \qquad \textbf{(3.7)}$$

$$N_S^+ = k_{reg}\,[I^-] / (k^+_{sub(TiO_2)} \times [\text{4-TBP}]); \quad [\text{4-TBP}] \sim 0.7\ \text{M}, [I^-] = 0.5\ \text{M}) \qquad \textbf{(3.8)}$$

The N numbers of 4.3×10^8 and 2.1×10^6 were calculated using the mean values for the three highest [17] and two lowest [18] reported values for **N3** dye regeneration rates by iodide. The calculated N numbers were then translated to the dye lifetimes of ~ 85 years and ~ 0.4 years respectively through equation (2.11).

$$\text{Lifetime of S} = 20\ \text{years} \times N / (1 \times 10^8) \qquad \textbf{(2.11)}$$

The results of the above calculations are summarized in Table 3.5. As it can be seen the divergence in published dye regeneration rates has led to two remarkably different lifetime estimation of the **N719** dye.

3.4.6. On the mechanism of the substitution reaction of SCN^- ligand by 4-TBP

In order to further verify the suggestion that the **N719** dye substitution reaction with **4-TBP** occurs from the dye oxidized state, an electrochemical oxidation of the **N719** dye was carried out in the presence of **4-TBP** additive. Analysis of the reaction mixture at different time intervals during the progress of the electrolysis process showed no evidence of the formation of the additive substituted product. This observation may be explained by the fact that the homogeneous degradation reaction rate of the dye is much higher than the reaction between the oxidized **N719** dye and **4-TBP** additive. Further examination was carried out by electrooxidation of the uncarboxylated analogue of **N3** dye, $RuL'_2(NCS)_2$ (L′=2,2′ bipyridine) in the presence of **4-TBP** additive. This compound was chosen because of its stable oxidized state which is manifested by its stable blue colour. Electrochemical oxidation of the $RuL'_2(NCS)_2$ was continued until the completion of more than 90% of the reaction. Very fast colour change was observed from blue to the light purple upon addition of the **4-TBP** to the solution. Comparison of the UV/Vis spectrum of the $\mathrm{RuL'_2(NCS)_2}$ and the product formed between $[\mathrm{Ru^{(III)}L'_2(NCS)_2}]$ and **4-TBP** showed a blue shift indicating the ligand substitution reaction.

3.5. Conclusion

3.5.1. Summary

In this work we have shown that solar cell dye sensitizer **N719** can be involved in a substitution reaction with **4-TBP** additive producing the substitution product $[\mathrm{Ru(dcbpyH)_2(NCS)(4\text{-}TBP)}]^-$, $\mathrm{Bu_4N^+}$. Experimental results suggest that this reaction can occur either thermally by heating a solution mixture of the **N719** dye and **4-TBP** additive or photochemically by visible light illumination of the homogeneous dye/additive or heterogeneous **N719**–$\mathrm{TiO_2}$/**4-TBP** solutions. It was also found that the amount of the additive substituted product increases upon adsorption of the dye on $\mathrm{TiO_2}$ nanoparticles. Based on this observation and other findings we concluded that the substitution product is predominantly formed through the dye oxidized stat, S^+. Quantum yield of photosubstitution reaction from S^+ state of the sensitizer dye adsorbed on $\mathrm{TiO_2}$ nanoparicles, $\phi^+_{\mathrm{sub(TiO_2)}} = 7 \times 10^{-5}$ was determined using a simple model system as used for the dye photooxidative degradation rate determination (see section 2.2). Substitution of this value and back electron transfer rate of $k_{\mathrm{back}} = 176\ \mathrm{S}^{-1}$ into equation 3.6 gives $k^+_{\mathrm{sub(TiO_2)}} = 0.07\ \mathrm{M^{-1}\ s^{-1}}$ as the heterogeneous photosubstitution reaction rate between $\mathrm{TiO_2}\,|\,S^+$ and **4-TBP.** Back electron transfer reaction rate was obtained as described in chapter 2 (see section 2.4.3). Another kinetic expression, equation 3.5 gives the $k^+_{\mathrm{sub(TiO_2)}} = 0.011\ \mathrm{M^{-1}\ s^{-1}}$. The discrepancy between the results obtained from two different kinetic expressions was ascribed to the low back electron transfer rate which was determined in the absence of **4-TBP** additive. Influence of this photosubstitution reaction on the **N719** dye lifetime was evaluated via calculating dye turnover number, N assuming that this reaction is the only side reaction involving the **N719** dye sensitizer. Literature values on the **N3** dye regeneration reaction, k_{reg} differs by more than a factor of 100 [17, 18]. Using the mean values of the two lowest and three highest k_{reg} values of 2.1×10^5 and $4.2 \times 10^7\ \mathrm{M^{-1}s^{-1}}$ gives two different N numbers of 2.1×10^6 and 4.3×10^8 respectively. These two N numbers could be translated to dye lifetime of ~ 0.4 years and ~ 86 years respectively.

3.5.2. Relevance to nc-DSSC

In a functioning nc-DSSC any side reaction involving sensitizer dye will result in loss of cell performance. It has generally been accepted that the addition of **4-TBP** as an additive into the nc-DSSC electrolyte solution improves the cell performance by influencing V_{oc} and also sensitizer dye stability [11a]. Although the additive may improve cell performance, it is however apparent from our findings that the dye stability can be affected. In spite of the fact that our investigations were carried out in a model system in place of a real nc-DSSc, the obtained results clearly suggest that the occurrence of the substitution reaction of the solar cell additive **4-TBP** with sensitizer dye **N719** is inevitable under the effect of both heat and visible light illumination and should be considered in view of its outcome for long term stability of the dye and consequently nc-DSSC performance. The two very different turnover numbers for the dye and as a consequence dye lifetime are associated with the large divergence in the literature value of k_{reg}. Again measuring dye regeneration rate, k_{reg} and back electron transfer rate, k_{back} under our experimental conditions will allow us to predict the **N719** dye lifetime more reliably.

References:

1) McEvory, A.J.; Grätzel, M. Sol. Energy Mater. Sol. Cells, **1994,** 32, 221.

2) O'Regan, B.; Grätzel, M. *Nature* **1991**, *353*, 737.

3) (a) Vlachopoulous, N.; Liska, P.; Augustynski, J.; Grätzel, M.; J. Am. Chem. Soc. **1998**, 110, 1216. (b) Desilvestro, J.; Grätzel, M.; Kavan, L.; Moser, J. E.; Augustynski, J., J. Am. Chem. Soc. **1985**, 107, 2988.

4) (a) Hagfeldt, A.; Grätzel, M. *Chem. Rev.* **1995**, *95*, 49 (b) Hagfeldt, A.; Grätzel, M. *Acc. Chem. Res.* **2000**, *33*, 269, (c) Smestad, G.; Bignozzi, C.; Argazzi, A., Sol. Energy Mater. Sol. Cells, **1994**, 32, 259, (d) gratzel, M. ; Nature, **2001**, 414, 338, e) Grätzel, M.; Prog. Photovolt. Res. Appl, **2000,** 8, 171.

5) Kalyanasundaram, K.; Grätzel, M. *Coordination Chem. Rev.* **1998**, *77*, 347.

6) Nazeeruddin, M. K.; Kay, A.; Rodicio,I.; Humphry-Baker, R.; Müller, E.; Liska, P.; Vlachopoulos, N.; Grätzel, M. *J. Am. Chem. Soc.* **1993**, *115*, 6382.

7) Kohle, O.; Grätzel, M.; Meyer, A. F.; Meyer, T. B., *Adv. Mater.* **1997**, *9*, 904.

8) (a) Tachibana, Y.; Nazeeruddin, Md. K.; Grätzel, M.; Klug, D. R.; Durrant, J. R. Chem. Phys. **2002**, 285, 127. (b) Argazzi, R.; Bignozzi, C. A.; Inorg. Chem., **1994**, 33, 5741.

9) (a) Hinsch, A.; Kroon, J. M.; Spath, M.; van Roosmalen, J. A. M.; Bakker, N. J.; Sommeling, P.; van der Burg, N.; Kinderman, R.; Kern, R.; Ferber, J.; Schill, C.; Schubert, M.; Meyer, A.; Meyer, T.; Uhlendorf, I.; Holzbock, J.; Niepmann, R.; 16th European Photovoltaic Solar Energy Conference and Exhibition, Glasgow, **2000,** (b) Rijnberg, E.; Kroon, J. M.; Wienke, J.; Hinsch, A.; van Roosmalen, J. A. M.; Sinke, W. C.; Scholtens, B. J. R.; de Vries, J. G.; de Koster, C. G.; Duchateau, A. L. L.; Maes, I. C. H.; Henderickx, H. J. W. Proc. World Conf. PVSEC. 2nd. **1998**, 47 (c) Hinsch, A.; Kroon, J. M.; Kern, R.; Uhlendorf, I.; Holzbock, J.; Meyer, A.; Ferber, J. Prog. Photovolt: Res. Appl. **2001**, 9, 425.

10) (a) Grunwald, R.; Tributsch, H. *J. Phys. Chem. B.* **1997**, *101*, 2564, (b) Macht, B.; Turrión, M.; Barkschat, A.; Salvador, P.; Ellmer, K.; Tributsch, H. *Sol. Energy Mater. Sol. Cells* **2002**, *73*, 163.

11) (a) Greijer, H. A.; Lindgren, J.; Hagfeldt, A. J. Phys. Chem. B. **2001** , 105 , 6314, (b) Greijer-Agrell, H.; Lindgren, J.; Hagfeldt, A. Solar Energy **2003**, 75, 169 (c) Greijer Agrell, H.; Lindgren, J.; Hagfeldt, A. J. Photochem. and Photobio. A: Chem. **2004**, 164, 23.

12) Cecchet, F.; Gioacchini, A. M.; Marcaccio, M.; Paolucci, F.; Roffia, S.; Alebbi, M.; Bignozzi , C. A. *J. Phys. Chem. B.* **2002**, *106*, 3926.

13) Bond, A. M.; Deacon, G. B.; Howitt, J.; MacFarlane, D. R.; Spiccia, L.; Wolfbauer, G. J. Electrochem. Soc. **1999**, 146, 648.

14) Hansen, G.; Gervang, B.; Lund, T. Inorg. Chem. **2003**, 42, 5545.

15) (a) Kallioinen, J.; Lehtovuori, V.; Myllyperkiö, P.; Korppi-Tommola, J. Chem. Phys. Lett. **2001**, 340, 217. (b) Tachibana, Y.; Haque, S. A.; Mercer, I. P.; Durrant, J. R.; Klug, D. R.; J. Phys. Chem. B. **2000** , 104 , 1198 (c) Ellingson, R. J.; Asbury, J. B.; Ferrere, S.; Ghosh, H. N.; Sprague, J. R.; Lian, T.; Nozik, A. J. J. Phys. Chem. B. **1998** , 102 , 6455.

16) (a) Kuciauskas, D.; Monat, J. E.; Villahermosa, R.; Gray, H. B.; Lewis, N. S.; McCusker, J. K. ; J. Phys. Chem. B. **2002** , 106, 9347. (b), Tachibana, Y.; Moser, J. E.; Gratzel, M.; Klug, D. R.; Durrant, J. R. J. Phys. Chem. **1996** , 100 , 20056, (c) Hannappel, T.; Burfeindt, B.; Storck , W.; Willig, F. J. Phys. Chem. B. **1997** , 101 , 6799. .

17) (a) Haque, S. A.; Tachibana, Y.; Klug, D. R.; Durrant, J. R. J. Phys. Chem. B. **1998,** 102, 1745, (b) Pelet, S.; Moser, J.-E.; Gratzel, M. J. Phys. Chem. B. **2000** , 104 , 1791, (c) Heimer, T. A.; Heilweil, E. J.; Bignozzi, C. A.; Meyer, G. J. J. Phys. Chem. A. **2000** , 104 , 4256.

18) Kuciauskas, D.; Freund, M. S.; Gray, H. B.; Winkler, J. R.; Lewis, N. S. J. Phys Chem.B. **2001**, 105, 392, (b) Montanari, I.; Nelson, J.; Durrant, J. R. J. Phys. Chem. B. **2002** , 106, 12203.

19) (a) Nasr, C.; Hotchandani, S.; Kamat, P. V. J. Phys. Chem. B. **1998**, 102, 4944. (b) Alebbi, M.; Bignozzi, C. A.; Heimer, T. A.; Hasselmann, G. M.; Meyer, G. J. J. Phys. Chem. B. **1998**, 102, 7577, (c) Fitzmaurice, D. J.; Frei, H. Langmuir **1991**, 7, 1129.

20) Amirnasr, M.; Nazeeruddin, Md. K.; Grätzel, M. Thermochim. Acta **2000**, 348, 105.

21) Lund, T. et al. in preparation.

22) The use of Aberchrome 540 in chemical actinometry, School of Chemistry and Applied Chemistry, University of Wales College of Cardiff.

23) Cole, R. B; "Electrospray Ionization Mass spectrometry", John Wiley & Sons, New York, 1997.

24) Boschloo, G.; Hagfeldt, A. Chem. Phys. Lett. **2003**, 370, 381.

25) Moser, J.E.; Noukakis, D.; Bach, U.; Tachibana, Y.; Klug, D. R.; Durrant, J. R.; Humphry-Baker, R.; Gratzewl, M. J. Phys. . Chem. B. **1998**, 102, 3649.

26) Kang, T-S.; Chun, K-H.; Hong, J. S.; Moon, S-H.; Kim, K-J.; J. Electrochem. Soc.; **2000**, 147, 3049.

27) Schlichthrol, G.; Huang, S.Y.; Spragne, J.; frank, A.J. J.Phys.Chem.B **1997,** 101, 8141.

28) Huang,S.Y.; Schlichthrol, G.; Nozik,A.J.; gratzel,M. Frank,A.J. J.Phys.Chem.B **1997,** 101, 2576.

29) Kusama, H.; Arakawa, H.; J. Photochem. & Photobio. A: Chemistry, **2003,** 160, 171.

30) H. Kusama, H. Arakawa, J. Photochem.& Photobio. A: Chemistry, **2004,** 162, 441.

31) Kusama, H.; Konishi, K.; Sugihara, H.; Arakawa, H.; Sol. Energy Mater Sol. Cells,**2003**, 80, 167.

32) Kusama, H.; Arakawa, H.; Sol. Energy Mater. Sol. Cells, **2004**, 81, 87.

33) H. Kusama, H. Arakawa, Sol. Energy Mater. Sol. Cells, **2004,** 82, 457.

34) H. Kusama, H. Arakawa, Sol. Energy Mater. Sol. Cells, **2005,** 85, 333.

35) (a) Grätzel, M.; K. Kalyanasundaram, Curr. Sci. **1994,** 66, 706, (b) Grätzel, M., Platinum Met. Rev. **1994,** 38, 151.

36) (a) Hoggard, P. E.; Porter, G. B.; J. Am. Chem. Soc. **1978,** 100, 1457, (b) Pinnick, D. V.; Durham, B.; Inorg. Chem. **1984**, 23, 1440.

37) Allen, L. R.; Craft, P. P.; Durham, B.; Walsh J., Inorg. Chem. 26 (1987) 53.

38) Nazeeruddin, Md. K.; Zakeeruddin, S. M.; Humphry-Baker, M.; Jirousek, M.; Liska, P.; Vlachopoulos, N.; Shklover, V.; Fischer, Christian-H.; Grätzel, M. Inorg. Chem. **1999,** 38, 6298.

Electrochemical Synthesis of Some Arylsulfones and 2,5-disubstituted Aminobenzoquinones

1. An Introduction to electroorganic synthesis

The history of the electrochemical synthesis of organic compounds is more than a century and half. Even though it was Faraday who first discovered the formation of alkanes via electrooxidative decarboxylation of carboxylate anions, the real beginning of the technique is ascribed to Kolbe, who interpreted the reaction and used it purposefully to synthesis of alkanes. Since that time electroorganic synthesis has achieved remarkable progress from both practical and theoretical view points and there is much information on various kinds of anodic and cathodic reactions in the literature [1-7]. Electrochemistry may be considered as a unique non-thermal procedure to activate the molecules to take part in the reactions. By increasing the electrode potential some reactions having high activation energy can be performed on the electrode surface at room temperature. In another point of view it is an alternative way to the redox chemical reactions. If a chemical reagent acts via electron transfer and not atom transfer, the similarity of the products is expected. However many differences are observed between chemical and electrochemical processes [5b]. Many advantageous have been reported for electrosynthesis of organic compounds in comparison to the normal chemical synthetic methods [3a]. One of the most important characteristics of the electrochemical synthetic methods is the possibility to control the electrode potential selectively to oxidize a specific part of a complex molecule [2a]. This characteristic has made this technique a valuable tool in synthesizing complex molecules. Moreover, performing the reactions at the electrode solution interface which is specific to this technique brings about some preferences in comparison to the normal synthetic methods [3b]. Selective product formation via modifying the electrode surface, solvent–supporting electrolyte system, using specific electrolysis equipment, doing the reactions at room temperature and finally performing the reactions between two substrates having same polarity (Umpoling), the situation which is rarely achieved in normal synthetic organic chemistry are another opportunities offered by these methods [2a,5b]. From the environmental point of view electroorganic reactions are less pollutant than the normal synthetic methods.

2. Fundamental concepts used in electroorganic synthesis [2a]

2.1. Dipole inversion [3b]

The first step in a typical electroorganic reaction is an electron transfer between the substrate and the electrode. During this process and depending on the electrode reaction (oxidation or reduction) the substrate may be converted to a cation radical, an anion radical or a dianion as shown in equation 1. If the substrate is a radical or ionic species the conversion follows the pathway shown in equation 2.

$$S^{2-} \underset{+e^-}{\overset{-e^-}{\rightleftharpoons}} S^{\cdot -} \underset{+e^-}{\overset{-e^-}{\rightleftharpoons}} S \underset{+e^-}{\overset{-e^-}{\rightleftharpoons}} S^{+\cdot} \underset{+e^-}{\overset{-e^-}{\rightleftharpoons}} S^{2-} \qquad (1)$$

$$S^{-} \underset{+e^-}{\overset{-e^-}{\rightleftharpoons}} S^{\cdot} \underset{+e^-}{\overset{-e^-}{\rightleftharpoons}} S^{+} \qquad (2)$$

As is obvious from equations 1 and 2, formation of an active species via electron exchange reaction is accompanied by change of the polarity of the reactant. Therefore, in contrast to the normal organic reactions, in electroorganic synthesis the reaction between two reactants with the same polarity, for example two nucleophiles or two electrophiles are possible.

2.2. Electron transfer reaction (E process) and chemical reaction (C process) [2a]

Electrochemical reactions of organic compounds are often composed of two processes, electron transfer reaction at the electrode surface (E process) which is then followed by a chemical reaction which occurs in the electrolysis medium (C process) (Scheme 1).

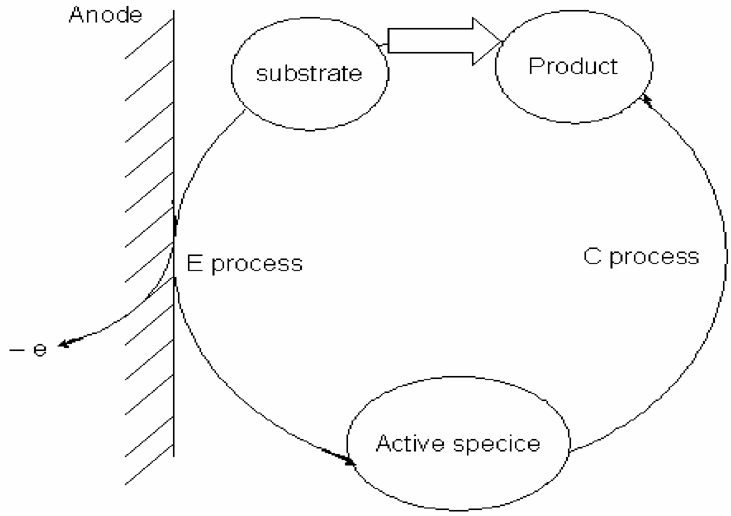

Scheme1 Electroorganic reaction by a combination of electron transfer and chemical processes [2a].

Activity of the intermediate species which is selectively produced through the E process is controlled by the C process. It means that the fate of the electrogenerated intermediates are often under the influence of the solvent-supporting electrolyte system, additives and electrodes through the occurrence of different reactions such as substitution, addition, elimination and so on. Equation 3 is an illustrative example for a substrate S-H which is oxidized via an ECEC mechanism [2a].

$$\text{S-H} \xrightarrow[\text{E}]{-e^-} [\text{S-H}]^{+\cdot} \xrightarrow[\text{C}]{-\text{H}^+} \text{S}^{\cdot} \xrightarrow[\text{E}]{-e^-} \text{S}^{+} \xrightarrow[\text{C}]{+\text{Y}} \text{S-Y} \tag{3}$$

3. Aim of the electrosynthesis project

The presence of an ortho- or para-quinone ring as a reactive centre of electron transfer in the structure of many natural compounds [8a] and biological materials [8b] is an indication of the importance of the quinone containing compounds. Therefore, elucidation of the electrochemical behaviour and also developing suitable procedures for the electrochemical synthesis of compounds containing ortho- or para-quinone rings could be very valuable. Many investigations have been made to propose proper electrochemical routes to produce the compounds containing ortho- or para-quinone rings in their framework [9]. In this direction and in view of the outstanding advantageous of the electrochemical synthetic methods we prompted to investigate the applicability of electrochemical methods to synthesis some arylsulfones and aminobenzoquinones as valuable compounds containing ortho- and para-dihydroxybenzene rings via electrochemical oxidation of pyrocatechols/hydroquinone and hydroquinone in the presence of some sulfinic acids and aliphatic amines respectively.

4. Electrochemical Synthesis of Sulfones

Investigations have shown that sulfones by virtue of their diverse chemistry are valuable synthetic intermediates [10]. They have been used in the total synthesis of biologically active natural compounds [11]. It was claimed that these compounds possess anticancer and carcinogenesis activity [12]. Chemical synthesis of arylsulfones using dihydroxybenzens as starting materials requires addition of an adequate oxidant to the reaction medium in order to transform the starting compounds to the corresponding quinones [13]. This transformation can be achieved easily by anodic oxidation of dihydroxybenzene compounds at a given potential. Therefore, this part of the thesis is aimed at the electrochemical synthesis of some arylsulfones by electrochemical oxidation of pyrocatechol (**1a**), 4-methylpyrocatechol (**1b**) and hydroquinone (1,4-dihydroxybenzene) (**4**) in the presence of *p*-toluenesulfinic acid (**I**) and benzenesulfinic acid (**II**) (Table 1). The optimum reaction conditions were obtained from cyclic voltammetric investigation of these compounds in the presence of the mentioned nucleophiles.

Table 1 molecular Structure of pyrocatechol, 4-methylpyrocatechol, hydroquinone, *p*-toluenesulfinic acid and benzenesulfinic acid.

1a	1b	4	I	II
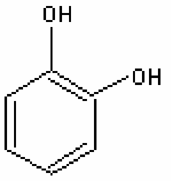	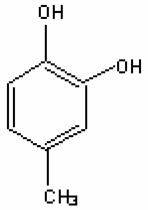	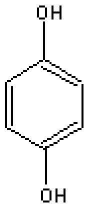	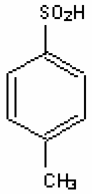	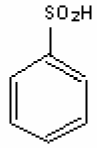

4.1. Electrochemical oxidation of pyrocatechols in the presence and absence of nucleophiles

Electrochemical oxidation of pyrocatechol and some of its derivatives have been extensively investigated in different solvents including methanol [14], ethanol [15] and water [16] and in the presence of different nucleophiles like 4-hydroxy coumarin [17], β-diketones and β-diesters [18]. In general, electrooxidation of pyrocatechol and its derivatives leads to the corresponding *o*-quinones by release of two electrons and two protons. The formed *o*-quinones are quite reactive and can be attacked as Michael acceptors by solvent, supporting electrolytes and additives producing various compounds through the 1,4-addition (Michael) reactions. Depending on the substitute introduced, the new formed pyrocatechol can again be oxidized and lead to the corresponding *o*-quinone. These reactions can be summarized as in Scheme 2.

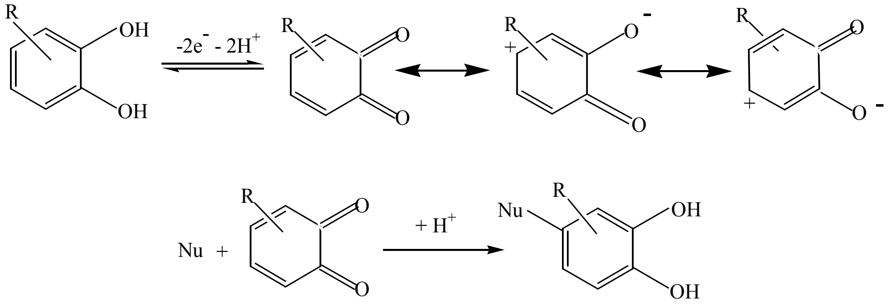

Scheme 2

4.1. 1. Electrochemical oxidation of pyrocatechols in aqueous solutions

Based on the literature, electrooxidation of pyrocatechol and its derivatives in aqueous solutions and in the absence of any stronger nucleophiles than water follows the reaction mechanism ECE as shown in Scheme 3 leading to the hydroxylated hydroquinones [16, 19]. As the oxidation potential of the formed 1,2,4-trihydroxybenzene is smaller than that of the catechol (E2 < E1), the latter compound can be oxidized again. There is also the probability of the polymerization reactions of anion or dianion of the pyrocatechol with the formed *o*-quinones (P) [20]. The resulting compounds can further be oxidized and the reaction continues.

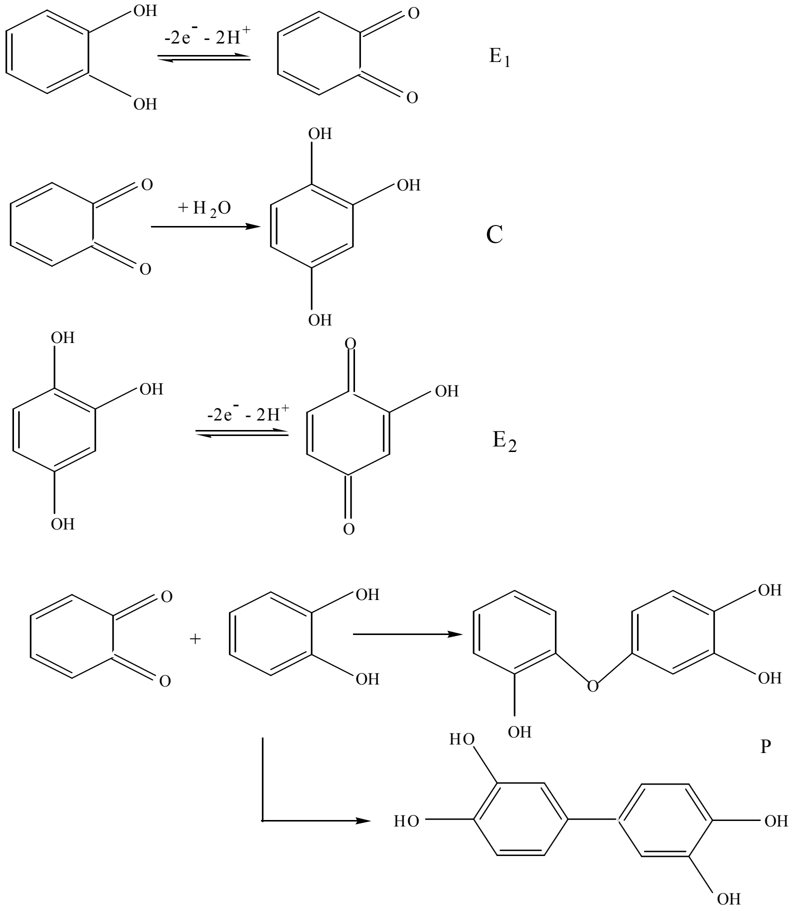

Scheme 3

4.2. Electrochemical synthesis of 4-(4-Toluenesulfonyl)-pyrocatechol (3a) and 5-(4-Toluenesulfonyl)-4-methylpyrocatechol (3b)

In view of the value of cyclic voltammetry in finding optimum reaction conditions and also elucidating the reaction mechanisms, first the cyclic voltammetric behaviour of the reacting pyrocatechols was investigated in the absence and in the presence of the used nucleophiles. Then, based on the obtained results the targeted compounds were electrochemically synthesised and characterised by IR, ^{1}H NMR, MS and elemental analysis after purification.

4.2.1. Electrochemical behaviour of pyrocatechol in an aqueous solution

Figure 1a shows a typical cyclic voltammogram of a pyrocatechol in an aqueous sodium acetate solution as the supporting electrolyte. The voltammogram shows one anodic peak and its cathodic counterpart with the cathodic to anodic peak current ratio of ~ 1 which is representative of a quasi-reversible behaviour for the pyrocatechol/*o*-quionone system obtained in this solvent-supporting electrolyte system [9h, 19c]. Under repetitive cycling (Figure 1b), there is no remarkable evidence of the occurrence of any hydroxylation or other coupling reactions which indicates that these reactions are very slow compared to the time scale of the experiment. On the other hand the cathodic to anodic peak current ratio decreases and peak separation, ΔE_p increases by increasing the catechol concentration [31]. The same effects are also obtained by staying at the switching potential. These results clearly are an indication of polymer formation reactions via coupling of anionic or dianionic catechols with the electrooxidatively formed *o*-quinones. At high amount of catechol concentration the rate of these coupling reactions are comparable to the time window of the cyclic voltammetry experiment.

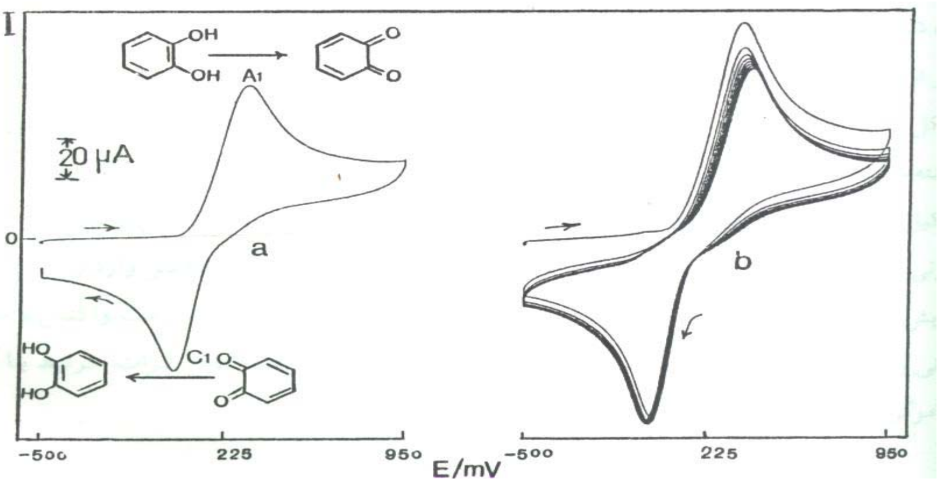

Figure1 Cyclic voltammograms of 1 mM catechol in 0.15 M aqueous sodium acetate solution at glassy carbon electrode. Scan rate: 100 m v s $^{-1}$, (b) Scan rate: 200 m v s $^{-1}$, 10 repetitive potential cycles. T = 25 ± 1°C [31].

4.2.2. Electrochemical behaviour of pyrocatechol/4-methylpyrocatechol in an aqueous solution in the presence of p-toluenesulfinic acid

Figure 2 shows the cyclic voltammograms of 1 mM catechol (**1a**) (curve b), and 1 mM *p*-toluenesulfinic acid (**I**) (curve a) in an aqueous solution containing 0.15 M sodium acetate as the supporting electrolyte. Under these conditions, (**I**) exhibits only an irreversible peak at more positive potentials.

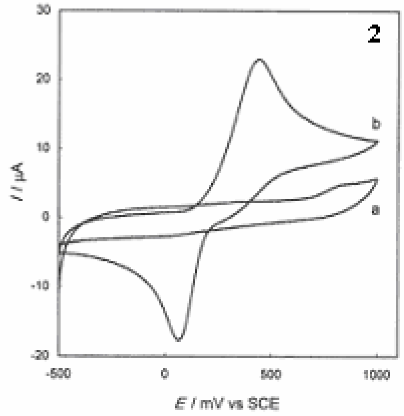

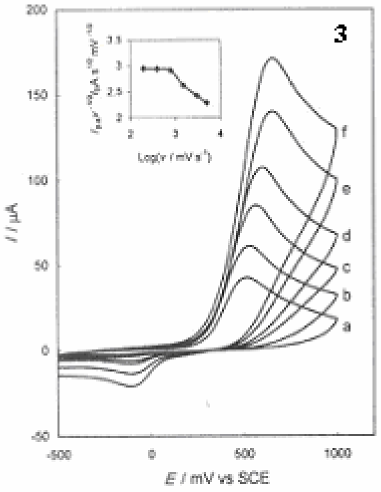

Figure 2 cyclic voltammetry of 1 mM (a) *p*-toluenesulfinic acid and (b) catechol at a glassy carbon electrode in 0.15 M sodium acetate solution. Scan rate: 100 mV s^{-1}.

Figure 3 cyclic voltammograms of a solution containing 1mM catechol and 1 mM *p*-toluenesulfinic acid at different scan rates at a glassy carbon electrode. Supporting electrolyte: 0.15 M sodium acetate. Scan rate: (a) 200, (b) 400, (c) 800, (d) 1500, (e) 3000, (f) 5000 mV s^{-1}. Inset: the variation of current function as a function of scan rate (log v**)**.

In the presence of 1 mM *p*-toluenesulfinic acid, the cathodic peak for the reduction of *o*-benzoquinone is nearly absent at lower scan rates and considerably diminished at higher scan rates (Figure 3, curves a-f). Such behaviour is an indication of an EC mechanism [21]. The product of the EC reaction is electroinactive in the accessible potential range by virtue of its insolubility in the given solvent–supporting electrolyte system. This is manifested as a considerable decrease in the anodic peak height in the second cycle and the lack of any new cathodic or anodic peak. This process also inhibits the performance of the electrode process extensively. Cyclic voltammetry of 4-methylcatechol (**1b**) in the same solvent-supporting electrolyte system as used for catechol also represents its quasi-reversible behaviour. The same behaviour as catechol is observed for electrooxidation of 4-methylcatechol in the presence of *p*-tolouenesulfinic acid indicating that the presence of electron donating methyl group has little effect on the reactivity of the 4-methyl-*o*-benzoquinone formed. The anodic peak current function confirms the EC mechanism.

4.2.3. Reaction mechanism of electrochemical oxidation of 1,2-dihydroxybenzene in the presence of *p*-toluenesulfinic acid (I)

According to the results obtained from the above cyclic voltammetric investigations and the mechanism proposed by Ogata et al. [22], the following reaction pathway as shown in Scheme 4 was proposed for the electrooxidation of (**1a, b**) in the presence of (**I**).

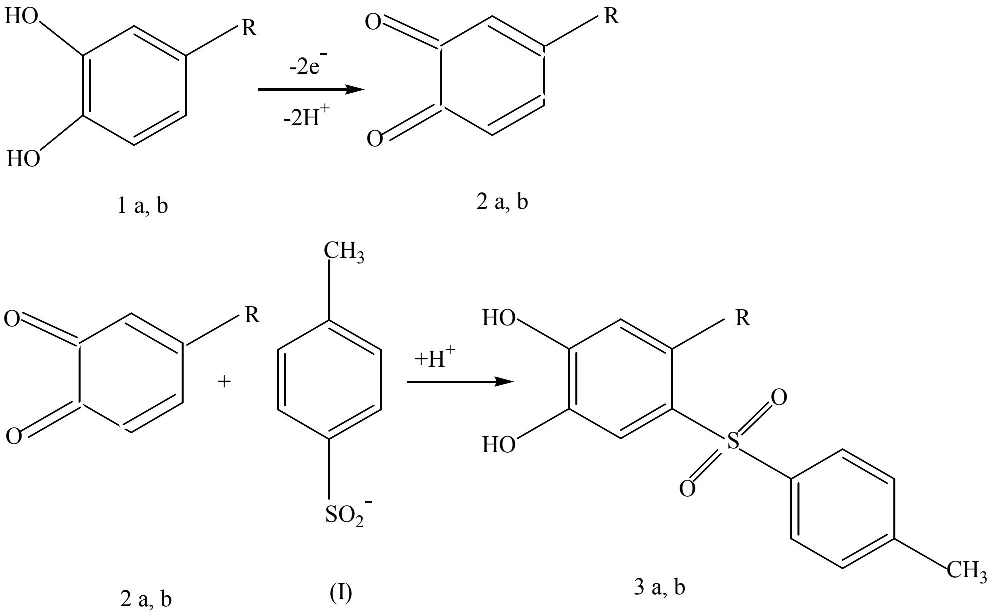

1 a, 2 a, 3 a R = H

1 b, 2 b, 3 b R = CH_3

Scheme 4

4.3. Electrochemical synthesis of 2-(4-Toluenesulfonyl)-hydroquinone (6) and 2-Benzensulfonyl-hydroquinone (7).

4.3.1. Electrochemical behaviour of 1, 4-dihydroxybenzene (4) in the absence and presence of p-toluenesulfinic acid (I) and benzensulfinic acid (II)

Cyclic voltammogram of 1 mM 1, 4-dihydroxybenzene (**4**) in 0.2 M acetic acid solution (Figure 4, curve a) is representative of a quasi-reversible two-electron process corresponding to the transformation of 1,4-dihydroxybenzene to the corresponding *p*-benzoquinone (**5**) and vice versa. The peak current ratio of ~1 during the repetitive cycling of potential is considered as the stability of the *p*-quinone formed in this solvent-supporting electrolyte system. At the same condition anodic oxidation of *p*-toluenesulfinic acid (**I**) occurs irreversibly at more positive potentials (Figure 4, curve b).

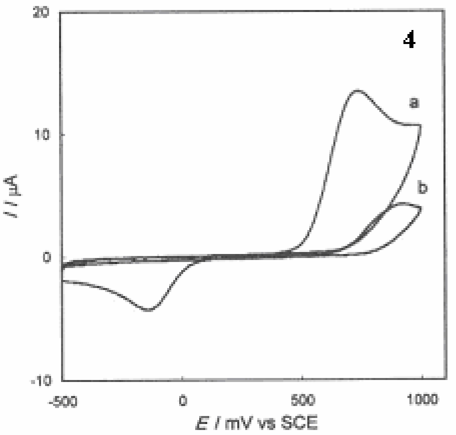

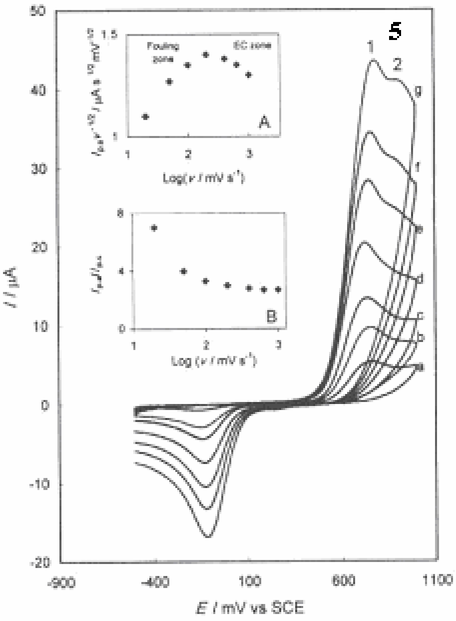

Figure 4 Cyclic voltammetry of: (a) 1 mM 1,4-dihydroxybenzene, (b) 1 mM *p*-toluenesulfinic acid at a glassy carbon electrode in 0.2 M acetic acid solution. Scan rate: 100 mV s^{-1}.

Figure 5 Cyclic voltammograms of 1 mM 1,4-dihydroxy benzene in the presence of 1 mM *p*-toluenesulfinic acid at a glassy carbon electrode in 0.2 M acetic acid solution at scan rates: (a) 20, (b) 50, (c) 100, (d) 200, (e) 400, (f) 600, (g) 1000 mV s $^{-1}$. Inset A: variation of the anodic peak current function ($I_{pa}/v^{1/2}$) as a function of scan rate (log v).

Electrochemical oxidation of 1, 4-dihydroxybenzene (**4**) in the presence of *p*-toluenesulfinic acid (**I**) is followed by a chemical reaction involving *p*-quinone formed and *p*-toluensulfinic acid. This is evident from the disappearance of the cathodic peak for the reduction of *p*-benzoquinone at very low scan rates and an increase of the cathodic peak height proportional to the increasing scan rate (Figure 5). The anodic to cathodic peak current ratio and the anodic peak current function fully confirms the occurrence of this follow up chemical reaction. Observation of a decrease in the anodic peak current height and also positive and negative shift of the anodic and cathodic peak potentials during the multicyclic voltammetry is an indication of the fouling of the electrode surface via deposition of the product formed on the electrode surface. The product insolubility also makes the compound electroinactive in the accessible potential range, showing no new anodic or cathodic peak. As can be seen in Figure 5, increasing the potential scan rate suppress the follow up chemical reaction manifested as splitting of the anodic peak and as a decrease in peak current function, $I_{pa}/v^{1/2}$, (Figure 5, Inset A, EC zone). By increasing the potential scan rate, oxidation of the 1,4-di-hydroxybenzene can occurs via an EC and E mechanism appearing as anodic peaks 1 and 2 respectively. The two fouling zone and EC zone represent these two mechanisms occurring at low and high scan rates respectively. Electrooxidation of (**4**) in the presence of benzenesulfinic acid (**II**) as a nucleophile in water follows the same pathway observed in the presence of *p*-toluenesulfinic acid, which again is in agreement with the occurrence of a following chemical reaction via an EC mechanism and producing an insoluble reaction product which is deposited on the electrode surface.

4.3.2. Reaction Mechanism of electrochemical oxidation of 1,4-dihydroxybenzene in the presence of *p*-toluenesulfinic acid (I) and benzenesulfinic acid (II)

based on the results of cyclic voltammetric experiments and results obtained from the reaction of chemically generated *p*-benzoquinone with benzensulfinic acid [23] the following pathways as in Scheme 5 was proposed for the electrooxidation of 1, 4-dihydroxy benzene (**4**) in the presence of *p*-toluenesulfinic acid (**I**) and benzenesulfinic acid (**II**).

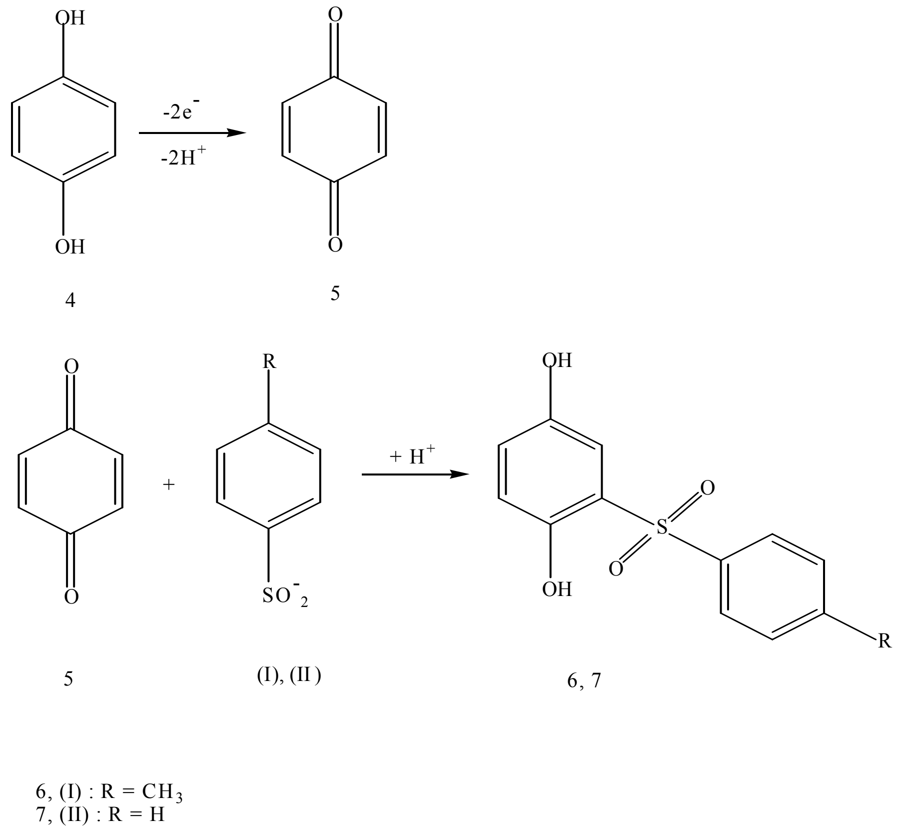

Scheme 5

5. Electrochemical Synthesis of 2, 5-Disubstituted amino Benzoquinones (11a,b,c)

Aminoquinones are desired for testing as possible antimalarial or antitumoral agents [24]. Addition of amines to 1,4-benzoquinones has already been published [25]. Chemical procedures for the preparation of bis-(dialkylamino)-quinones from *p*-benzoquinone suffers from the low yield of the product formed [26]. This is because of the consumption of two-thirds of the quinone as an oxidizing agent to oxidize the intermediate compounds. Considering the outstanding advantageous of the electrochemical methods by using the electrode potential as an oxidizing agent, which eliminates the problems as mentioned, this part of the work was focused on the applicability of the electrochemical methods to synthesize the aminobenzoquinones. To reach this goal the electrochemical behaviour of 1,4-dihydroxybenzene (**4**) was investigated in the absence and in the presence of dimethyamine (**a**), piperidine (**b**) and morpholine **(c)**. Based on the cyclic voltammetric investigations the 2,5-diaminosubstituted benzoquinones (**11a**), (**11b**) and (**11c**) were synthesized respectively.

5.1. Electrochemical investigation of 1,4-dihydroxybenzene in methanol

Figure 6 shows the cyclic voltammogram of 1,4-dihydroxybenzene in methanol containing 0.1 M CH_3COOK as supporting electrolyte and at different scan rates.

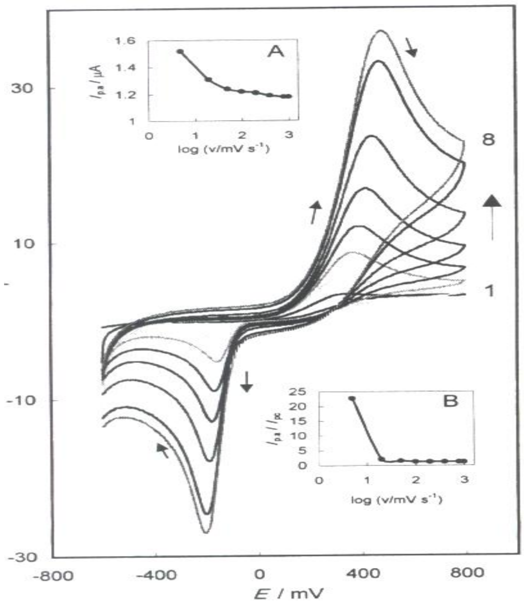

Figure 6 cyclic voltammograms of a 1 mM solution of 1,4-dihydroxybenzene in methanol containing 0.1 M CH_3COOK as supporting electrolyte and at scan rates: (1) 5, (2) 20, (3) 50, (4) 100, (5) 200, (6) 400, (7) 800 and (8) 1000 mV s^{-1}. Inst A: Variation of positive peak current, I_{pa} *vs*. scan rate, log *v*. Inset B: Variation of peak current ratio, I_{pa} / I_{pc} vs. scan rate.

There is one anodic peak at about 0.34 V/Ag/AgCl/KCl (sat.) at very low scan rates without any cathodic counterpart. This peak is assigned to the electrooxidation of the 1,4-dihydroxybenzene. With increasing scan rate the anodic peak height increases parallel with the appearance and increase of a cathodic peak which can be related to the cathodic reduction of positively generated *p*-benzoquinone. The observed behaviour is an indication of a following chemical reaction with the involvement of the electrochemically generated *p*-benzoquinone which is further confirmed by plotting the variation of anodic peak current function and also the anodic to cathodic peak current ratio vs. the scan rate (Inset A and B of Figure 6). The following chemical reaction can be related to the metoxylation of the electrochemically generated *p*-benzoquinone producing methoxyhydroquinones [14]. However, a nearly constant peak current ratio at higher scan rates, particularly during reparative cycling of the potential reveals that any metoxylation or dimerization reaction are too slow to be observed in the time scale of cyclic voltammetry.

5.2. Electrochemical investigation of 1,4-dihydroxybenzene in the presence of some aliphatic amines.

Electrochemical behaviour of 1,4-dihydroxybenzene (**4**) was studied in the presence of dimethylamine (**a**)**,** piperidine (**b**) and morpholine (**c**) as a function of amine concentration and at different scan rates. Figure 7 depicts the cyclic voltammetric behaviour of 1, 4-dihydroxybenzene in the presence of different concentrations of dimethylamine. In general the voltammograms indicate the occurrence of the follow up chemical reactions coupled to the electrooxidation of 1,4-dihydroxybenzene. This is evident from the disappearance of the cathodic counterpart of the anodic oxidation peak of 1,4-dihydroxybenzene (peak c_1) at lower scan rates in parallel with the appearance and increase of other newly formed peaks corresponding to mono-substituted (peak c_2) and di-substituted (peak c_3) amino-hydroquinones which is observed as a function of increasing scan rates . This is also fully confirmed by the plots of anodic peak current function (see inset of the Figure 8). Evolution of the voltammograms for the electrooxdation of (**4**) in the presence of piperidine (**b**) and at the same conditions as in case of dimethylamine is nearly the same. Electrooxidation of 1,4-dihydroxybenzen in the presence of morpholine (**c**) shows nearly the same behaviour as that observed in the presence of dimethylamine and piperidine at different amine concentration and also at different scan rates. However, it is noteworthy that even in the presence of an excess amount of morpholine and at low scan rates, no negative peak showing the formation of the di-morpholino product is discernable, while peak relating to mono-morpholino product is observed.

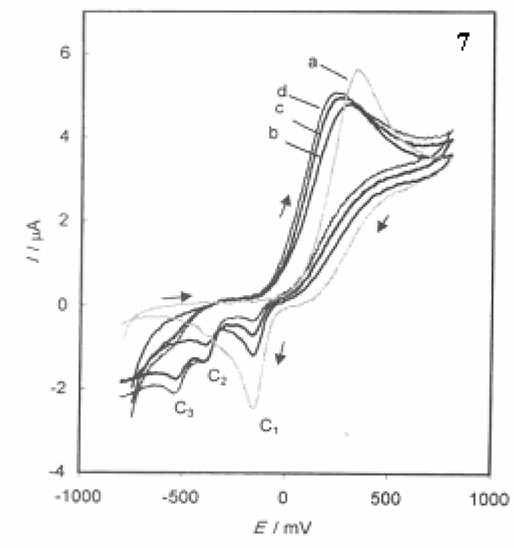

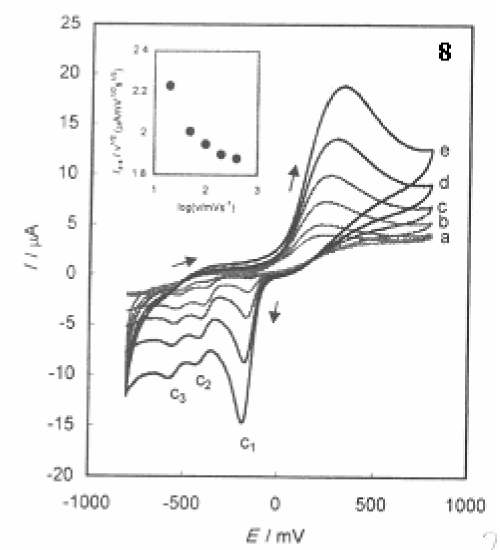

Figure7 Cyclic voltammograms of 1 mM 1,4-dihydroxybenzene (a) in the absence and in the presence of (b) 2 mM (c) 4 mM (d) 6 mM dimethylamine in methanol containing 0.1 M CH_3COOK as supporting electrolyte. Scan rate: 20 mV s^{-1}. Initial potential: -750 mV vs. Ref.

Figure8 Cyclic voltammograms of 1 mM 1, 4- dihydroxybenzene in the presence of 6 mM dimethylamine in methanol containing 0.1 M CH3COOk as supporting electrolyte and at scan rates: (a) 20, (b) 50, (c) 100, (d) 200 and (e) 400 mV s^{-1}. Inset shows the variation of anodic peak current function.

These findings indicate that the second following chemical reaction is so much slower that it can not proceed in the limited time scale of cyclic voltammetry. It also means that morpholine behaves as the weaker nucleophile amongst those employed in this work. However, in the time scale of macro-scale electrolysis this product can be formed, but in a low yield in comparison to the products (**11a**) and (**11b**)**.** Coulometry at controlled potential of the compound (**4**) in the presence of the mentioned amines gave 6 electrons per molecule of (**4**) in each case.

5.3. Reaction Mechanism of electrochemical oxidation of 1,4-dihydroxy benzene in the presence of dimethyl amine, piperidine and morpholine

Based on the results obtained from the above investigations the following ECECE mechanism as in scheme 6 can be proposed for electrooxidation of 1,4-dihydroxybenzene in the presence of above mentioned amines. Based on the proposed mechanism the positively produced 1,4-benzoquinone is attacked by the amine present in solution via a Michael addition reaction. The product of the chemical reaction is more easily oxidizable than the parent compound and consequently is oxidized and takes part in a second Michael addition reaction with the second molecule of the amine. Final oxidation of this di-substituted product leads to di-substituted benzoquinone. The results of spectroscopic analysis of the electrolysis products fully confirm the proposed mechanism.

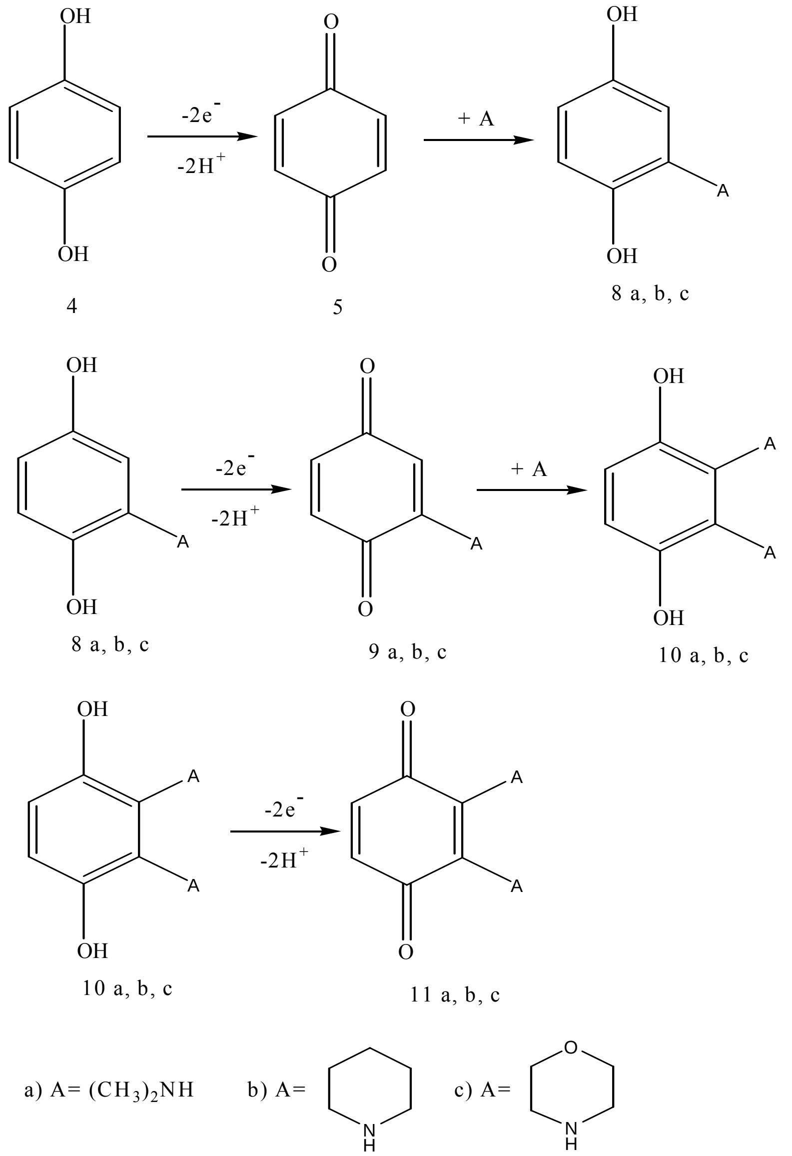

Scheme 6

6. Conclusion

The results of the above investigations have shown that *o*- and *p*-benzoquinones obtained from the oxidation of corresponding hydroquinones can behave as Michael acceptors and easily be attacked in an aqueous solution by nucleufiles like sulfinic acids and amines leading to sulfones and

2,5-diaminosubstituted benzoquinones respectively. A mechanism has deduced for the nucleophilic attack of these nucleophiles to the electrochemically generated *o*- and *p*-benzoquinones using data obtained from cyclic voltammetry and controlled potential coulometry. Electrolysis of the *o*- and *p*-dihydroxybenzenes in the presence of the above mentioned nucleophiles were led to the electrosynthesis of the expected products in good yield and purity.

7. References:

1) (a) H. Lund, O. Hammerich, “Organic Electrochemistry”, Marcel Dekker, New York, **2001**. (b) H. Lund, M. M. Baizer, “Organic Electrochemistry”, 3rd edn. Marcel Dekker, New York, **1991**. (c) M. M. Baizer (Ed.), “Organic Electrochemistry”, Marcel dekker, New York, **1983**.
2) (a) S. Torii, “Novel Trends in Electroorganic Synthesis”, Springer Verlag, Tokyo, Berlin, Heidelberg, New York, **1998**. (b) S. Torii, “Electroorganic Synthesis: Oxidations, methods and applications”, Part I, Kodansha / Verlag Chemie, Tokyo / Weinhem, **1985**.
3) (a) T. Shono, “Electroorganic Synthesis”, Academic Press, New York, **1991**. (b) T. Shono, “Electroorganic chemistry as a new tool in organic synthesis”, Springer, Berlin, Heidelberg New York, **1984**.
4) (a) N. L. Weinberg (Ed.), “Technique of electroorganic Synthesis”, parts I-III, Wiley-Interscience, New York, **1974, 1975, 1982**. (b) S. D. Ross, M. Finkelstein, e. J. Rudd, “anodic Oxidation”, Academic Press, New York, **1975**. (c) R.N. Adams, ”Electrochemistry at solid electrodes”, Marcel Dekker, New York, **1966**.
5) (a) A. J. Fry, “Synthetic Organic Electrochemistry”, Harper & Row, New York, **1972**. (b) R. D. Little et al., “Electrochemistry VI, Electroorganic Synthesis, Bond Formation at Anode and Cathode”, Springer Verlag, Berlin, Heidelberg, New York.
6) (a) J. Volke, F. liska, “Electrochemistry in Organic Synthesis”, Springer-Verlag, Berlin, Heidelberg, **1994.** (b) D. Kyriacou, “Modern Electroorganic Chemistry”, Springer-Verlag, Berlin, Heidelberg, **1994.**
7) M. R. Riffi, F. H. Covitz, “Introduction to Organic Electrochemistry”, Marcel Dekker, New York, **1974**,
8) (a) H. Thomson, “Naturally Occurring Quinones”, Chapman and HALL, London, 3rd. edn. **1987.** (b) K. Hostettmann and I. P. Lea, “Biologically Active Natural Products”, Oxford University Press, Oxford, **1988**.
9) (a) J. Y. Becker and T. A. Coch, Electrochim. Acta, **1993**, 38, 357. (b) S. Torii, H. Tanaka, S. Nakane, Bull. Chem. Soc. Jpn, **1982,** 55, 1673. (c) J. A. Richards, P. E. Whiston, D. H. Evans, J. Electroanal. Chem., **1975**, 63, 311. (d) M. Petek, S. Brockenstein, B. Fernstein, R. N. Adams, J. Electroanal. Chem., **1973**, 42, 397. (e) D. W. Leedy, J. Electroanal. Chem., **1973,** 45, 467. (f) W. E. Britton, C. Steelink, Tetrahedron Lett. **1974**, 33, 2873. (g) B. R. Eggins and R. arwood, J. Electroanal. Chem., **1977**, 83, 347. (h) L. papouchado, G. Pertrie, N. Adams, J. Electroanal. Chem., **1972**, 38, 389.

10) (a) F. Catural, C. Najera, Tetrahedron **1997,** 53, 11449. (b) V. K. Aggarwal, A. Ali, M. P. Coogan, Tetrahedron **1999**, 55, 293.

11) N. E. Prilezhaeva, Russ. Chem. Rev. **2000**, 69,367.

12) (a) P. E. Reddy, R. M. V. Reddy, PCT Int. Appl. Wo9918068, **1999,** (Chem. Abstr. 1999 130: P 281870). (b) J. K. Konopa, M. T. Koniecny, B. J. Horowaska, A. J. Kunikowski, T. Asoa, H. Nishino Y. Yamada, Jpn. Patent JP 9003037, 1997 (Chem. Abstr., 1997, 126: P 185889).

13) H. W. Wanzlik, M. L. Horchler, S. Mohmann, R. Gritzky, H. Heiderpriem, P. Pankow, Angew. Chem. Int. Ed. **1964,** 3, 401.

14) (a) D. Nematollahi, S. M. Golabi, J. Electroanal. Chem., 405, **1996**, 133. (b) D. Nematollahi, S. M. Golabi, J. Electroanal. Chem., 481, **2000**, 208.

15) S. M. Golabi, D. Nematollahi, Bull. Electrochem. 13, **1997**, 156.

16) L. Papouchado, G. Petrie, J. H. Sharp, R. N. Adams, J. Am. Chem. Soc., **1968**; 90, 5620.

17) (a) I. Tabakovic, z Grujic, Z, Bejtovic, J. Heterocyclic Chem, 20, **1983**, 635. (b) Z. Grujic, I. Tabakovic, M. Tokovnik, Tetrahedron Lett., **1976**, 4823. (c) S. M. Golabi, D. Nematollahi, J. Electroanal. Chem., 420, **1997**, 127. (d) S. M. Golabi, D. Nematollahi, J. Electroanal. Chem., 430, **1997**, 141. (e) D. Nematollahi, S. M. Golabi, Bulletin of Electrochemistry, 14, **1998**, 97.

18) (a) M. A. Azzem, M. Zahran, E. Hagagg, Bull. Chem. Soc. Jpn., 67, **1994**, 1390. (b) D. Nematollahi, S. M. Golabi, Iranian J Sci Thechnol, 21, **1997**, 121. (c) D. Nematollahi, M. Rafiee, Green Chem., 7, **2005**, 638.

19) (a) A. Brun, R. Rosset, J. Electroanal. Chem, 49, **1974**, 287. (b) E. Bishop and W. Husein, Analyst, 109, **1984**, 627(229). **(**c) M. D. Ryan, A. Yueh, Wen-Yu Chen, J. Electrochem. Soc., 127, **1980**, 1489.

20) A. W. Sternson, R. Mccreey, B. Feinberg, R. N. Adams, J. Electroanal Chem., 46, **1973**, 313.

21) A. J. Bard, L. R. Faulkner, “Electrochemical Methods, Fundamentals and Applications”, Second edn. Wiley, New York, **2001**, p. 496.

22) (a) Y. Ogata, Y. Sawaki, M. Isono, Tetrahedron, 25, **1969**, 2715. (b) Y. Ogata, Sawaki, M. Isono, Tetrahedron, 26, **1970**, 731.

23) J. M. Bruce, P. L. Williams, J. Chem. Soc., Perkin Trans. I, **1992**, 2877.

24) R. E. Lutz, T. A. Martin, J. F. Codington, T. M. Amaker, R. K. Allison, N. H. Leake, R. J. Rowlett, Jr, J. D. Smith, J. W. Wilson, J. Org. Chem., 14, **1949**, 982.

25) (a) Crosby, A. H.; Lutz, R. E.; J. Am. Chem. Soc. **1956,** 78, 1233. (b) Shurman, J. V.; Becker, E. I. J. Org. Chem. **1953**, 18, 211.

26) R. Bultzly, E. Lorz, JACS, 70, **1948**, 861.

27) A. Mottram Couper, D. Pletcher and F. C. Walsh, Chem. Rev., 90, **1990**, 837.

28) L.F. Fieser and M. A. Peters, Jacs, 53, **1931**, 793

29) G. Sivaramaih and V. R. Krishnan, Indian J. Chem., 4, **1967**, 541.

30) J. Chem. Soc., (London), **1951**, 703.

31) D. Nematollahi, Ph.D. Thesis, Tabriz University, 1996.

Appendices

Appendix I:

Determination of the Light-Induced Degradation Rate of the Solar Cell Sensitizer N719 on TiO_2 Nanocrystaline Particles. .

F. Nour-Mohammadi, N. D. Sau, G. Boschloo, A. Hagfeldt, T. Lund.

J. Phys. Chem. B, 109, 2005, 22413.

J. Phys. Chem. B **2005,** *109,* 22413−22419

Determination of the Light-Induced Degradation Rate of the Solar Cell Sensitizer N719 on TiO_2 Nanocrystalline Particles

Farahnaz Nour-Mohhamadi,† Sau Doan Nguyen,† Gerrit Boschloo,‡,§ Anders Hagfeldt,‡,§ and Torben Lund*,†

Department of Life Sciences and Chemistry, Roskilde University, DK-4000, Denmark, and Department of Physical Chemistry, Uppsala University, Box 579, SE-72123 Uppsala, Sweden

Received: May 26, 2005; In Final Form: September 28, 2005

The oxidative degradation rate, k_{deg}, of the solar cell dye $(Bu_4N^+)_2[Ru(dcbpyH)_2(NCS)_2]^{2-}$, referred to as **N719** or $[RuL_2(NCS)_2]$, was obtained by applying a simple model system. Colloidal solutions of **N719**-dyed TiO_2 particles in acetonitrile were irradiated with 532-nm monochromatic light, and the sum of the quantum yields for the oxidative degradation products $[RuL_2(CN)_2]$, $[RuL_2(NCS)(CN)]$, and $[RuL_2(NCS)(ACN)]$, Φ_{deg}, was obtained at eight different light intensities in the range of 0.1−16.30 mW/cm^2 by LC−UV−MS. The Φ_{deg} values decreased from 3.3×10^{-3} to 2.0×10^{-4} in the applied intensity range. By using the relation $k_{deg} = \Phi_{deg}k_{back}$ and back electron-transfer reaction rates, k_{back}, obtained with photoinduced absorption spectroscopy, it was possible to calculate an average value for the oxidative degradation rate of **N719** dye attached to TiO_2 particles, $k_{deg} = 4.0 \times 10^{-2}$ s^{-1}. The stability of **N719** dye during solar cell operation was discussed based on this number, and on values of the electron-transfer rate between $[Ru^{(III)}L_2(NCS)_2]$ and iodide ion that are available in the literature.

Introduction

Nanocrystalline dye-sensitized titanium dioxide solar cells (nc-DSSC), developed by O'Regan and Grätzel,[1] have attracted significant attention because of their high solar-to-electric power conversion efficiency and low cost compared to those of silicon solar cells.[2−4] The best performing dye-sensitized solar cells reported to date are based on a nanocrystalline TiO_2 film sensitized with ruthenium polypyridyl complexes and having an overall light-to-electricity conversion efficiency $\eta \sim$ 10−12% and excellent stability.[5−7] For practical applications, the long-term stability of the nc-DSSC is very important. The stability of various cell components has been investigated by several research groups and much information has been obtained about the factors and mechanisms that control their stability and efficiency.[6−17] On the basis of accelerated illumination tests, some authors have estimated DSSC lifetimes to be between 5 and 10 years under outdoor illumination conditions,[11,12] while others have claimed that such long cell lifetimes are not achievable.[8,9] The most important single component in the nc-DSSC is the sensitizer dye, and the long-term stability and efficiency of the cells is thus related to its stability. Most investigations have focused on the ruthenium dye $[RuL_2(NCS)_2]$ (L = 4,4′-dicarboxylic acid 2,2′-bipyridyl) and its tetrabutylammonium salt, referred to as **N3** and **N719**, respectively.

The operating principle of a nanocrystalline dye-sensitized titanium dioxide solar cell with **N3** dye as the sensitizer is as shown in eqs 1−3.

$$TiO_2|Ru^{(II)}L_2(NCS)_2 + h\nu \rightarrow TiO_2|Ru^{(II)}L_2(NCS)_2^* \quad (1)$$

$$TiO_2|Ru^{(II)}L_2(NCS)_2^* \rightarrow TiO_2 + e^-|Ru^{(III)}L_2(NCS)_2^+ \quad (2)$$

$$TiO_2|Ru^{(III)}L_2(NCS)_2^+ + I^- \rightarrow TiO_2|Ru^{(II)}L_2(NCS)_2 + I^\bullet \quad (3)$$

The ruthenium dye, which is anchored to the TiO_2 surface by bidentate coordination,[18] is excited by the incoming light (eq 1) and transformed to the oxidized form by an ultrafast electron injection process from the excited state to the conduction band of the TiO_2 semiconductor (eq 2).[19−20] The chemistry of the photoanode is completed by the regeneration of the starting complex by an electron transfer from the mediator I^- (eq 3).[21,22,27b] To achieve 20 years of solar cell operation under outdoor illumination conditions, the ruthenium dye sensitizer should be able to sustain more than 10^8 cell cycles and the rate of possible side reactions should be as low as possible. The sensitizer dye may in principle degrade from its ground state, S, excited state, S*, or oxidized state, S^+. The *cis*-$[Ru^{(II)}L_2(NCS)_2]$ complex has been shown to be thermally very stable[23] and the injection rate of eq 2 so fast ($k_{inj} > 1 \times 10^{13}$ s^{-1}) that side reactions initiated from the exited state can be ruled out. Therefore, the most likely degradation pathway occurs from the Ru(III) oxidized state. The instability of $[Ru^{(III)}L_2(NCS)_2]^+$ is apparent from the irreversible voltammograms of the complex[10,24] and from the fact that electrochemical oxidation of $[RuL_2(NCS)_2]$ in acetonitrile does not produce the blue color (λ = 740 nm) characteristic of a $Ru^{(III)}$ complex.[25] The stability of the dye during solar cell operation is therefore dependent on the rate of regeneration of the $Ru^{(II)}$ dye (eq 3) compared with the rate of degradation of the $Ru^{(III)}$ complex (eq 4).

---

* Address correspondence to this author. Fax: 45-46743011. E-mail: tlund@ruc.dk.

† Roskilde University.

‡ Uppsala University.

§ Current address: Department of Chemistry, Royal Institute of Technology, SE-10044 Stockholm, Sweden.

10.1021/jp052792v CCC: $30.25

$$\mathrm{TiO_2|Ru^{(III)}L_2(NCS)_2^+} \xrightarrow{k_{\mathrm{deg}}} \text{degradation products} \qquad (4)$$

$$\mathrm{TiO_2} + \mathrm{e^-|Ru^{(III)}L_2(NCS)_2^+} \xrightarrow{k_{\mathrm{back}}} \mathrm{TiO_2|Ru^{(II)}L_2(NCS)_2} \qquad (5)$$

Knowledge of the oxidation products of $[\mathrm{Ru^{(II)}L_2(NCS)_2}]$ and the oxidative degradation rate, k_{deg}, are essential parameters for the prediction of the long-term stability of the dye under solar cell operation. Though several reports have focused on the degradation products,[10,26] to our knowledge no one has previously attempted to obtain the degradation rate, k_{deg}.

The aim of this research is to obtain the degradation rate, k_{deg}, of $[\mathrm{Ru^{(III)}L_2(NCS)_2}]^+$ attached directly onto the nanocrystalline $\mathrm{TiO_2}$ particles. The complicated solar cell system is replaced by a simpler model system based on a stirred suspension of **N719**-dyed $\mathrm{TiO_2}$ particles in acetonitrile irradiated by monochromatic light ($\lambda = 532$ nm). As iodide is absent in this experiment, oxidized dye molecules will recombine with electrons injected into the $\mathrm{TiO_2}$ particles (eq 5) or take part in a degradation reaction, as illustrated in Figure 1.

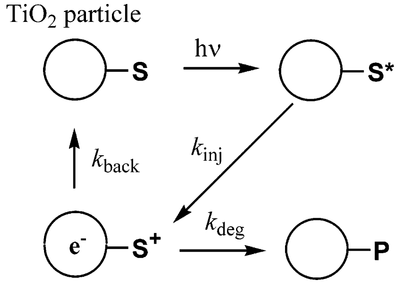

Figure 1. Schematic representation of the model system used in the photolysis experiments.

The total amount of degradation products, $\sum n_{\mathrm{deg}}$, generated during the illumination of dyed $\mathrm{TiO_2}$ particles is quantitatively monitored by high-pressure liquid chromatography (HPLC) coupled to a UV−vis detector and a mass spectrometer (MS). The quantum yield of all degradation products, Φ_{deg}, may be calculated according to eq 6, where N_{a} is the number of absorbed photons. The quantum yield depends on the competition between the degradation reaction (eq 4) and back electron-transfer reaction (eq 5) and may be related to the rate of these reactions through eq 7.

$$\Phi_{\mathrm{deg}} = \sum n_{\mathrm{deg}}/N_{\mathrm{a}} \qquad (6)$$

$$\Phi_{\mathrm{deg}} = \frac{k_{\mathrm{deg}}}{k_{\mathrm{deg}} + k_{back}} \sim k_{\mathrm{deg}}/k_{\mathrm{back}}; \qquad k_{\mathrm{back}} \gg k_{\mathrm{deg}} \qquad (7)$$

The rate of the back electron-transfer reaction has been measured by laser flash photolysis and photoinduced absorption (PIA), and values in the range of 10^3 to 10^6 $\mathrm{s^{-1}}$ have been reported.[27−29] Considering the light intensity dependence of the back electron-transfer reaction rate,[29] in order to use this rate as a basis for calculating the rate of the degradation reaction, it is necessary to obtain k_{back} under the same light intensity and experimental conditions as used in the photolysis experiments. In this work we obtained back electron-transfer reaction rates at different light intensities by means of PIA measurements.

Experimental Section

Materials. The bistetrabutylammonium salt of the complex *cis*-bis(isothiocyanato)bis(2,2′-bipyridyl-4,4′-dicarboxylato)ruthenium(II), with the trade name Ruthenium 535-bis TBA, and referred to as **N719**, was obtained from Solaronix. HPLC-grade acetonitrile (Merck) was dried by passing the solvent through a column of activated neutral alumina particles. The actinometer Aberchrome 540, (*E*)-α-(2,5-dimethyl-3-furylethylidene)isopropylidene succinic anhydride, was purchased from Aberchromics Ltd., Wales.

The dye degradation experiments were performed by two different methods described below.

Method 1: *Preparation of Dye-Covered Nanocrystalline TiO₂ Films*. A colloidal $\mathrm{TiO_2}$ suspension was prepared by mixing Degussa P25 titanium dioxide (∼2 g) with ∼20 mL of absolute ethanol. Small glass balls ($d = 5$ mm) were added and the mixture was ground by shaking overnight. Nanocrystalline $\mathrm{TiO_2}$ films were prepared by spraying the colloidal $\mathrm{TiO_2}$ suspension onto nonconductive glass plates (length 7 cm, width 1.5 cm), using an airbrush (Olympos Airbrush model HP-100C with nozzle diameter of 0.3 mm), followed by heating the plates under an air atmosphere for 30 min at 450 °C. The titanium dioxide coverage of the plates was between 16 and 25 mg (1.52−2.38 mg/cm^2). Dye coating was made by soaking the $\mathrm{TiO_2}$ glass plates in **N719** dye solution in absolute ethanol (6×10^{-5} M) overnight and at room temperature. All the dyed plates were stored in absolute ethanol in the dark.

Photolysis Experiments by Method I. The degradation experiments were carried out in a UV cuvette prepared as described below. The dyed titanium dioxide particles prepared as thin films were removed from the glass plates as small aggregates and transferred into a cuvette ($1 \times 1 \times 3$ cm^3) capped with an airtight membrane. The cuvette was filled with acetonitrile (3 mL) and then the oxygen was removed by argon gas (99.995%, $\mathrm{O_2} < 10$ ppm) bubbling for about 20 min. During illumination the colloidal solution was magnetically stirred. In all photolysis experiments the cuvettes were placed in the black box of the photon-counting device. The active area of the cuvette exposed to the light was approximately 2 cm^2.

Dye Extraction Procedure. At the end of every photolysis experiment the dyed titanium dioxide particles were transferred into a test tube. After centrifugation, most of the solvent was removed with use of a Pasteur pipet. The dye on the remaining $\mathrm{TiO_2}$ particles was extracted by treatment with a mixture of aqueous NaOH (0.1 M, 2 mL) and absolute ethanol (1 mL). After centrifugation, the red solution containing the dye and its degradation products was decanted and, after acidifying with 15 μL of concentrated formic acid, was analyzed with LC−UV−MS. Control experiments showed that **N719** and its photodegradation products were stable in 0.10 M NaOH at room temperature.

Preparation of the Standard Solutions. Standard solutions of **N719** were prepared in absolute ethanol (1×10^{-5} to 1×10^{-4} M) and the LC−MS chromatograms obtained. An external standard curve was constructed and used to quantify the amount of degradation products in the photolysis experiments. The quantitative analysis of photolysis mixtures was based on the approximation that **N719** dye and its degradation products would all have the same sensitivity in the MS detector.

Method II: *Preparation of Dye-Covered TiO₂ Particles.* Degussa P25 $\mathrm{TiO_2}$ (600 mg) was magnetically stirred in 250 mL of an **N719** dye solution ([**N719**] = 6.06×10^{-5} mol/L) in absolute ethanol. After 24 h all of the dye molecules in the solution were completely adsorbed onto the surface of the titanium dioxide particles. Centrifuging an aliquot of this mixture resulted in a colorless liquid above the pink solid (dyed $\mathrm{TiO_2}$), confirming the complete adsorption of the dye onto the $\mathrm{TiO_2}$ particles. After removing the colorless liquid by rotary evaporation, the red-colored nanocrystalline TiO_2 particles were transferred into a brown bottle that was wrapped in aluminum foil and stored in the dark.

Preparation of the Dyed TiO_2 Colloidal Solution. The dyed nanocrystalline TiO_2 powder (12 mg of dye with 0.304 μmol of **N719**) was placed into a cuvette containing 3 mL of dry acetonitrile. The mixture was degassed with a flow of argon gas for 20 min. After degassing, a "homogeneous" stable dyed TiO_2 colloidal solution was obtained by sonification of the cuvette for 1 h.

Photolysis Experiments. The cuvette containing the dyed colloidal TiO_2 solution was placed into the black box of a photon-counting device. The sample was irradiated with continuous laser light (532 nm) of known intensity (0.1−16 mW/cm^2) for the duration needed to obtain the predefined light doses. Six photolysis experiments with light doses of $(1-6) \times 10^5$ counting numbers (1×10^5 counting numbers $= 3.18 \times 10^{-5}$ mol of photons) were performed at each laser light intensity. After irradiation, the dyed TiO_2 colloidal solution was transferred into a round-bottom flask and the acetonitrile was removed by means of rotary evaporation.

The degradation products from the photolysis experiments that were still bound to the TiO_2 particles were extracted by means of treatment with a solution comprised of 2 mL of 0.1 M NaOH and 1 mL of ethanol. The red extract in the flask was transferred into a clean test tube and then centrifuged. After the white TiO_2 particles were removed, the red liquid was transferred to another test tube and 15 μL of formic acid was added. The acidified solution was then transferred into an HPLC vial and analyzed with LC−UV.

Instrumentation. *HPLC−UV/Vis−MS Equipment.* The LC−MS instrument was equipped with a UV diode array detector with a 5-cm flow cell in series with an MS detector. The HPLC instrument was a TSP Spectra System equipped with an AS3000 auto sampler, a P4000 gradient pump, a vacuum degasser, and a UV 6000 LP diode array detector. Separation was performed with a linear gradient program starting with 100% A (5% acetonitrile + 94% water + 1% formic acid) ending after 21.6 min with 100% B (acetonitrile). Elution with 100% B continued for a further 10 min, followed by a return to 100% A after a further 5 min. The flow rate was 0.2 mL/min. The analytical column was a 50-mm Xterra MS RP C18 column from Waters with an i.d. of 2.1 mm. The mass detector was an LCQ-Deca ion-trap instrument from ThermoFinnigan equipped with an electrospray ionization interface (ESI) run in positive mode. A positive potential (+4.5 kV) was applied to the silica needle, while the other details of the setup were as follows: discharge current 19−20 mA, capillary voltage 23 V, capillary temperature 350 °C, tube lens offset 5 V, and sheath gas (N_2) and auxiliary gas (N_2) 78 and 45 arbitrary units, respectively. UV−vis absorptions were recorded between 400 and 600 nm. The ion trap was run in the data-dependent MS scan mode. The scan event was obtained in the 400−800 *m*/*z* interval. The parent mass list was *m*/*z* 643.1, 648.1, 674.9, and 706, while the reject mass list was *m*/*z* 547, 569, 585, 591, 613, 629, 636, and 592. The isolation *m*/*z* width was 6, the normalized collision energy was 35, the activation time was 30 ms, and minimum signal required 10^5 counts. Xcalibur 1.2 LCQ software controlled the chromatographic and mass spectrometric analysis.

Light Sources. Three light sources were used. Low-intensity light was generated by an Oriel, 300-W tungsten−halogen lamp in combination with a 435-nm cutoff filter and a 525 ± 5-nm interference filter. The light intensity of this source was 0.2 mW. Approximately two-thirds of the cuvette (2 cm^2) was illuminated, corresponding to an intensity of 0.1 mW/cm^2. A second light source was a slide projector equipped with a 250-W halogen lamp in combination with an IR water filter and a UV−vis 525 ± 5-nm interference filter. The intensity of this source was 1.07 mW or ∼0.54 mW/cm^2. The third light source was a 532-nm laser with a light intensity of 16.3 mW/cm^2. The intensity of the laser light could be reduced by using neutral density filters (Oriel).

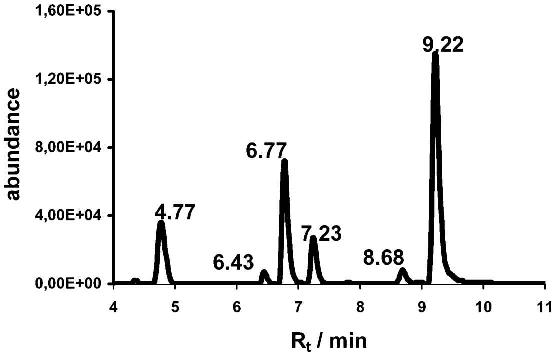

Figure 2. LC−UV chromatogram of a dye extract obtained after laser light illumination of a colloidal solution of **N719**-dyed TiO_2 particles in deoxygenated acetonitrile, prepared using method II: laser light intensity, 2.86 W/cm^2; excitation wavelength, 532 nm; mol of absorbed photons, 1.91×10^{-4} mol.

Photon-Counting Device. A homemade photon-counting device was used in the photolysis experiments. The device consisted of a black box, a cuvette holder, and a light-splitting system in which 90% of the light was directed toward the sample and 10% to a photodiode. The electrical response of the diode was monitored and integrated electronically.

Actinometry Experiment. Aberchrome 540 in toluene (5 mM) was used as a chemical actinometer in the visible region to calibrate the photon-counting device. The Abercrome solution (3 mL) was first irradiated with UV light until a red-colored solution of absorbance ∼2 was obtained. Then, the red solution was exposed to the visible light source, i.e., the 532-nm laser light, and the absorbance decrease of the solution was obtained as a function of the counting number obtained from the photon-counting device.

Photoinduced Absorption Spectroscopy. The photoinduced absorption (PIA) apparatus has been described elsewhere.[29] Briefly, a 1.0-mm path-length cuvette containing the dyed TiO_2 sample was illuminated with chopped light from a 532-nm He−Ne continuous wave laser. Resulting absorption changes at 800 nm were probed with light from a filtered tungsten−halogen lamp ($\lambda > 715$ nm), using a monochromator, a Si-detector, and a lock-in amplifier set at the chopping frequency (range 400 to 4 Hz). Neutral density filters were used to attenuate the laser beam. Time constants were obtained with a nonlinear, least-squares fit of the frequency domain data.

Results and Discussion

Identification of the Dye Degradation Products. Figure 2 shows the LC−UV chromatogram of a dye extract obtained from a representative laser irradiation experiment performed on a pink colloidal solution of **N719**-dyed TiO_2 particles prepared following method II. In all the photolysis experiments that involved applying different light sources and intensities, six peaks were observed in the chromatograms. The degradation products observed in the photolysis experiments were similar to those observed as resulting from the electrochemical oxidation of **N719** in acetonitrile and dimethylformamide.[26] The UV and MS spectra of these oxidative degradation products have recently been described,[26] and a list of λ_{max} and important *m*/*z* values of

TABLE 1: Data of Retention Times, Absorption Maxima, and Characteristic *m/z* Values of N719 and Its Degradation Products Obtained from Degradation Experiments Performed on N719-Dyed TiO_2 Nanocrystalline Particles in Acetonitrile

complex	formula[a]	r_t/min	characteristic *m/z* values	λ_{max}
1	$[RuL_2(NCS)_2]$	9.22	706, 648	525
2	$[RuL_2(NCS)(SCN)]$	8.70	706, 648	521
3	$[RuL_2(CN)_2]$	4.78	643	470
4	$[RuL_2(NCS)(CN)]$	6.77	675,648	497
5	$[RuL_2(NCS)(ACN)]$	7.25	689, 648	481
6	$[RuL_2(NCS)(H_2O)]$	6.45	667, 648	512

[a] L = 4,4′-dicarboxylic acid 2,2′-bipyridyl. ACN = CH_3CN.

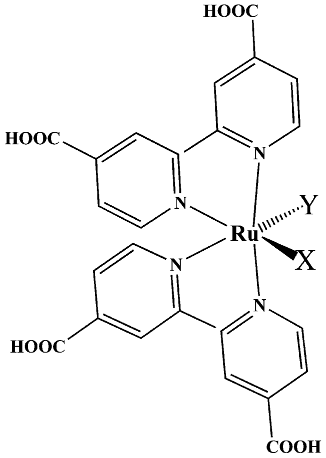

	X	Y
1	**NCS**	**NCS**
2	**SCN**	**NCS**
3	**CN**	**CN**
4	**NCS**	**CN**
5	**NCS**	**CH_3CN**
6	**NCS**	**H_2O**

Figure 3. Structure of **1**−**6**.

the products is shown in Table 1**.** The structures of the starting dye molecule and its degradation products are shown in Figure 3.

Compound **1** is the main component of the acidified dye extracts. This product is the fully protonated form of the unreacted starting **N719** complex. Compound **2** is the S/N thiocyanate isomer of **1**. A sample of the **N719** starting material contains approximately 5% of the complex, with one S- and one N-bound thiocyanate ligand. Compounds **3**−**5** are the main degradation products. Compound **4** is characterized by its mass spectrum, which shows ruthenium isotope patterns around the ions, *m/z* 675, $[RuL_2(NCS)(CN) + H]^+$, and *m/z* 648, $[RuL_2(NCS)]^+$. The latter ion is formed by the elimination of an $NCS^{\bullet -}$ radical from the molecular ion. Product **4** is produced through an internal oxidation mechanism in the complex, initiated by the electron-transfer process between the NCS^- ligand and the $Ru^{(III)}$ center.[7] Complex **3** is characterized by its yellow color ($\lambda_{max} = 470$ nm) and a ruthenium isotope pattern around the ion, *m/z* 643, which may be assigned to the ion $[RuL_2(CN)_2 + H]^+$. Interestingly, compound **3** was also observed in the electrochemical oxidation of **N719** in dimethylformamide, but not from the electrolysis of **N719** in acetonitrile.[26] Product **3** is likely produced by a further photooxidation of **4**. Compound **5** is characterized by its *m/z* value of 689, corresponding to the $[RuL_2(NCS)(ACN)]^+$ ion. The complex was also observed in the electrolysis of **N719** in acetonitrile, and is believed to be formed via a solvent-dependent mechanism.[26] The mass spectrum of the peak at $R_t = 6.45$ min (**6**) showed a low-intensity ruthenium isotope pattern around the *m/z* value of 667, which may be assigned to the $[RuL_2(NCS)(H_2O) + H]^+$ ion. Compound **6** was observed as an impurity (<1%) in the starting material**.** The concentration of **6** was constant during the photolysis experiments, and the presence of **6** was therefore explained as an **N719** impurity and not a product produced during the photolysis.

Quantum Yield Determination. Table 2 shows the results of six laser photolysis experiments with a laser light intensity of 9.58 mW/cm^2 along with the moles of absorbed photons in each experiment. Degradation products **3**−**5** were quantified from the LC−UV chromatograms by dividing the area of each product peak by the total peak areas of compounds **1**−**5** and multiplying this ratio by n_{dye} , the starting number of moles of **N719** dye in the cuvette. In these calculations it is assumed that compounds **1**−**5** all have the same extinction coefficient at their respective visible absorption maxima. Parts a and b of Figure 4 show the evolution of degradation products **3**, **4**, and **5** and the total amount of these three products as a function of the moles of absorbed photons. The results presented in Figure 4a,b were obtained by using method II with a laser light intensity of 9.58 mW/cm^2 and by using method I with a light intensity of 0.10 mW/cm^2, respectively. As observed from Figure 4a,b, reasonably straight lines are obtained for all three products. The intercepts with the *y*-axis of **3** and **5** are nearly zero, as expected, whereas an intercept is observed for **4**, indicating an initial degradation of **N719** to **4** before the start of photolysis. The origin of this initial degradation is unknown; however, impurity defects in the Degussa P25 nanoparticles may be responsible for the observed oxidative thermal degradation. The slopes of the lines representing the sum of the three oxidative degradation products, **3**−**5**, in Figure 4a,b are equal to the total quantum yield of oxidative degradation products at the respective intensities. The quantum yields of degradation at 9.58 and 0.10 mW/cm^2 were $(3.1 \pm 0.4) \times 10^{-4}$ and $(3.2 \pm 0.2) \times 10^{-3}$, respectively. The lower the light intensity, the higher the value of Φ_{deg}.

Determination of k_{back}. Photoinduced absorption measurements[29] were performed on a colloidal solution of **N719**-dyed TiO_2 particles prepared by using method I and laser light intensities in the range of 0.5 to 5 mW/cm^2. Magnetic stirring of the solution was eliminated by using ultrasound waves to make a stable colloidal solution during the experiment. The back electron-transfer time, τ_{back}, was extracted from the frequency dependence of the PIA signals. Figure 5 shows τ_{back} as a function of the incident light intensity, *I*. τ_{back} decreases with the increasing intensity of the excitation laser light. The back electron-transfer rate appears to follow a power-law dependence on the light intensity ($\lambda = 532$ nm); see eq 8.

$$k_{back} = \frac{1}{\tau_{back}} = \frac{1}{0.0127 I^{-0.4043}} = 78.74 I^{0.4043} \qquad (8)$$

Determination of k_{deg}. The oxidative degradation rate of the dye, k_{deg}, may be calculated from the back electron-transfer reaction rate, k_{back}, and the total quantum yield of all degradation products, according to eq 7. A complication arises, however, due to the change in the light intensity throughout the length of the light pathway inside the cuvette. This results from the light absorption by the dyed TiO_2 particles and causes the light intensity to decrease continuously throughout the length of the cuvette. As discussed in the previous paragraph, k_{back} depends on the excitation light intensity (see eq 8), and therefore will decrease from a high value, $k_{back}(I_0)$, at the front of the cuvette ($l = 0$ cm), to a value near zero at $l = 1$ cm. The uncorrected degradation rate constant, k^u_{deg}, may be calculated from eq 9. This rate is too fast compared to the actual degradation rate, because $k_{back}(I_0)$ is too high compared to a weighted average of k_{back}. The correction factor, f_c, defined as in eq 10, is derived from the mathematical

TABLE 2: Data from Photolysis Experiments with Laser Intensity of 9.58 mW/cm^2

compd	R_t/min	expt 1[a]	expt 2[a]	expt 3[a]	expt 4[a]	expt 5[a]	expt 6[a]
3	4.78	2.05×10^{-9}	2.37×10^{-9}	4.67×10^{-9}	3.32×10^{-9}	6.78×10^{-9}	9.39×10^{-9}
4	6.78	1.72×10^{-8}	2.20×10^{-8}	2.27×10^{-8}	3.39×10^{-8}	3.71×10^{-8}	3.53×10^{-8}
5	7.25	5.72×10^{-9}	1.21×10^{-8}	1.17×10^{-8}	1.89×10^{-8}	2.70×10^{-8}	2.54×10^{-8}
2	8.70	1.93×10^{-8}	2.23×10^{-8}	2.20×10^{-8}	2.06×10^{-8}	1.94×10^{-8}	1.83×10^{-8}
1	9.22	2.61×10^{-7}	2.39×10^{-7}	2.30×10^{-7}	2.14×10^{-7}	2.03×10^{-7}	1.97×10^{-7}
n_{dye}		3.14×10^{-7}	3.06×10^{-7}	3.01×10^{-7}	3.04×10^{-7}	3.04×10^{-7}	2.95×10^{-7}
n_{DP}		2.50×10^{-8}	3.65×10^{-8}	3.91×10^{-8}	5.61×10^{-8}	7.09×10^{-8}	7.01×10^{-8}
n_{photon}		3.18×10^{-5}	6.36×10^{-5}	9.54×10^{-5}	1.27×10^{-4}	1.59×10^{-4}	1.91×10^{-4}

[a] All numbers in the columns are in moles.

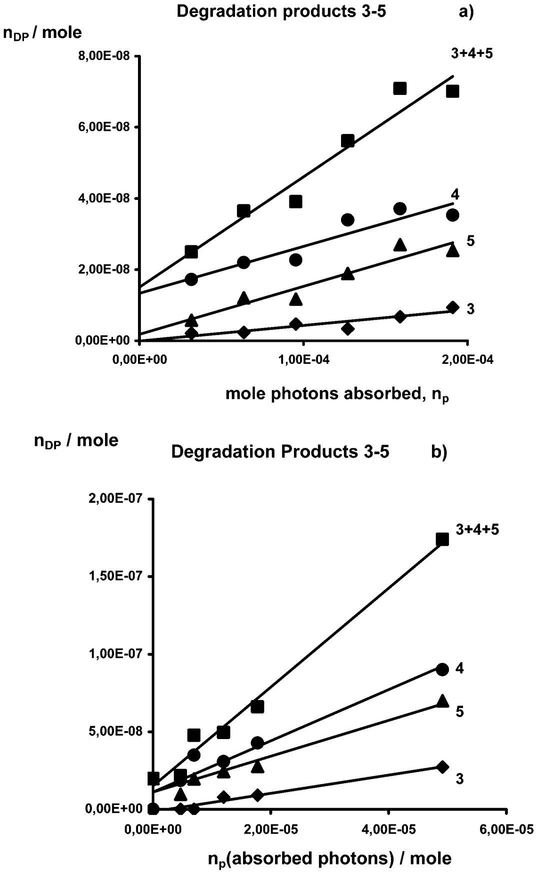

Figure 4. (a) Plot of the moles of each of degradation products **3**−**5** and the sum, n_{DP}, of products **3** + **4** + **5** as a function of the moles of absorbed photons, n_p, from extracted solutions of illuminated colloidal **N719**-dyed TiO$_2$ particles in deoxygenated acetonitrile: laser light intensity, 9.58 mW/cm^2; method II; $n(\mathbf{3} + \mathbf{4} + \mathbf{5}) = (3.1 \times 10^{-4})n_p + 1.5 \times 10^{-8}$; $R^2 = 0.946$. (b) Tungsten−halogen lamp; 525-nm filter; light intensity, 0.10 mW/cm^2; method I; $n(\mathbf{3} + \mathbf{4} + \mathbf{5}) = (3.2 \times 10^{-3})n_p + 1.5 \times 10^{-8}$; $R^2 = 0.948$.

expressions for the corrected rate of degradation, k^c_{deg} (see the Appendix).

$$k^u_{deg} = \Phi_{deg} k_{back}(I_0) \tag{9}$$

$$f_c = \frac{k^c_{deg}}{k^u_{deg}} = 0.60 \tag{10}$$

The mathematical treatment shows that f_c is a constant of 0.60 and does not depend on the incoming laser light intensity, I_0.

The results of all the photolysis experiments performed with both methods I and II are presented in Table 3. The applied light intensity, I_0, was 1−160 W/m^2, which is low relative to the 1000 W/m^2 intensity of standard AM1.5 solar illumination.

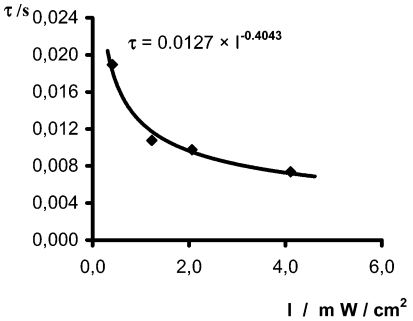

Figure 5. τ_{back} obtained by photoinduced absorption (PIA) measurements as a function of the laser light intensity. $\tau_{back} = 0.0127 \times I^{-0.4043}$.

In the applied intensity interval, k_{back} increases by a factor of 8 from 31 to 243 s^{-1}, while the measured Φ_{deg} decreases by a factor of 15 from 3×10^{-3} to 2×10^{-4}. The degradation rate of the [Ru$^{(III)}$L$_2$(NCS)$_2$]$^+$, k^c_{deg}, is reasonably constant, with an average value of $(4.0 \pm 1.0) \times 10^{-2}$ s^{-1}. Taking into consideration the large variation of the I_0 values and the application of two different experimental procedures (methods I and II), the relatively low standard deviation (≈20%) is quite remarkable. In method I the TiO$_2$ particles are sintered at 450 °C, producing large aggregates of TiO$_2$ particles, whereas in method II much smaller, nonsintered particles are used. The relatively constant k_{deg} values suggest that our simple kinetic scheme, eqs 1, 2, 4, and 5, does represent the chemistry of the photolysis experiments reasonably correctly.

The half-life, τ_{deg}, of [Ru$^{(III)}$L$_2$(NCS)$_2$]$^+$ attached to the TiO$_2$ surface is remarkably long ($\tau_{deg} = \ln 2/k_{deg} \approx 17$ s) compared to its half-life in acetonitrile, $\tau_{ACN} = 0.2$ ms, measured by using cyclic voltammetry experiments.[10] Apparently the attachment to the TiO$_2$ surface stabilizes, by some unknown mechanism, the Ru(III) form against oxidative degradation.

Determination of the Turnover Number in a DSSC. The turnover number, N, of the dye in a dye-sensitized solar cell may be calculated from eq 11, where k_3 is the regenerative electron-transfer reaction rate between the iodide ion and the Ru$^{(III)}$ complex (eq 3). In most solar cells the iodide ion concentration is 0.5 M.

$$N = \text{turnover number} = \frac{k_3[I^-]}{k_{deg}} \tag{11}$$

The regeneration rates, k_3, of **N719** attached to nanocrystalline TiO$_2$ have been obtained by several groups using the mean results of laser flash photolysis experiments.[27−28] An overview of the k_3 values presented in the literature is shown in Table 4. The results obtained by Haque,[27a] Pelet,[27b] and Heimer[27c] gave high values of k_3 with a mean value of 4.2×10^7 M^{-1} s^{-1}, whereas the k_3 values obtained by Kuciauskas[28a] and Montanari[28b]

TABLE 3: Oxidative Degradation Rates, k_{deg}, of N719 Attached to TiO_2 Particles

light source	I_0, mW/cm^2	τ,[a] s	k_{back},[b] s^{-1}	Φ_{deg}[c]	$10^2k^{u}_{deg}$,[d] s^{-1}	$10^2k^{c}_{deg}$,[e] s^{-1}
tungsten−halogen lamp [f,g]	0.10	3.22×10^{-2}	31	3.2×10^{-3}	9.9	5.9
halogen lamp [f,g]	0.54	1.63×10^{-2}	61	1.4×10^{-3}	8.3	5.0
laser [h,i]	0.93	1.31×10^{-2}	76	7.7×10^{-4}	5.6	3.3
laser	2.86	1.27×10^{-2}	120	5.5×10^{-4}	6.6	4.0
laser	4.65	6.82×10^{-3}	147	4.1×10^{-4}	6.0	3.6
laser	9.58	5.09×10^{-3}	196	3.1×10^{-4}	6.1	3.6
laser	6.79	5.85×10^{-3}	171	3.8×10^{-4}	6.4	3.9
laser	16.30	4.11×10^{-3}	243	2.0×10^{-4}	5.0	3.0
average ± sdv					6.7 ± 1.6	**4.0 ± 1.0**

[a] Measured using the PIA method. [b] $k_{back} = 1/\tau$. [c] Relative standard deviations of Φ_{deg} are between 6% and 15%. [d] Uncorrected degradation rates. [e] Corrected rates, see text. [f] 525 ± 10 nm, band-pass filter used. [g] Method 1 used. [h] $\lambda = 532$ nm. [i] Method 2 used.

TABLE 4: Regeneration Rates, k_3, of N3 Obtained from the Literature

ref	experimental conditions	k_3/M^{-1} s^{-1}	N[c]
Haque[27a]	0.3 M KI in propylene carbonate/ethylene carbonate[a]	2.3×10^7	2.8×10^8
Pelet[27b]	propylene carbonate, $[I^-] = 0.1$ M, $[Li^+] > 10^{-2}$ M[b]	3.6×10^7	4.5×10^8
Heimer[27c]	MeOH, 0.5 M NaI	7.1×10^7	8.9×10^8
Kuciauskas[28a]	CH_3CN, 0.5 M LiI	2.6×10^5	2.5×10^6
Montanari[28b]	propylene carbonate	1.6×10^5	2.0×10^6

[a] $t_{1/2} = 100$ ns, $k_3 = \ln 2/(t_{1/2} \times [I^-])$. [b] $1/t_{1/2} = 6 \times 10^6$ s^{-1}. [c] N calculated from eq 9 (see text).

are more than 200 times slower, with a mean value of $k_3 = 2.1 \times 10^5$ M^{-1} s^{-1}. It is not obvious to us why there is such a large divergence in the obtained regeneration rates. Based on the average of the two slowest regeneration rates obtained for **N719** and assuming that the degradation rate, $k_{deg} = 4.0 \times 10^{-2}$ s^{-1}, obtained for our simple model system is valid for a nc-DSSC, a turnover number N equal to 2.6×10^6 may be calculated with eq 9. This number corresponds to 0.5 years of normal solar cell operation, which is clearly insufficient for practical purposes. In contrast, when the average of the three highest values of k_3 is used, $N = 5.3 \times 10^8$ is obtained, indicating an **N719** sensitizer dye that is nearly perfectly stable under solar cell operation with respect to oxidative degradation. The corresponding solar cell lifetime would then be more than 20 years.

Our calculations of **N719** dye lifetimes are based on the assumption that the dye oxidative degradation rate, k_{deg}, under real nc-DSSC operation conditions is the same as that obtained from our simple model system. Observation of the same degradation products **3**−**5** as found in our model experiments from LC−UV−MS analysis of dye extracts of long-time illuminated complete dye sensitized solar cells[30] supports this assumption. Therefore, in a qualitative way our model system represents the more complex real nc-DSSC reasonably well. Hinsh et al. have reported nc-DSSC stability equivalent to 10 years of normal solar cell operation after 8300 h of light soaking at 2−5 sun.[14] This can be taken as an intrinsic stability of **N719** equivalent to at least 10 years, which is relatively close to the predicted lifetime based on our model system, applying the high average value of dye regeneration rate, k_3. The dye degradation kinetics based on our model system therefore seems to simulate the dye degradation kinetics in a real nc-DSSC reasonably well. Even though the dye degradation rates obtained from the simple model experiments may not be able to predict the lifetimes of solar cell dyes in real nc-DSSC better than within a factor of 2−3, the k_{deg} values may be used to rank the relative stability of various solar cell dyes in an experimentally simple and fast way. Investigations on dye degradation kinetics in real nc-DSSC are in progress.

Conclusion

The oxidative degradation rate, k_{deg}, of solar cell dye **N719** was obtained by applying a simple model system. Colloidal solutions of **N719**-dyed TiO_2 particles in acetonitrile were irradiated by 532-nm monochromatic light, and the sum of the quantum yields of the oxidative degradation products $[RuL_2(CN)_2]$, $[RuL_2(NCS)(CN)]$, and $[RuL_2(NCS)(ACN)]$, Φ_{deg}, were obtained at eight different light intensities in the range 0.1−16.30 mW/cm^2 by LC−UV−MS. The Φ_{deg} values decreased from 3.19×10^{-3} to 2×10^{-4} in the applied intensity range. By using the relation $k_{deg} = \Phi_{deg}k_{back}$ and back electron-transfer reaction rates, k_{back}, obtained from photoinduced absorption spectroscopy, it was possible to calculate an average value for the oxidative degradation rate of **N719** dye attached to the TiO_2 particles, $k_{deg} = 4.0 \times 10^{-2}$ s^{-1}. The stability of **N719** dye during solar cell operation was discussed, based on both this number and literature values of the regeneration reaction rate between $[Ru^{(III)}L_2(NCS)_2]$ and iodide. Five values for the **N719** dye regeneration rate constant, k_3, were found in the literature, the lowest and highest such values differing by more than a factor of 100. On the basis of the average of the three highest k_3 values, $N = 5.3 \times 10^8$ was obtained. This high turnover number indicates that an almost perfectly stable **N719** dye that could remain stable for more than 20 years under normal solar cell operating conditions, provided that oxidative degradation is the only route of dye degradation. A low value, $N = 2.6 \times 10^6$, was calculated based on the two lowest k_3 values corresponding to a lifetime of less than half a year under solar cell operation conditions. Obviously more measurements are needed to reach a consensus on the $Ru^{(II)}$ regeneration rate constant.

Appendix

The quantum yield of degradation, Φ, depends on the intensity of the absorbed light, I, according to eq A1. In this equation, k^{c}_{deg} is the rate of oxidative degradation of the Ru(III) state, and the back electron-transfer rate, $k_{back}(I)$, is given by eq A2, with $\alpha = 0.4043$. The experimentally obtained quantum yield, Φ, may be calculated as the average $\langle\Phi(I)\rangle$ over the intensity interval $[0, I_0]$ (see eq A3). Substitution of eqs A1 and A2 into eq A3 gives eq A4. The uncorrected rate of degradation, k^{u}_{deg}, is defined by eq A5. By inserting the expressions k^{c}_{deg} and k^{u}_{deg} (eqs A4 and A5) into the definition of f_c, a value close to 0.60 may be calculated (eq A6).

$$\Phi(I) = \frac{k_{\mathrm{deg}}^{\mathrm{u}}}{k_{\mathrm{back}}(I)} \tag{A1}$$

$$k_{\mathrm{back}} = \beta I^{\alpha} \tag{A2}$$

$$\Phi = \langle \Phi(I) \rangle = \frac{1}{I_0}\int_0^{I_0} \Phi(I)\, \mathrm{d}I \tag{A3}$$

$$\Phi = \frac{k_{\mathrm{deg}}^{\mathrm{c}}}{\beta I_0}\int_0^{I_0} I^{-\alpha}\, \mathrm{d}I = \frac{k_{\mathrm{deg}}^{\mathrm{c}}}{\beta} I_0^{-\alpha} \frac{1}{(1-\alpha)} \tag{A4}$$

$$\Phi = \frac{k_{\mathrm{deg}}^{\mathrm{u}}}{k_{\mathrm{back}}(I_0)} = \frac{k_{\mathrm{deg}}^{\mathrm{u}}}{\beta} I_0^{-\alpha} \tag{A5}$$

$$f_{\mathrm{c}} = \frac{k_{\mathrm{deg}}^{\mathrm{c}}}{k_{\mathrm{deg}}^{\mathrm{u}}} = (1-\alpha) = (1-0.4043) \approx 0.60 \tag{A6}$$

References and Notes

(1) O'Regan, B.; Grätzel, M. *Nature* **1991**, *353*, 737.

(2) Hagfeldt, A.; Grätzel, M. *Chem. Rev.* **1995**, *95*, 49.

(3) Grätzel, M. *Coord. Chem. Rev.* **1998**, *77*, 347.

(4) Hagfeldt, A.; Gratzel, M. *Acc. Chem. Res.* **2000**, *33*, 269.

(5) Vlachopoulos, N.; Liska, L.; Augustynski, J.; Grätzel, M. *J. Am. Chem. Soc.* **1988**, *110*, 1216.

(6) Nazeeruddin, M. K.; Kay, A.; Rodicio, I.; Humphry-Baker, R.; Müller, E.; Liska, P.; Vlachopoulos, N.; Grätzel, M. *J. Am. Chem. Soc.* **1993**, *115*, 6382.

(7) Kohle, O.; Grätzel, M.; Meyer, A. F.; Meyer, T. B. *Adv. Mater.* **1997**, *9*, 904.

(8) Grunwald, R.; Tributsch, H. *J. Phys. Chem. B* **1997**, *101*, 2564.

(9) Macht, B.; Turrión, M.; Barkschat, A.; Salvador, P.; Ellmer, K.; Tributsch, H. *Sol. Energy Mater. Sol. Cells* **2002**, *73*, 163.

(10) Cecchet, F.; Gioacchini, A. M.; Marcaccio, M.; Paolucci, F.; Roffia, S.; Alebbi, M.; Bignozzi, C. A. *J. Phys. Chem. B* **2002**, *106*, 3926.

(11) Hinsch, A.; Kroon, J. M.; van Roosmalen, J. A. M.; Bakker, N. J.; Sommeling, P.; van der Burg, N.; Kinderman, R.; Kern, R.; Feber, J.; Chill, C.; Schubert, M.; Meyer, A.; Meyer, T.; Uhlendorf, I.; Holzbock, J.; Niepmann, R. 16th European Photovoltaic Solar Energy Conference and Exhibition, Glasgow, 2000.

(12) Rijnberg, E.; Kroon, J. M.; Wienke, J.; Hinsch, A.; van Roosmalen, J. A. M.; Sinke, C.; Scholtens, B. J. R.; de Vries, J. G.; de Koster, C. G.; Duchateau, A. L. L.; Maes, I. C. H.; Henderickx, H. J. W. *Proc. World Confe. PVSEC 2nd* **1998**, 47.

(13) Nazeeruddin, Md. K.; Amirnasr, M.; Comte, P.; Mackay, J. R.; McQuillan, A. J.; Houriet, R.; Gratzel, M. *Langmuir* **2000**, *16*, 8525.

(14) Hinsch A.; Kroon, J. M.; Kern, R.; Uhlendorf, I.; Meyer, A.; Ferber, J. *Prog. Photovolt. Res.* **2001**, *9*, 425.

(15) Greijer, H. A.; Lindgren, J.; Hagfeldt, A. *J. Phys. Chem. B* **2001**, *105*, 6314.

(16) Greijer, H. A.; Lindgren, J.; Hagfeldt, A. *J. Photochem. Photobiol. A* **2004**, *164*, 23.

(17) Greijer-Agrell, H.; Lindgren, J.; Hagfeldt, A. *Solar Energy* **2003**, *75*, 169.

(18) Finnie, K. S.; Bartlett, J. R.; Woolfrey, J. L. *Langmuir* **1998**, *14*, 2744.

(19) (a) Kallioinen, J.; Lehtovuori, V.; Myllyperkiö, P.; Korppi-Tommola, J. *Chem. Phys. Lett.* **2001**, *340*, 217. (b) Tachibana, Y.; Haque, S. A.; Mercer, I. P.; Durrant, J. R.; Klug, D. R. *J. Phys. Chem. B* **2000**, *104*, 1198. (c) Ellingson, R. J.; Asbury, J. B.; Ferrere, S.; Ghosh, H. N.; Sprague, J. R.; Lian, T.; Nozik, A. J. *J. Phys. Chem. B* **1998**, *102*, 6455.

(20) (a) Kuciauskas, D.; Monat, J. E.; Villahermosa, R.; Gray, H. B.; Lewis, N. S.; McCusker, J. K. *J. Phys. Chem. B* **2002**, *106*, 9347. (b) Tachibana, Y.; Moser, J. E.; Gratzel, M.; Klug, D. R.; Durrant, J. R. *J. Phys. Chem.* **1996**, *100*, 20056. (c) Hannappel, T.; Burfeindt, B.; Storck, W.; Willig, F. *J. Phys. Chem. B* **1997**, *101*, 6799.

(21) (a) Nasr, C.; Hotchandani, S.; Kamat, P. V. *J. Phys. Chem. B* **1998**, *102*, 4944. (b) Alebbi, M.; Bignozzi, C. A.; Heimer, T. A.; Hasselmann, G. M.; Meyer, G. J. *J. Phys. Chem. B* **1998**, *102*, 7577.

(22) Fitzmaurice, D. J.; Frei, H. *Langmuir* **1991**, *7*, 1129.

(23) Amirnasr, M.; Nazeeruddin, Md. K.; Grätzel, M. *Thermochim. Acta* **2000**, *348*, 105.

(24) Bond, A. M.; Howitt, J.; MacFarlane, D. R.; Spiccia, L.; Wolfbauer, G. *J. Electrochem. Soc.* **1999**, *146*, 648.

(25) Das, S.; Kamat, P. V. *J. Phys. Chem. B* **1998**, *102*, 8954.

(26) Hansen, G.; Gervang, B.; Lund, T. *Inorg. Chem.* **2003**, *42*, 5545.

(27) (a) Haque, S. A.; Tachibana, Y.; Klug, D. R.; Durrant, J. R. *J. Phys. Chem. B* **1998**, *102*, 1745. (b) Pelet, S.; Moser, J.-E.; Gratzel, M. *J. Phys. Chem. B* **2000**, *104*, 1791. (c) Heimer, T. A.; Heilweil, E. J.; Bignozzi, C. A.; Meyer, G. J. *J. Phys. Chem. A* **2000**, *104*, 4256.

(28) (a) Kuciauskas, D.; Freund, M. S.; Gray, H. B.; Winkler, J. R.; Lewis, N. S. *J. Phys. Chem. B* **2001**, *105*, 392. (b) Montanari, I.; Nelson, J.; Durrant, J. R. *J. Phys. Chem. B* **2002**, *106*, 12203.

(29) Boschloo, G.; Hagfeldt, A. *Chem. Phys. Lett.* **2003**, *370*, 381.

(30) Lund, T. Manuscript in preparation.

Appendix II:

An investigation of the substitution reaction between the sensitizer N719 dye and the solar cell additive 4-tert-butylpyridin.

F. Nour-Mohammadi, T. Lund.

The results have been collected in a manuscript for publication.

Correspondence and proofs to:

Torben Lund
Department of Life Sciences and Chemistry
Roskilde University
DK-4000 Roskilde
Denmark

Running title: Lund *et al.* N719 and 4-*tert*-butylpyridine

Title**: An investigation of the substitution reaction between the sensitizer N719 dye and the solar cell additive 4-*tert*-butylpyridin.**

Farahnaz Nour-Mohammadi and Torben Lund*

Department of Life Sciences and Chemistry, Roskilde University, DK-4000, Denmark.

Corresponding author, Fax.: 45-46743011, e-mail: tlund@ruc.dk

1. Introduction

Nanocrystalline dye-sensitized titanium dioxide solar cells (nc-DSSC) have attracted significant attention because of their high efficiency of the solar-to-electric power conversion and low cost compared to those of silicon solar cells [1–6]. The chemistry at the photo anode is shown in eqs.1-3.

$$TiO_2|S + h\nu \rightarrow TiO_2|S^* \qquad (1)$$

$$TiO_2|S^* \rightarrow TiO_2 + e^-|S^+ \qquad (2)$$

$$TiO_2|S^+ + red \rightarrow TiO_2|S + ox \qquad (3)$$

The sensitizer S is excited by a photon followed by an ultrafast electron injection from S* to the conduction band of the TiO_2 semiconductor. The cell cycle is finished after regeneration of S by the reduced form of the mediator which in most cases for nc-DSSC is iodide. One of the most popular sensitizes has been the ruthenium dye $[Ru(Hdcbpy)_2(NCS)_2]^{2-}$, 2 $(n\text{-}C_4H_9)_4N^+$, (H_2dcbpy = 2,2′-bipyridine-4,4′-dicarboxylic acid) due to its high efficiency and stability [1-4]. The molecular structure is shown in Figure 1a.

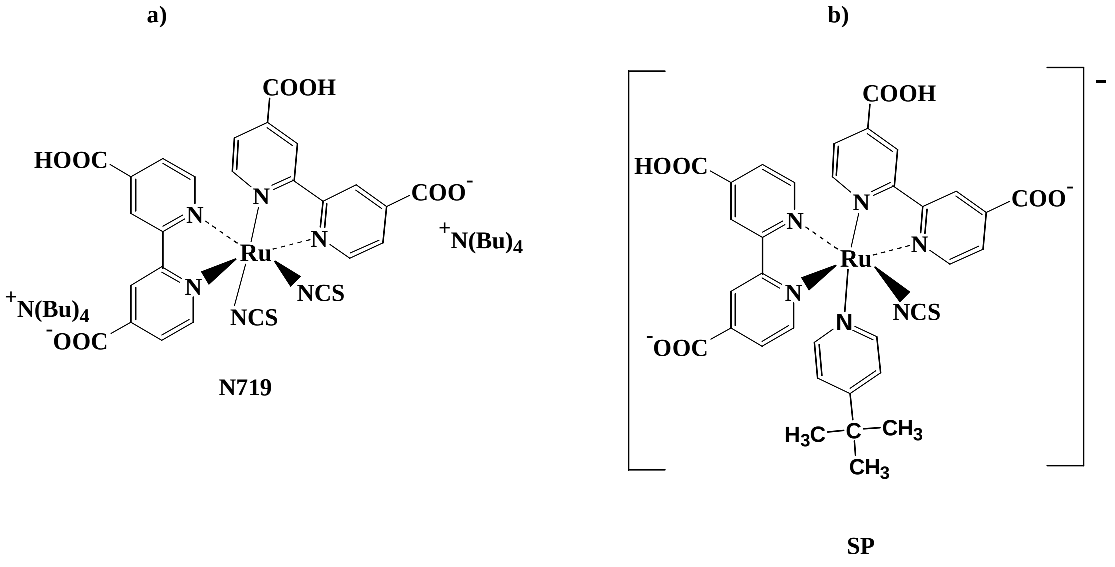

N719

SP

Figure 1

Various types of additives have been introduced to the cell electrolyte to improve the cell performance [7-13]. 4-*tert*-butylpyridin (**4-TBP**) is one of the most commonly used additives as it has been shown to increase the open circuit voltage V_{oc} of the cell by 80-100 mV by suppressing the dark current from the recombination of electrons in the conduction band with the oxidized form of the mediator (I^-_3) [14].

Recently we found the substitution product SP = $[Ru(Hdcbpy)_2(NCS)(4\text{-}TBP)]^-$ (see Figure 1b) in dye extracts from light exposed nc-DSSC with **N719** as the sensitizer [15]. To our knowledge there have been no previous reports of possible side reactions of **N719** with 4-*tert*-butylpyridine in solar cells. The observation prompted us to investigate kinetics of the substitution reaction to be able to evaluate the influence of this reaction on the long term stability of nc-DSSC.

The 4-*tert*-butylpyridine may react with the sensitizer in all its three states, S, S* and S^+. The substitution product, however, was mainly found in solar cells which had been exposed to light at room temperature [15]. This indicates that the substitution product SP at room temperature is mainly formed through the dye states S* or S^+. The injection rate of S* to the conduction band of the TiO_2 semiconductor is extremely fast ($k_2 = 10^{13}\ s^{-1}$) [16] and the pyridine additive will therefore have no time to react with S*. It is therefore most likely that the substitution reaction during solar cell operation occurs from the oxidized state of the sensitizer S^+ (eq. 4).

$$TiO_2|S^+ + 4\text{-TBP} \xrightarrow{k_4} TiO_2|SP \quad (4)$$

$$TiO_2|S^+ \xrightarrow{k_5} TiO_2|DP \quad (5)$$

$$TiO_2 + e^-|S^+ \xrightarrow{k_6} TiO_2|S \quad (6)$$

In this work we have measured the quantum yield of SP, Φ_{SP}, and the quantum yield of the sum of the oxidative degradation products DP, Φ_{DP}, through model experiments similar to the experiments in which we obtained the rate of the oxidative degradation reaction $k_5 = 0.04\ s^{-1}$ [17]. The quantum yield experiments were performed by irradiating colloidal solutions of **N719** dyed nanocrystaline TiO_2 particles in acetonitrile in the presence of high concentrations of 4-*tert*-butylpyridine. The chemistry of the model experiments are described by eqs. 1, 2, 4, 5 and 6. The rate constant of substitution k_4 may be calculated from the quantum yields Φ_{SP}, Φ_{DP} and k_5 or from Φ_{SP} and k_6. Based on the k_4 value it is possible to evaluate the effect of **4-TBP** addition on the long term stability of **N719** in light exposed solar cells.

2. Experimental

2.1 Chemicals

The bis(tetrabutylammonium) salt of the complex *cis*-bis(isothiocyanato) bis (2,2′-bipyridyl-4,4′-dicarboxylato) ruthenium (II) with the trade name Ruthenium 535–bis TBA and referred to as **N719** was obtained from Solaronix**.** *N*,*N*-Dimethylformamide (DMF) and acetonitrile (ACN) were HPLC grade (Merc). 4-*tert*-butylpyridine was purchased from Aldrich and was used as received. The applied titanium dioxide was Degussa P25.

2.2 Instrumentation

The HPLC–UV/Vis–MS equipment and procedure, the light sources and the photon counting device have recently been described [17]. ^1H NMR was obtained by a 600 MHz Varian Inova instrument.

2.3 Synthesis of Bu_4N^+, $[Ru(Hdcbpy)_2(NCS)(4\text{-}TBP)]^-$

N719 (25 mg, 0.021 mmole) and 4-*tert*-butylpyridine (320 µl, 2.14 mmole) were dissolved in dimethylformamide (5 ml). The solution was deareated with argon and heated to about 120 °C under a small argon flow. After ~ 24 hours the solvent was removed by rotary evaporation and the remaining solid was dissolved in a small amount of methanol. The solution was separated on a column packed with sephadex LH20 resin and with application of the starting eluent water/acetonitrile/formic acid (95/5/15). Methanol was added during the elution process until all ruthenium complexes had been eluted. The eluted fractions were then analysed by LC-UV/Vis-MS and the fractions containing the desired substitution product were collected and the solvent was removed by rotary evaporation. The remaining solid product was dissolved in 1.1 g D_2O and 40 µL of a basic solution of 1 g D_2O and 100 mg NaOD and the solution was analyzed by ^{1}H-NMR.

2.4 Preparation of the dyed TiO_2 colloidal solution.

The preparation of dye-covered Degussa P25 TiO_2 particles has recently been decribed [17]. The dyed nanocrystalline TiO_2 powder (12 mg dyed with 0.304 µmole **N719**) was placed into a cuvette containing 3 ml of dry acetonitrile and 320 µl of 4-*tert*-butylpyridin (2.18 mM , [**4-TBP**] = 0.7 M). The mixture was degassed with a flow of argon for 20 minutes. After degassing, a “homogenous” stable dyed TiO_2 colloidal solution was obtained by sonification of the cuvette for 1 h.

2.5 Photolysis of N719 dyed TiO_2 particles in the presence of 4-TBP.

The cuvette containing the dyed colloidal TiO_2 solution was placed in the black box of a photon-counting device. The sample was irradiated with continuous laser light (532 nm) of 7.33 mW/cm^2 for 200 minutes corresponding to a light doses of 1.23×10^6 counting numbers (1×10^5 counting numbers = 3.17×10^{-5} mole of photons). After the photolysis was stopped the dyed TiO_2 colloidal solution was transferred into a round-bottom flask and the acetonitrile was removed by means of rotary evaporation. Degradation products from the photolysis experiments that were still bound to the TiO_2 particles were extracted by treatment with a solution composed of 2 ml of 0.1 M NaOH and 1 ml of ethanol. The red extract in the flask was transferred into a clean test tube and centrifuged. The red supernatant was transferred into another test tube and 15 µl of formic acid was added. The acidified solution was then transferred into an HPLC vial and analyzed using LC-UV/Vis-MS. LC-UV/Vis chromatograms were plotted in the maximum absorption mode in the wave length interval 400-800 nm. LC-MS chromatograms were plotted as the total ion chromatogram of the m/z values 643, 648, 675, 689, 706 and 783.

2.6 Response factor calculations

UV/Vis and MS response factors of $Bu4N^+$, $[Ru(Hdcbpy)_2(NCS)(4\text{-}TBP)]^-$ relative to **N719** were obtained from samples with known concentrations of the isolated substitution product SP and **N719**. The following values were obtained: $(R_{SP}/R_{N719})_{UV} = 1.22$ and $(R_{SP}/R_{N719})_{MS} = 3.15$.

3. Results and Discussion

3.1 Identification of the substitution product.

Figure 2a shows a LC-MS chromatogram of a dimethylformamide solution of the **N719** dye and 4-**TBP** after 9 hours heating at 120 ^{0}C.

Figure 2a, b

The peak which eluted after 9.01 min was identified as the fully protonated starting complex $[Ru(H_2dcbpy)_2(NCS)_2]$. The complex was characterized by its visible absorption spectrum λ_{max} = 525 nm and a characteristic ruthenium isotope pattern around the M^+ ion $[Ru^{(III)}(H_2dcbpy)_2(NCS)_2]^+$ m/z = 706 [17,18]. The peak with the retention time 10.15 min has a maximum in the visible spectrum at λ_{max} = 509 nm and an intense ruthenium isotope pattern in the mass spectrum around the ion m/z = 783 which fits with the mass of the molecular ion $[Ru^{(II)}(H_2dcbpy)_2(NCS)(TBP)]^+$ (see Figure 2b). The fragment ion m/z = 648 corresponds to the ion $[Ru^{(II)}(H_2dcbpy)_2(NCS)]^+$ formed by elimination of the **4-TBP** ligand from the molecular ion.

In order to confirm the structure by ^{1}H-NMR the reaction was performed on a larger scale followed by purification of the **4-TBP** substituted complex on a sephadex column with an eluent mixture of water, acetonitril and formic acid. The ^{1}H-NMR spectrum of the purified product shows 14 non equivalent aromatic protons (Figure 3) and a singlet at 1.5 ppm. The molecule has twelve aromatic bipyridine signals which indicate a complex with the structure $[Ru(H_2dcbpy)_2XY]$ in which the two bipyridyl groups are non equivalent. The four H3 and H3´ protons of the two bipyridyl rings can be identified from their small doublet splitting, $^4J \approx 1$ Hz and the eight H5, H6, H5´and H6´ protons by their doublet splitting ^3J = 6-7 Hz. The last two aromatic signals at 7.34 and 7.33 ppm are due to the four aromatic protons on the pyridine ring and the signal at 1.5 ppm due to the *tert*-butyl group. MS and ^{1}H-NMR spectra are therefore consistent with the structure shown in Figure 1b.

Figure 3

3.2 $TiO_2|S^+$ + 4-TBP

Figure 4a and 4b shows the LC-UV and LC-MS chromatograms respectively of a dye extract obtained from a model experiment in which a colloidal solution of **N719** dyed nanocrystalline TiO_2 particles in acetonitrile containing **4-TBP** (0.7 M) have been irradiated with 532 nm laser light. In the LC-UV chromatogram (Figure 4a) five peaks are observed. The two peaks at R_t = 8.83 and 8.30 min are due to the starting complex $[Ru(H_2dcbpy)_2(NCS)_2]$ and its minor isomer $[Ru(H_2dcbpy)_2(NCS)(SCN)]$ respectively. The peak at R_t = 9.93 min is identified as the 4-*tert*-butylpyridine substitution product whereas the peaks at R_t = 6.36, and R_t = 4.30 min were identified as the **N719** oxidative degradation products $[Ru(H_2dcbpy)_2(NCS)(CN)]$ and $[Ru(H_2dcbpy)_2(CN)_2]$, respectively. The substitution product peak intensity in the LC-MS chromatogram is higher than that in the LC-UV chromatogram. This is caused by the 3 times higher ESI-MS detector sensitivity of the substitution product relative to the other ruthenium complexes. In Table 1 the λ_{max} and the characteristic m/z values are shown for the identified products together with their quantum yields.

Figure 4a +b

Table 1

3.3 Calculation of k_4

The rate of substitution, k_4, may be calculated from eqs. (7) and (8) which were derived by application of the steady state approximation on eqs. 1, 2, 4, 5 and 6 and use of the equation $k_6 >> k_4$.

$$k_4 \approx f_c \times \Phi_{SP} \times k_6/[\text{4-TBP}], \quad f_c = 0.60 \qquad (7)$$

$$k_4 = k_5 \times (\Phi_{SP}/\Phi_{DP})\,/[\text{4-TBP}] \qquad (8)$$

The back electron transfer rate k_6 between the electrons in the TiO_2 particles and S^+ is dependent on the light intensity I_0 used in the photolysis experiments. High light intensity will produce a high steady state concentration of electrons in the TiO_2 particles which will lead to a high back electron transfer rate k_6. We have recently obtained back electron transfer rates of the model system by means of photo induced absorption experiments (PIA) and based on these measurements it is possible to calculate $k_6 = 176\ s^{-1}$ for the applied laser light intensity $I = 7.33\ mW/cm^2$. [17] The correction factor f_c in eq. 7 compensates for the fact that the light intensity decreases from its initial value I_0 at the entrance of the photolysis cuvette to a very small value after passing the 1 cm dyed TiO_2 colloidal solution. This will cause back electron transfer rate to decrease throughout the cell. [17]

Applying the values $\Phi_{SP} = 7.1\times10^{-5}$, $\Phi_{DP} = (5.6 + 0.6)\times10^{-5} = 6.2\times10^{-5}$ (see Table 1), $k_5 = 0.04\ s^{-1}$, $k_6 = 176\ s^{-1}$ and [4-TBP] = 0.7 M in eqs. 7 and 8 the following substitution rates may be calculated: k_4 (eq. 7) = $0.011\ M^{-1}s^{-1}$ and k_4 (eq. 8) = $0.07\ M^{-1}s^{-1}$. Two quite different rate constants are obtained from the two kinetic expressions. A possible explanation may be that the back electron transfer rate k_6 is too low. The rate is obtained from PIA measurements without the addition of **4-TBP**. The effect of **4-TBP** on k_6 has not been investigated, however it is known that **4-TBP** affects the conduction band level and it is therefore likely that the addition of **4-TBP** will affect the back electron transfer rate. The k_4 = 0.07 $M^{-1}s^{-1}$ value based on eq. 8 is therefore likely to be the most reliable value.

3.4 Evaluation of N719 dye stability in solar cells with 4-TBP addition

The evaluation of the **N719** dye stability is based on a simple life time estimation in which it is assumed that the reaction between $TiO_2|S^+$ and **4-TBP** (eq. 4) is the only side reaction in the solar cell and that the kinetics of the simple model system is similar to the degradation kinetics of a real solar cell. [17] The lifetime calculation of the sensitizer is based on the prediction of the corresponding N value, where N is the number of cell cycles which a single sensitizer molecule should be able to sustain. N may be estimated by the following simple expression (eq. 9):

$$N = k_3\,[I^-] / (k_4 \times [\text{4-TBP}]) \qquad (9)$$

It has previously been estimated that the sensitizer should be able to sustain 1×10^8 cell cycles in order to obtain a life time of the dye equal to 20 years of normal solar cell operation [4]. The estimated N number may therefore be translated into a life time by eq. 10

$$\text{Life time of S} = 20\ \text{years} \times N / 1\times10^8 \qquad (10)$$

Calculations of N and the life time of **N719** are shown in Table 2. The regeneration rates, k_3, of **N3** (the fully protonated form of **N719**) attached to the nanocrystalline TiO_2 have been obtained by several groups by using laser flash photolysis experiments [19-20]. The results obtained by Haque [19a], Pelet [19b], and Heimer [19c] gave high values of k_3 with a mean value of $4.3\times10^7\ M^{-1}\ s^{-1}$, whereas the k_3 values obtained by Kuciauskas [20a] and Montanari [20b] are more than 100 times lower, with a mean value of $k_3 = 2.1 \times 10^5$ M^{-1} s^{-1}. It is not obvious why there is such a large divergence in the obtained regeneration rates. Based on the slow regeneration rate obtained for **N3** and the rate $k_4 = 0.07$ M^{-1} s^{-1}, a turnover number N equal to 2.1×10^6 may be calculated using eq. 9. This number corresponds to ~ 0.4 years of normal solar cell operation, which is clearly insufficient for practical purposes. In contrast, when the high value of k_3 is used, $N = 4.3 \times 10^8$ is obtained, indicating an **N719** sensitizer dye that is nearly perfectly stable under solar cell operation with respect to the reaction between $TiO_2|S^+$ and **4-TBP**. The corresponding solar cell lifetime would then be 72 years.

4. Conclusion

The substitution product Bu_4N^+, $[Ru(Hdcbpy)_2(NCS)(4\text{-TBP})]^-$ may be synthesized in a simple homogeneous thermal reaction in DMF between the solar cell dye **N719** and the additive **4-TBP**. The same product is formed by photolysis of a colloidal solution of **N719** dyed TiO_2 particles in the presence of **4-TBP** (0.7 M) with a quantum yield $\Phi_{SP} = 7 \times 10^{-5}$. The heterogeneous rate of substitution between $TiO_2|$ S^+ and **4-TBP** was estimated to be $k_4 = 0.07$ M^{-1} s^{-1}. Based on this value and a low literature value of the regeneration reaction between $TiO_2|S^+$ and iodide, $k_3 = 2.1 \times 10^5$ a low life time ~ 0.4 years is predicted of the **N719** sensitizer under normal solar cell operation. However if the high value $k_3 = 4.3 \times 10^8$ $M^{-1}s^{-1}$ is used then a life time ~ 86 years is predicted indicating no degradation problems due to the 4-TBP addition.

The results of this work suggest that some concern should be paid to the possible substitution reaction of the solar cell additive 4-*tert*-butylpyrridine with sensitizers in nc-DSSC.

References

1) B. O'Regan, M. Grätzel, *Nature 353* (**1991)** 737.
2) A. Hagfeldt, M. Grätzel, *Chem. Rev*. 95 (**1995)** 49.
3) M. Grätzel, *Coordination Chem. Rev*. 77 (**1998)** 347.
4) M. Grätzel, A. Hagfeldt, *Acc. Chem. Res*. **33 (2000)** 269.
5) N. Vlachopoulos, L. Liska, J. Augustynski, M. Grätzel, *J. Am. Chem. Soc*. 110 (**1988)** 1216.
6) M. K. Nazeeruddin, A. Kay, I. Rodicio,R. Humphry-Baker, E. Müller, P. Liska, N. Vlachopoulos, M. Grätzel, *J. Am. Chem. Soc*. 115 (**1993)** 6382..
7) H. Kusama, H. Arakawa, *J. Photochem. & Photobio. A: Chemistry* 160 (**2003**) 171.
8) H. Kusama, K. Konishi,H. Sugihara,H. Arakawa, *Sol. Energy Mater. Sol. Cells* 80 (**2003**) 167.
9) H. Kusama, H. Arakawa, *Sol. Energy Mater. Sol. Cells* 81 (**2004**) 87.
10) H. Kusama, H. Arakawa, *J. Photochem.& Photobio. A: Chemistry* 162 (**2004**) 441.
11) H. Kusama, H. Arakawa, *Sol. Energy Mater. Sol. Cells* 82 (**2004**) 457.
12) O. Kohle, M. Gratzel, A. F. Meyer, T. B. Meywr, *Adv. Mater*. 9 (**1997**) 904.
13) G. Schlichthorl, S. Y. Huang,J. Sprague, A. J. Frank, *J. Phys. Chem. B* 101 (**1997**) 8139.
14) S. Y. Huang, G. Schlichtörl, A. J. Nozik, M. Grätzel, and A. J. Frank, *J. Phys. Chem. B* 101 (**1997**) 2576.
15) T. Lund et. al in preparation.
16) G. Benkö, P. Myllyperkiö, J. Pan, A. P. Yartsev, and V. Sundström, *J. Am. Chem. Soc.* 125 (**2003**) 1118-1119.
17) F. Nour-Mohammadi, S. D. Nguyen, G. Boschloo, A. Hagfeldt, T. Lund, *J. Phys. Chem. B* (**2005**), 109, 22413.
18) G. Hansen, B. Gervang, T. Lund, *Inorg. Chem*. 42 (**2003**) 5545.
19) (a) S. A. Haque, Y. Tachibana, D. R. Klug, J. R. Durrant, *J. Phys. Chem. B* 102 (**1998)**1 745 (b) **s.** Pelet, J. E. Moser, M. Gratzel, *J. Phys. Chem. B.* 104 (**2000)** 1791 (c) T. A. Heimer, E. J. Heilweil, C. A. Bignozzi, G. J. Meyer, *J. Phys. Chem. A* 104 (**2000)** 4256.
20) (a) **D.** Kuciauskas, M. S. Freund, H. B. Gray, J. R. Winkler, N. S. Lewis, *J. Phys. Chem. B* 105 (**2001)** 392. (b) **I.** Montanari, J. Nelson, J. R. Durrant, J. *Phys. Chem. B106* **(2002)** 12203.

Table 1 Identified products and their quantum yields obtained from the photolysis of **N719** dyed nanaocrystaline TiO_2 particles with 532 nm laser light.[a,b]

Compound	R_t/min	λ_{max}/nm	m/z	Mole $\times 10^8$	Φ $\times 10^5$
$[Ru(H_2dcbpy)_2(NCS)_2]$	8.83	525	706, 648	22.3	-
$[Ru(H_2dcbpy)_2(NCS)(SCN)]$	8.30	521	706, 648	1.93	-
$[Ru(H_2dcbpy)(Hdcbpy)$ $(NCS)(4\text{-}TBP)]$	9.93	509	783, 648	2.76	7.1
$[Ru(H_2dcbpy)_2(NCS)(CN)]$	6.35	497	675, 648	2.19	5.6
$[Ru(H_2dcbpy)_2(CN)_2]$	4.30	473	643	0.25	0.6

[a] Intensity of laser light = 7.33 mW/cm^2

[b] Total number of absorbed photons = 3.90×10^{-4} mole

Table 2 Intrinsic life time of **N719** dye in nc-DSSC with 0.7 M **4-TBP**.

Reaction	k / $M^{-1}s^{-1}$	N	Lifetime of **N719** (Years)
$TiO_2 \mid S^+$ + 4-TBP	0.07	$k_3 = 4.3 \times 10^7$ => $N = 4.3 \times 10^8$	~ 86
		$k_3 = 2.1 \times 10^5$ => $N = 2.1 \times 10^6$	~ 0.4

Figure Captions

Figure 2 a) Total ion chromatogram of a DMF solution of **N719** (0.2 mM) and **4-TBP** (0.2M) after 9 hours heating at 120 ^{0}C. b) Mass spectrum of the peak eluting at 10.15 min.

Figure 3 ^{1}H-NMR spectrum of the aromatic region of Bu_4N^+, $[Ru(Hdcbpy)_2(NCS)(4\text{-}TBP)]^-$

Figure 4 a) LC-UV/Vis chromatogram of the dye extract obtained from irradiation of ~ 12 mg colloidal solution of **N719** dyed nanocrystaline TiO_2 particles containing **4-TBP** (0.7 M). b) LC-MS chromatogram of the same solution as in a).

Figures

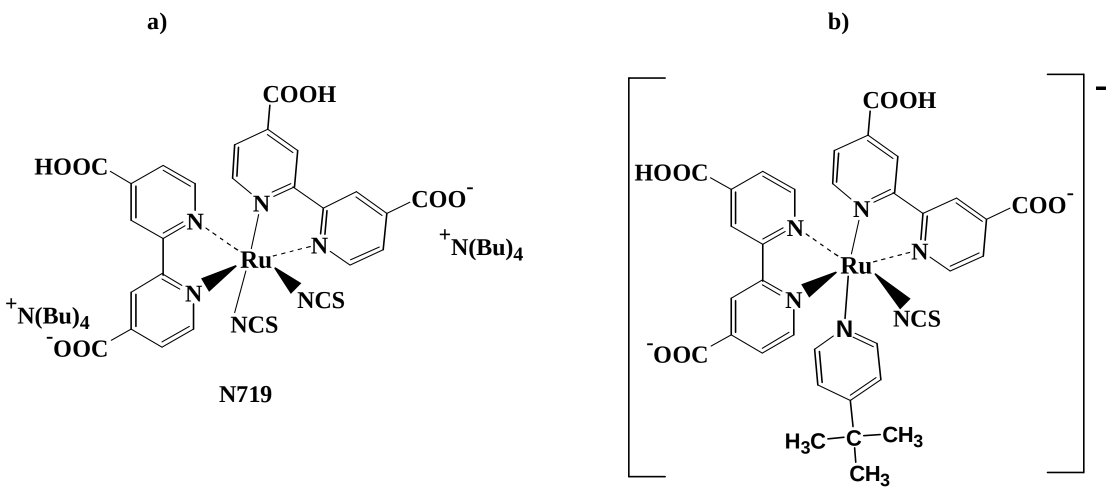

N719

SP

Figure 1

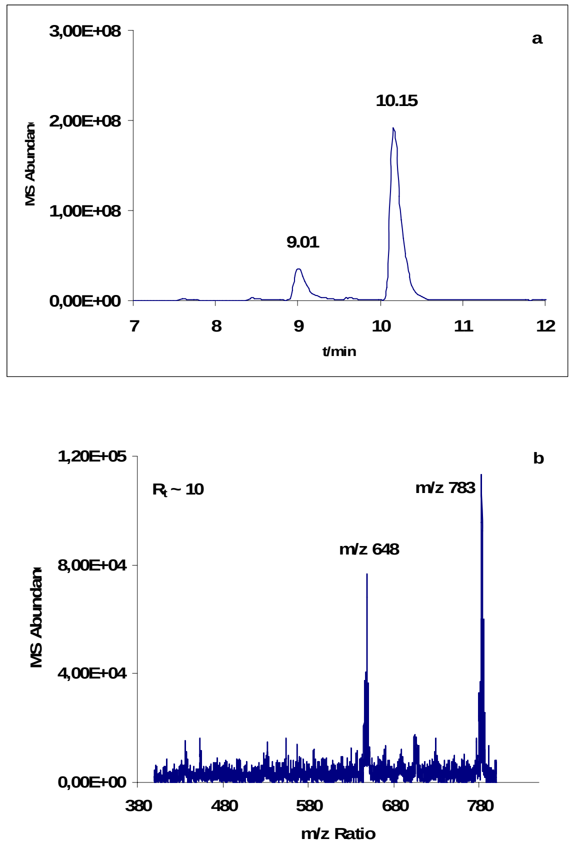

Figure 2

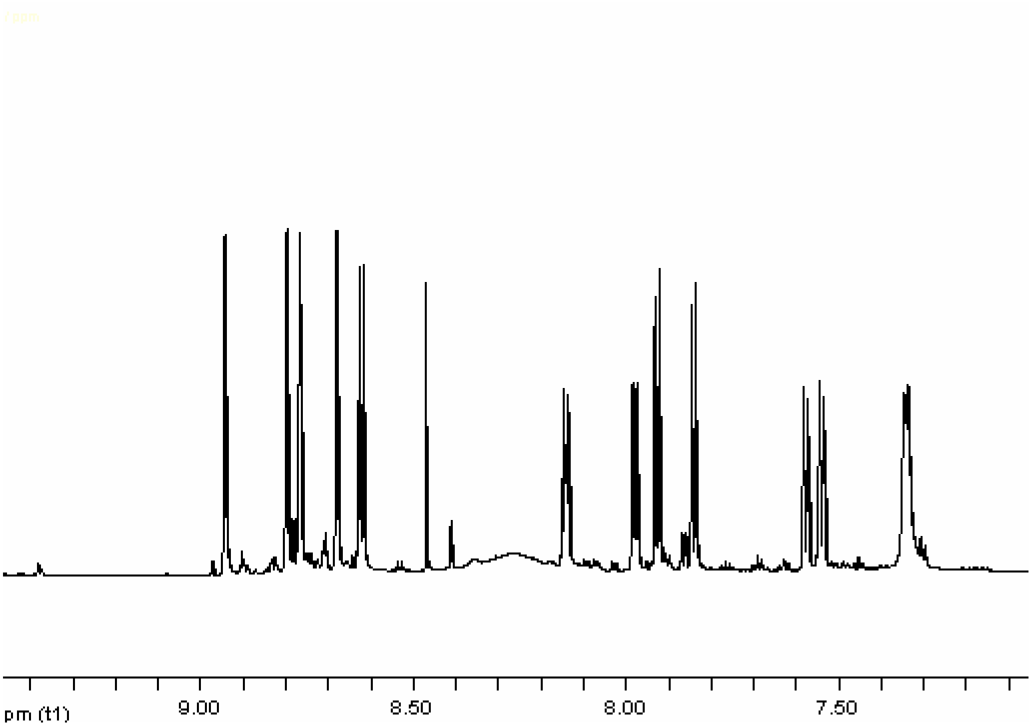

Figure 3

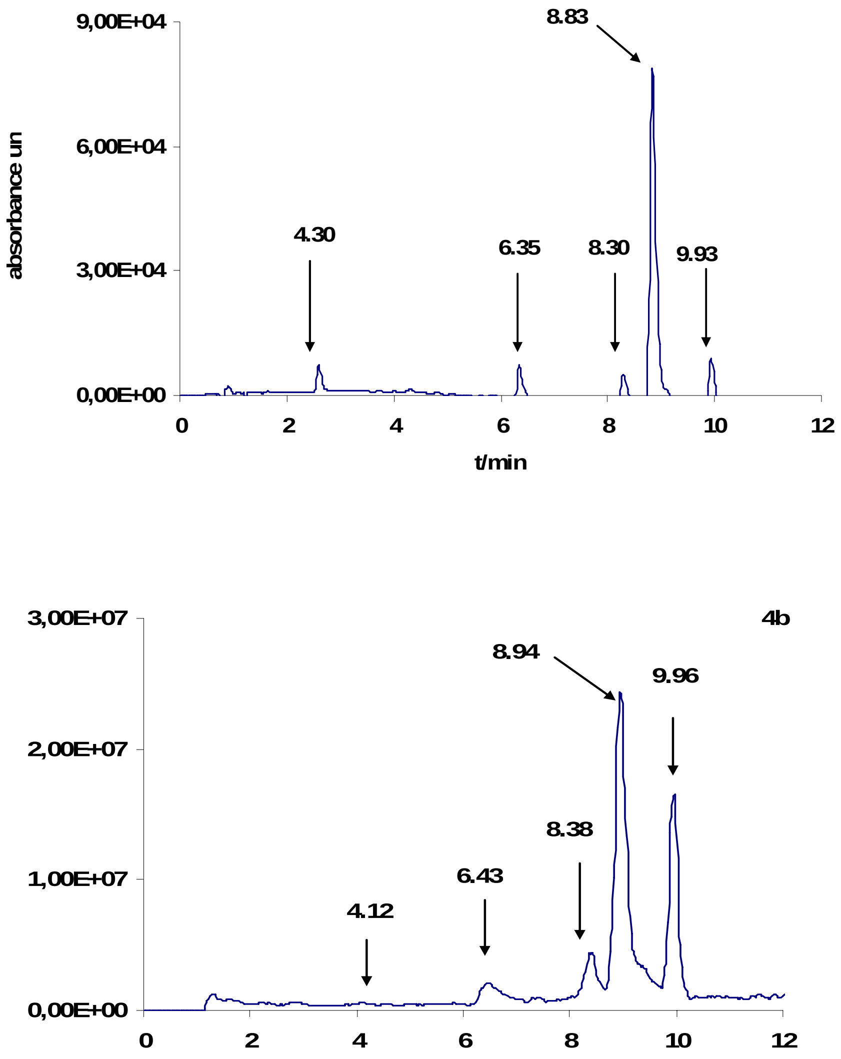
9,00E+04
6,00E+04
3,00E+04
0,00E+00
absorbance un
8.83
4.30
6.35
8.30
9.93
0
2
4
6
8
10
12
t/min
3,00E+07
2,00E+07
1,00E+07
0,00E+00
4b
8.94
9.96
8.38
6.43
4.12
0
2
4
6
8
10
12

Figure 4

Appendix III:

Electrochemical synthesis of organic compounds:1 Addition of sulfinic acids to electrochemically generated o- and p-benzoquinones.

F. Nourmohammadi, S. M. Golabi, A. Saadnia.

J. Electroanal Chem., 529, 2002, 12.

ELSEVIER

Journal of Electroanalytical Chemistry 529 (2002) 12–19

Journal of Electroanalytical Chemistry

www.elsevier.com/locate/jelechem

Electrochemical synthesis of organic compounds: 1. Addition of sulfinic acids to electrochemically generated *o*- and *p*-benzoquinones

F. Nourmohammadi [a], S.M. Golabi [a,*], A. Saadnia [b]

[a] *Electroanalytical Chemistry Laboratory, Faculty of Chemistry, University of Tabriz, Tabriz, Iran*
[b] *Organic Synthesis Laboratory, Faculty of Chemistry, University of Tabriz, Tabriz, Iran*

Received 23 November 2001; received in revised form 11 March 2002; accepted 23 April 2002

Abstract

Electrochemical oxidation of catechol (**1a**) and 4-methylcatechol (**1b**) in the presence of *p*-toluenesulfinic acid (**I**) and 1,4-dihydroxybenzene (**4**) in the presence of *p*-toluenesulfinic acid and benzenesulfinic acid (**II**) has been studied using cyclic voltammetry and controlled potential coulometry. The results indicate that compounds **1a** and **1b** react with **I**, and **4** reacts with **I** and **II** via a Michael addition reaction leading to the sulfones **3a**, **3b** and **6**, **7**, respectively. Products were obtained in good yield and purity. The mechanism of oxidation was deduced from voltammetric data and by coulometry at controlled potential. The products have been characterized after purification by IR, ^{1}H-NMR, and elemental analysis. © 2002 Elsevier Science B.V. All rights reserved.

Keywords: Electroorganic synthesis; Cyclic voltammetry; Sulfinic acids; *o*- and *p*-Benzoquinones

1. Introduction

Many papers have been published describing the oxidation of catechol and some of its derivatives in the presence of nucleophiles such as methanol [1,2], ethanol [3], 4-hydroxycoumarin [4–7], 3,3-dimethylbarbituric acid [8] and others [9]. While these investigations have led to the electrochemical synthesis of methoxy and ethoxy catechols, coumestan, dispiropyrimidine and benzofuran derivatives, only one paper has been published showing that electrochemically generated *p*-benzoquinone containing electron-withdrawing substituents can be attacked nucleophically by water as a nucleophile [10].

Investigations have shown that sulfones, by virtue of their diverse chemistry, are valuable synthetic intermediates [11,12]. Sulfones and sulfoxides have been used in the total synthesis of biologically active natural compounds [13]. An excellent review of sulfone chemistry has compiled by Simpkins [14]. It contains valuable information about the synthesis, properties and applications of sulfones. Most uses of sulfones involve sulfonylcarbanioens, which react with a wide range of electrophiles to produce new sulfones that may be further transformed to olefins by reduction, elimination or cyclization by a sulfur dioxide extrusion process. Vinyl sulfones are excellent acceptors in conjugate addition reactions and participate in cycloaddition processes. Vinyl sulfones have also been extensively studied due to their synthetic utility [15]. These compounds are pharmaceutically promising analogues of chalcones, (a class of natural products), in which the carbonyl group is replaced by the sulfone group which possesses a similar electrophilic character. It was claimed that these compounds possess anticancer and carcinogenesis-suppressing activity [16,17]. Biologically active flavonoids are usually polyhydroxylated in benzene rings of diphenyl vinyl sulfones [18–20]. On the other hand, the chemical synthesis of arylsulfones using hydroquinones as starting materials requires the addition of an adequate oxidant to the reaction medium in order to transform the hydroquinones to the corresponding quinones [21], whereas, in the electrochemical synthesis, this transformation can be achieved easily by anodic oxidation of hydroquinones at a given potential

---

* Corresponding author. Tel.: +98-411-334-8623/4; fax: +98-411-334-0191
E-mail address: golabi@tabrizu.ac.ir (S.M. Golabi).

PII: S0022-0728(02)00906-3

and for a given time. This can be regarded as an advantage of electrochemical procedures. For these reasons and because of the recent advances in the efficient electrochemical synthesis of organic compounds with high yield and purity, we aimed at the electrochemical synthesis of some arylsulfones. In the present work, the electrochemical oxidation of catechol (**1a**) and 4-methylcatechol (**1b**) in the presence of *p*-toluenesulfinic acid (**I**) and 1,4-dihydroxybenzene (**4**) in the presence of benzenesulfinic acid (**II**) and *p*-toluenesulfinic acid is described. Cyclic voltammetry studies and the preparative procedure for electrochemical synthesis of the products were involved. Finally, the products were characterized using spectroscopic methods and elemental analysis.

2. Experimental

2.1. Chemicals

All chemicals (catechol, 4-methylcatechol, 1,4-dihydroxybenzene, benzenesulfinic acid sodium salt and *p*-toluenesulfinic acid sodium salt hydrate) were reagent grade materials obtained from Aldrich and were used without further purification. All aqueous solutions were prepared with doubly distilled water. Supporting electrolyte solutions were made up from $NaCH_3COO$ and CH_3COOH that were pro-analysis grade from E. Merck. All experiments were carried out at room temperature.

2.2. Apparatus and procedure

Cyclic voltammograms were obtained with a 746 VA Trace Analyzer electrochemical system from Metrohm using a three-electrode electrochemical cell. The working electrode used in voltammetry was a glassy carbon disc (2 mm diameter) from Metrohm, and a platinum wire (Metrohm) was used as counter electrode. All potentials in voltammetry are quoted versus an Ag | AgCl | KCl (sat.) reference electrode. A personal computer was used for data storage and processing. Controlled potential coulometry and preparative electrolysis were performed using an Autolab PGSTAT 30 computer controlled potentiostat. The working electrode used in controlled potential macroscale electrolysis was an assembly consisting of two carbon rods (6 mm diameter and 5 cm length) and a large platinum sheet ($A \sim 4$ cm^2) constituted the counter electrode. The working electrode potential was adjusted versus a saturated calomel electrode (SCE).

2.3. Electroorganic synthesis of sulfones *3a*, *3b* and *6*, *7*

In a typical procedure, 40 ml of an aqueous solution containing 0.15 M sodium acetate as supporting electrolyte was pre-electrolyzed at 1.0 V (SCE) in a two compartment cell, then 1 mmol of **1a** or **1b** and 2 mmol of *p*-toluenesulfinic acid was added to the cell. The electrodes were washed with acetone several times during the electrolysis in order to remove their fouling by reaction products and to reactivate them. At the end of the electrolysis, the solutions were kept in the refrigerator (~ 2 °C) overnight. The precipitated solid was collected and purified as shown in Table 1. In the case of 1,4-dihydroxybenzen (**4**), 1 mmol of **4** and 2 mmol of **I** or **II** were added to 40 ml of 0.2 M acetic acid solution as supporting electrolyte. The performance of the electrolysis and the collection and purification of products were implemented similarly to the case of **1a** and **1b**. In both cases, after a charge consumption of about two electrons per molecule of quinone, (the coulombs required for total transformation of starting material to the products), the electrolysis was considered as terminated. Table 1 exhibits some information about the purification and the yield of the products.

2.4. Characteristics of the products

2.4.1. 4-(4-Toluenesulfonyl)-pyrocatechol (*3a*)

M.p. 182 °C. IR (KBr): ν_{max} 3593, 3493, 3245, 1503, 1455, 1387, 1302, 1155, 924, 824, 593, 577, cm^{-1}. ^1H-NMR, δ_{ppm} (DMSO-d_6): 9.5–10.5 (br, 2H, hydroxy protons); 7.70 (d, 2H, $J = 8.2$, C_6H_4–CH_3 ring), 7.36 (d, 2H, $J = 8.12$, C_6H_4–CH_3 ring), 7.20 (dd, 1H, $J = 2.27$, 8.3, pyrocatechol ring), 7.17 (d, 1H, $J = 2.24$, pyrocatechol ring), 6.85 (d, 1H, $J = 8.29$, pyrocatechol ring), 2.33 (s, 3H, methyl protons). Anal. Found: C, 59.03; H, 4.60. $C_{13}H_{12}O_4S$, Calc.: C, 59.07; H, 4.58%.

2.4.2. 5-(4-Toluenesulfonyl)-4-methylpyrocatechol (*3b*)

M.p. 159–160 °C. IR (KBr): ν_{max} 3439, 3269, 1503, 1518, 1449, 1294, 1148, 593 cm^{-1}. ^1H-NMR, δ_{ppm} (DMSO-d_6): 9.5–10.5 (br, 2H, hydroxy protons), 7.61 (d, 2H, $J = 8.16$, C_6H_4–CH_3 ring), 7.46 (s, 1H, hydroquinone ring), 7.37 (d, 2H, $J = 8.21$, C_6H_4–CH_3), 6.62 (s, 1H, hydroquinone ring), 2.34 (s, 3H, methyl pro-

Table 1
Preparative data

Conversion	Solvents used for purification by recrystallization	Product yield/%
1a–**3a**	Dichloromethane + toluene	87
1b–**3b**	Dichloromethane + toluene	94
4–**6**	Acetone + toluene	70
4–**7**	Acetone + toluene	80

tons), 2.13 (s, 3H, methyl protons). Anal. Found: C, 60.32; H, 5.01. $C_{14}H_{14}O_4S$, Calc.: C, 60.43; H, 5.03%.

2.4.3. 2-(4-Toluenesulfonyl)-hydroquinone (7)

M.p. 213–214 °C. IR (KBr): ν_{max} 3292, 1503, 1510, 1371, 1287, 1148, 824, 716 Cm^{1-}. ^{1}H-NMR δ_{ppm} (DMSO-d_6): 9.86 (s, 1H, hydroxy protons), 9.33 (s, 1H, hydroxy protons), 7.73 (d, 2H, $J=7.32$, C_6H_4–CH_3), 7.35 (d, 2H, $J=7.42$, C_6H_4–CH_3), 7.27 (d, 1H $J=2.18$, hydroquinone ring), 6.86 (dd, 1H, $J=3.0$, 8.7, hydroquinone ring), 6.68 (d, 1H, $J=8.74$, hydroquinone ring), 2.34 (s, 3H, methyl protons). Anal. Found: C, 57.32; H, 4.02. $C_{12}H_{10}O_4S$, Calc.: C, 57.6; H, 4%.

2.4.4. 2-Benzensulfonyl-hydroquinone (**6**)

M.p.195–196 °C. IR (KBr) ν_{max} 3300, 1510, 1454, 1294, 1148, 824, 739, 508, cm^{-1}. ^{1}H-NMR, δ_{ppm} (DMSO-d_6): 9.91 (s, 1H, hydroxy proton), 9.36 (s, 1H, hydroxy proton), 7.85 (d, 2H, $J=7.96$, C_6H_5), 7.63 (t, 1H, $J=7.18$, 7.56, C_6H_5) 7.55 (t, 2H, $J=7.71$, 7.64, C_6H_5), 7.29 (d, 1H, $J=3$, hydroquinone ring), 6.88 (dd, 1H, $J=3$,8, 7.4, hydroquinone ring), 6.70 (d, 1H, $J=8.75$, hydroquinone ring). Anal. Found: C, 58.86; H, 4.60. $C_{13}H_{12}O_4S$, Calc.: C, 59.90; H, 4.54%.

3. Results and discussion

3.1. Electrooxidation of catechol in the presence of *p*-toluenesulfinic acid

Sulfinic acids (RSO_2H) and their derivatives have been known as compounds with a propensity to disproportionate easily to thiosulfonate (RSO_2SR) and sulfonic acids (RSO_3H). However, there was some dispute concerning the rate of this process. There have been reports of essentially instantaneous reactions [22], whilst others have reported that the reaction takes about 20 months to complete [23]. The currently accepted mechanism for the disproportionation of sulfinic acids involves the path where sulfinyl and sulfonyl radicals are produced [24,25]. However, despite the tendency of sulfinic acid to disproportionate, it has been shown that it can participate, as an active nucleophile, in a Michael-type reaction with *p*-benzoquinone to give 2,5-dihydroxyphenylsulfone [26]. It has been claimed that the rate-determining step is the nucleophilic addition of sulfinate ion to the quinone ring at pHs lower than 3.1 [27]. Under such conditions, the electrosynthesis of sulfonated hydroquinones via electrooxidative production of related quinones may be achieved at lower pHs depending on the nature of the quinone and without the occurrence of nucleophile disproportionation.

In order to verify this assumption, the cyclic voltammetry of catechol **1a** in the absence and presence of *p*-toluenesulfinic acid (**I**) was studied as a function of scan rate in a solution containing 0.15 M sodium acetate. In the absence of nucleophile, the typical quasi-reversible behavior for the catechol–*o*-quinone system is obtained (Fig. 1, curve b) [1,28]. Under these conditions, nucleophile **I** exhibits only an irreversible peak at more positive potentials (Fig. 1, curve a).

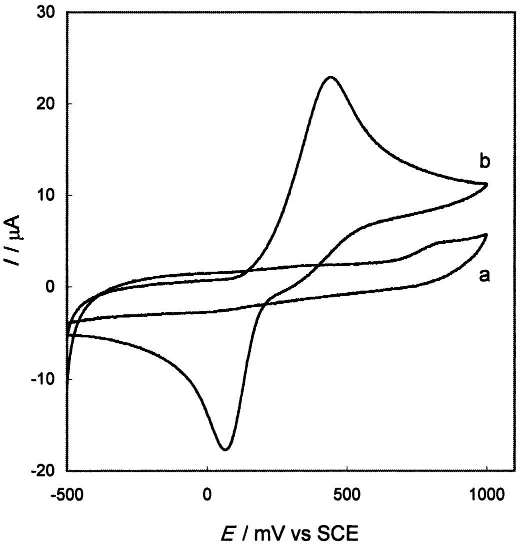

Fig. 1. Cyclic voltammetry of 1 mM (a) *p*-toluenesulfinic acid and (b) catechol at a glassy carbon electrode in 0.15 M sodium acetate solution. Scan rate: 100 mV s^{-1}.

The *o*-benzoquinone formed via oxidation can act as a Michael acceptor toward nucleophiles yielding substituted catechols [1–9]. This reaction can be followed by cyclic voltammetry. In the presence of 1 mM *p*-toluenesulfinic acid, the cathodic peak for the reduction of *o*-benzoquinone is nearly absent in scan rates below 600 mV s^{-1} and considerably diminished at higher scan rates (Fig. 2, curves a–f). Such behavior is an indicator of an EC mechanism [29] and is confirmed by plotting the anodic peak current function, $I_{pa}/v^{1/2}$, versus scan rate, v, and represented in inset A of Fig. 2. The height of the anodic peak in the second cycle is considerably reduced and no new cathodic or anodic peak appears indicating that the product of the EC reaction is electroinactive in the accessible potential range by virtue of its insolubility in the given solvent supporting electrolyte system. It is also deposited on the electrode surface, so that it inhibits the performance of the electrode process extensively (Fig. 3).

Controlled potential coulometry was performed in an aqueous solution containing 2 mM of **1a** and 4 mM of **I** at 1.0 V (SCE). Monitoring of the electrolysis progress was carried out by cyclic voltammetry (Fig. 4). As can be seen, the height of the anodic peak that is due to the electrooxidation of catechol in the presence of the nucleophile, is decreased as the electrolysis proceeds. After a charge consumption of about two electrons per molecule of **1a** the cyclic voltammogram (*c*) is obtained

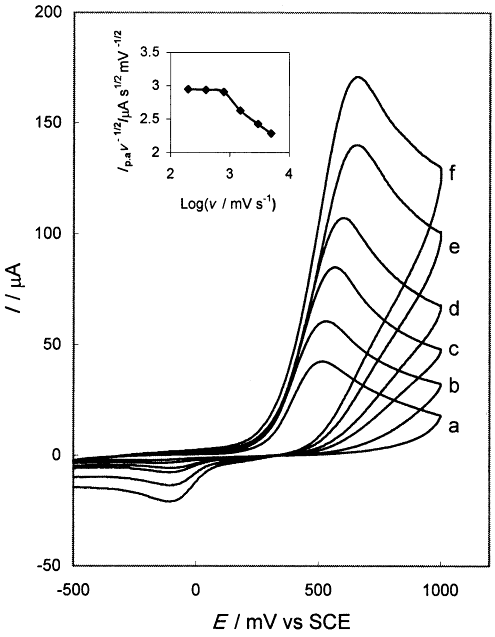

Fig. 2. Cyclic voltammograms of a solution containing 1 mM catechol and 1 mM p-toluenesulfinic acid at different scan rates at a glassy carbon electrode. Supporting electrolyte: 0.15 M sodium acetate. Scan rate: (a) 200, (b) 400, (c) 800, (d) 1500, (e) 3000 and (f) 5000 mV s^{-1}. Inset: The variation of current function ($I_{pa}/v^{1/2}$) as a function of scan rate (log v).

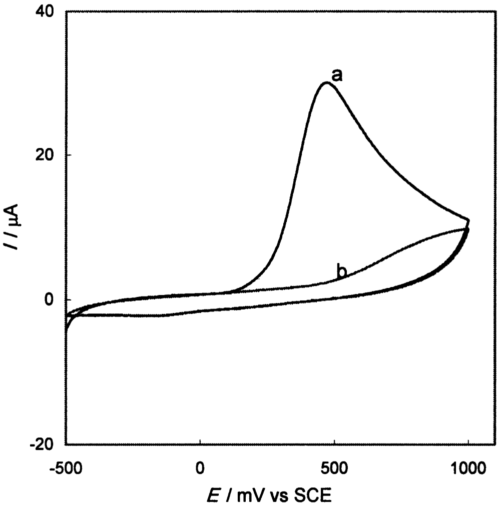

Fig. 3. Cyclic voltammograms of a solution containing 1 mM catechol and 1 mM p-toluenesulfinic acid at a glassy carbon electrode after: (a) first scan, (b) second scan. Supporting electrolyte: 0.15 M sodium acetate. Scan rate: 100 mV s^{-1}.

(Fig. 4). According to these observations and considering the mechanism proposed by Ogata et al. [26,27], we propose the following reaction pathway for the electrooxidation of **1a** in the presence of **I** (Scheme 1).

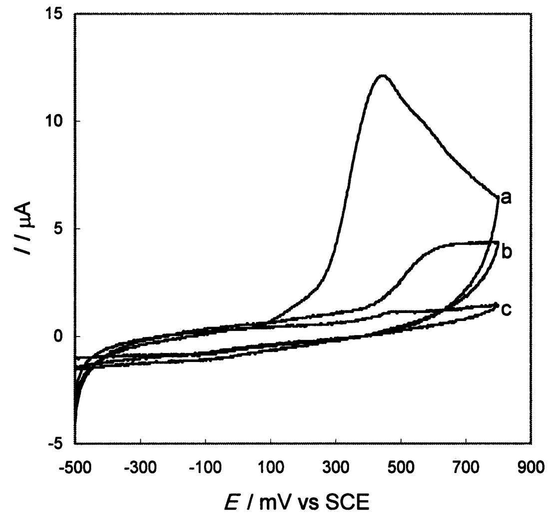

Fig. 4. Cyclic voltammograms of a solution containing 1 mM catechol and 2 mM p-toluenesulfinic acid at glassy carbon electrode: (a) at the beginning, (b) during and (c) at the end of electrolysis. Supporting electrolyte: sodium acetate 0.15 M. Scan rate: 50 mV s^{-1}.

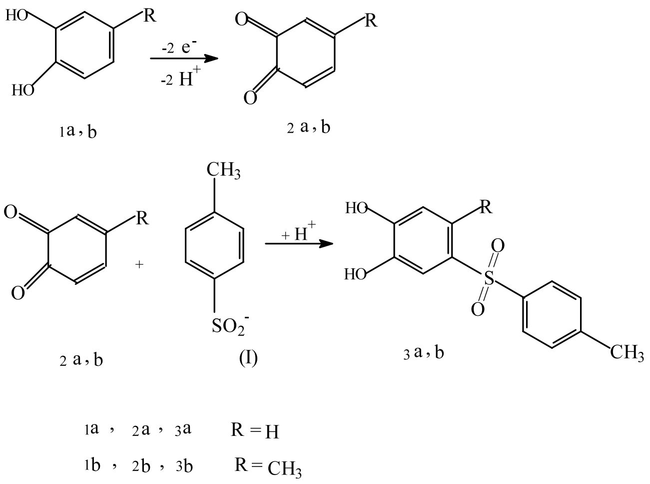

Scheme 1.

3.2. Electrooxidation of 4-methylcatechol (1b) in the presence of p-toluenesulfinic acid (I)

Fig. 5 shows the cyclic voltammograms of 4-methylcatechol in the presence and absence of p-toluenesulfinic acid in an aqueous sodium acetate solution as a solvent-supporting electrolyte system. As is shown, an anodic and a cathodic peak at 420 and ~10 mV versus Ag | AgCl | KCl (sat.) appears, respectively, due to the quasi-reversible transformation of 4-methylcatechol to 4-methyl-o-benzoquinone and vice versa, in the absence of a nucleophile (Fig. 5, curve a). The electrooxidation of 1 mM of **1b** in the presence of 1 mM of **I** proceeds in a way similar to that of **1a**. The presence of an electron donating methyl group has little effect on the reactivity of 4-methyl-o-benzoquinone formed (Fig. 5, curve b).

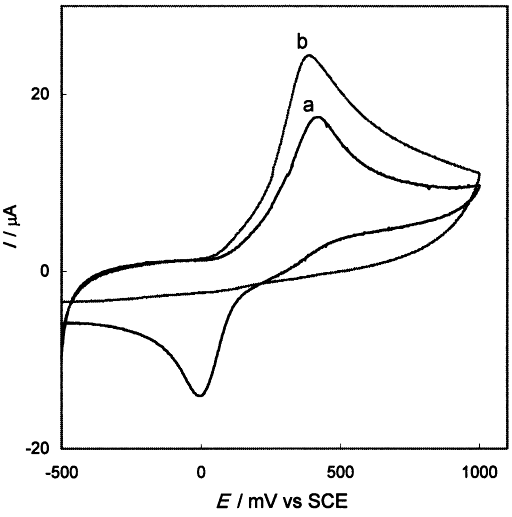

Fig. 5. Cyclic voltammograms of 1 mM 4-methylcatechol: (a) in the absence and (b) in the presence of 1 mM p-toluenesulfinic acid in 0.15 M sodium acetate solution. Scan rate: 100 mV s^{-1}.

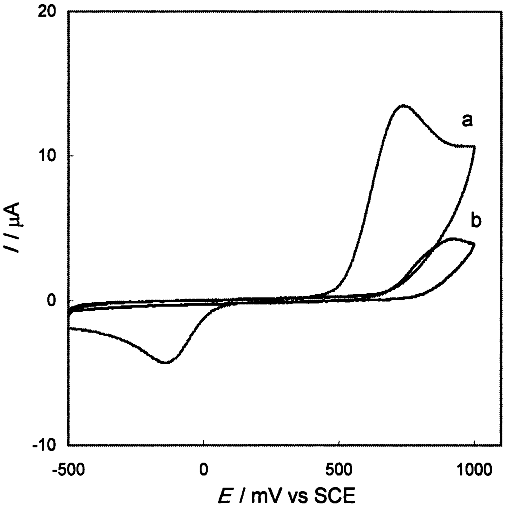

Fig. 6. Cyclic voltammograms of: (a) 1 mM 1,4-dihydroxybenzene and (b) 1 mM p-toluenesulfinic acid at a glassy carbon electrode in 0.20 M acetic acid solution. Scan rate: 100 mV s^{-1}.

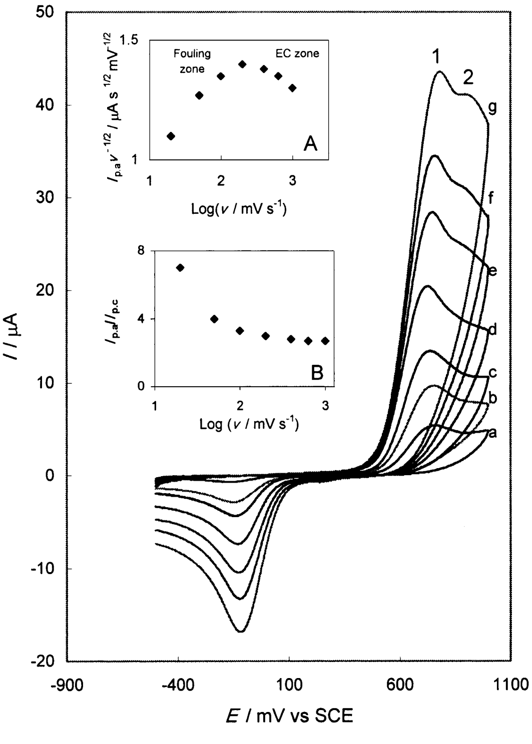

Fig. 7. Cyclic voltammograms of 1 mM 1,4-dihydroxybenzene in the presence of 1 mM p-toluenesulfinic acid at a glassy carbon electrode in 0.20 M acetic acid solution at scan rates: (a) 20, (b) 50, (c) 100, (d) 200, (e) 400, (f) 600, (g) 1000 mV s^{-1}. Inset A: variation of current function ($I_{pa}/v^{1/2}$) as a function of scan rate (log v). Inset B: variation of peak current ratio (I_{pa}/I_{pc}) as a function of scan rate (log v).

Similarly to **1a**, the occurrence of an EC mechanism is also confirmed by plotting the anodic peak current function, $I_{Pa}/v^{1/2}$ versus scan rate.

Cyclic voltammetry conducted during the electrolysis shows that parallel to the advancement of the coulometry, the height of the anodic peak that is due to the electrooxidation of 4-methylcatechol in the presence of **I** decreases. After a charge consumption of about two electrons per molecule of **1b**, the anodic peak disappears. The reaction pathway is similar to that of the catechol and leads to the compound **3b** (Scheme 1).

3.3. Electrooxidation of 1,4-dihydroxybenzene (*4*) in the presence of *p*-toluene-sulfinic acid (*I*)

Cyclic voltammetry of a 1 mM solution of 1,4-dihydroxybenzene in an aqueous solution containing 0.2 M acetic acid shows one anodic and a corresponding cathodic peak, with a peak separation of about 690 mV, corresponding to the transformation of 1,4-dihydroxybenzene to p-benzoquinone (**5**) and vice versa within a quasi-reversible two-electron process (Fig. 6, curve a). The peak current ratio, which is nearly constant, particularly during the repetitive cycling of potential, can be considered as a criterion for the stability of the p-benzoquinone produced at the surface of the electrode under the experimental conditions. The cyclic voltammogram of a 1 mM solution of p-toluenesulfinic acid shows an irreversible oxidation peak at more positive potentials (Fig. 6, curve b).

The electrooxidation of hydroquinone in the presence of **I** as a nucleophile in an aqueous solution was studied. Fig. 7 shows cyclic voltammograms obtained for a 1 mM solution of 1,4-dihydroxybenzene in the presence of 1 mM p-toluensulfinic acid (**I**) at different scan rates. It can be seen that the height of the cathodic counterpart of the 1,4-dihydroxybenzene oxidation peak increases proportionally to the increasing potential scan rate, which is indicative of a following chemical reaction by the oxidation product of **4**. At low scan rates, the

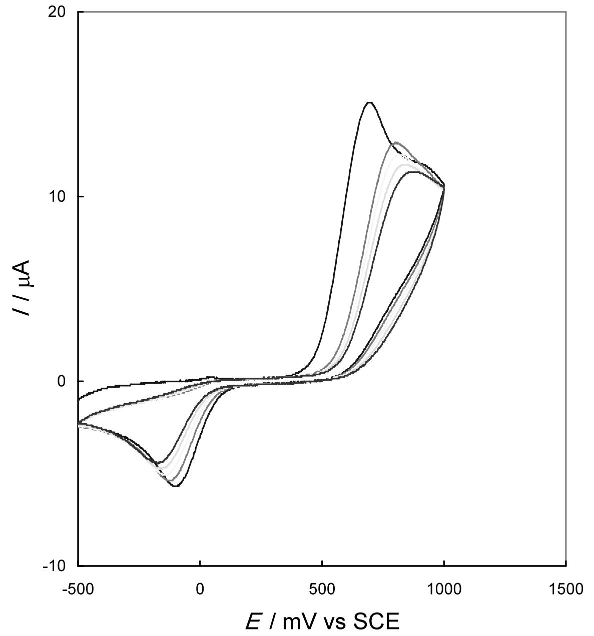

Fig. 8. Cyclic voltammograms of 1 mM 1,4-dihydroxybenzene in the presence of 1 mM p-toluenesulfinic acid in 0.20 M acetic acid solution during five repetitive potential cycles. Scan rate: 100 mV s^{-1}.

occurrence of an EC mechanism is fully confirmed by plotting the peak current ratio, I_{pa}/I_{pc}, versus scan rate, v. (Fig. 7, Inset (B). The multicyclic voltammetry of 1,4-dihydroxybenzene in the presence of **I** and at relatively low scan rates shows a decrease in the anodic and cathodic peak currents in parallel to the shift of the anodic and cathodic peaks in the positive and negative directions, respectively (Fig. 8). This behavior can be attributed to the deposition of the product at the electrode surface, and also there is no new anodic or cathodic peak that is indicative of electroinactivity of the product obtained under the experimental conditions. On the other hand, an increase of the potential sweep rate can diminish, to some extent, the progress of the following chemical reaction, which is manifested as a splitting in the anodic wave (Fig. 7, peaks 1 and 2 in curves e–g) and as a decrease in peak current function, $I_{pa}/v^{1/2}$, (Fig. 7, Inset A, EC zone). The two anodic peaks 1 and 2 in Fig. 7 correspond to the oxidation of **4** in the presence and in the absence of nucleophile **I** respectively. Inset A in Fig. 7 shows the variation of the anodic peak current function against scan rate. It is seen that the curve does not fully conform to an EC pattern. We believe that at low scan rates, the fouling of the electrode surface by the final product **6** or **7** makes it inactive for further progress of the electrode reaction and this provides a low value for the current function (Fig. 7, Inset A, fouling zone), whereas, at high scan rates, the fouling is partly suppressed and the peak current function begins to decrease proportionally to the sweep rate, which is indicative of an EC mechanism (Fig. 7, Inset A, EC zone). Controlled potential coulometry was performed in an aqueous solution containing 5 mM of **4** and 10 mM of **I** at 1.0 V (SCE). The progress of the electrolysis was monitored by cyclic voltammetry (Fig. 9). As can be seen, proportionally to the advancement of the coulometry, the anodic peak current of 1,4-dihydroxybenzene oxidation in the presence of **I** decreases and nearly disappears when the charge consumption becomes equal to about two electrons per molecule of 1,4-dihydroxybenzene. According to these results and the results obtained from the reaction of chemically generated p-benzoquinone with benzenesulfinic acid [30], we can propose the following pathway for the electrochemical oxidation of **4** in the presence of **I** (Scheme 2).

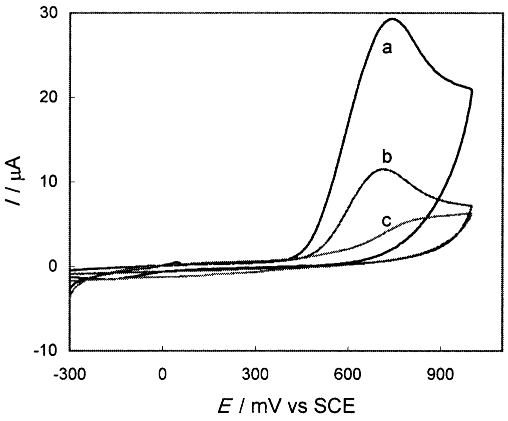

Fig. 9. Cyclic voltammograms of 1 mM 1,4-dihydroxybenzene in the presence of 2 mM p-toluenesulfinic acid in 0.20 M acetic acid solution: (a) before, (b) during and (c) at the end of electrolysis. Scan rate: 50 mV s^{-1}.

3.4. *Electrochemical oxidation of 1,4-dihydroxybenzene (**4**) in the presence of benzenesulfinic acid (**II**)*

The electrooxidation of **4** in the presence of benzenesulfinic acid as a nucleophile in water was studied by

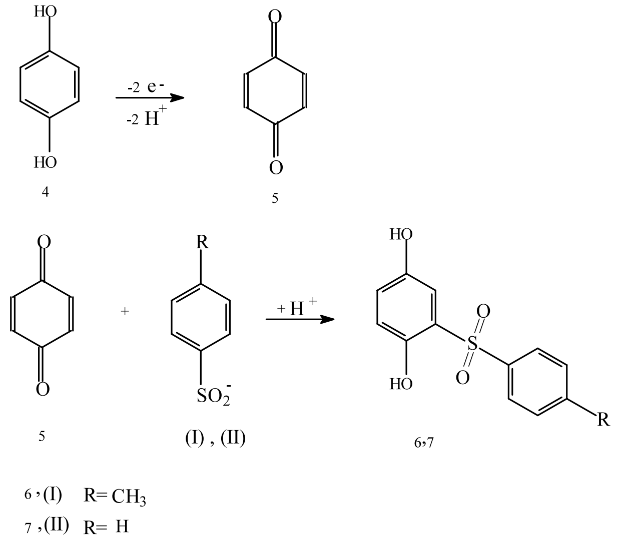

Scheme 2.

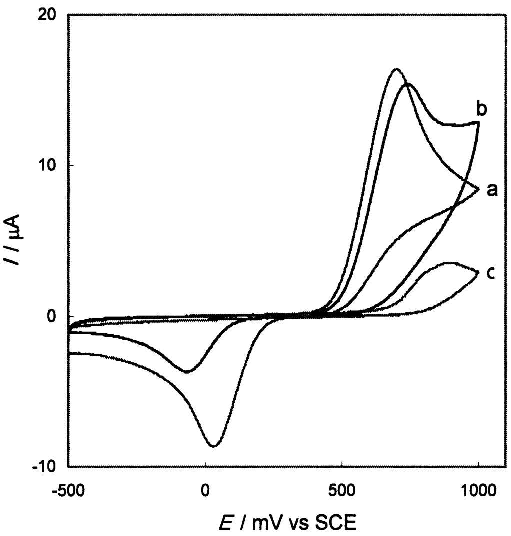

Fig. 10. Cyclic voltammograms of 1 mM 1,4-dihydroxybenzene (a) in the absence and (b) in the presence of 1 mM benzenesulfinic acid, (c)1 mM benzenesulfinic acid at a glassy carbon electrode in 0.20 M acetic acid solution. Scan rate: 100 mV s^{-1}.

cyclic voltammetry. Fig. 10 (curve a) shows the cyclic voltammogram of 1 mM **4** in an aqueous solution containing 0.2 M acetic acid. Similarly to the case of the electrooxidation of 1,4-dihydroxybenzene in the presence of *p*-toluenesulfinic acid, the cathodic peak height decreases significantly in the presence of **II**, while a small decrease is observed in the anodic peak. Moreover, both the anodic and cathodic peaks shift to more positive and more negative potentials, respectively, (Fig. 10, curve b). These observations are again in agreement with the occurrence of a following chemical reaction via an EC mechanism and also confirm the electrode surface fouling following the deposition of an electroinactive product formed during the electrode process. From the results obtained, a reaction pathway similar to the electrooxidation of **4** in the presence of **I** is proposed for the electrooxidation of **4** in the presence of **II** (Scheme 2).

At the end of this section, a brief discussion about the pH change in the anodic compartment during the progress of electrolysis seems to be interesting. On the basis of Schemes 1 and 2, the solution pH decreases during the progress of electrolysis following the release of protons in the course of *o*- and *p*-hydroquinone oxidation. Indeed, the Michael addition reaction presented in Scheme 2 should be carried out at lower pHs which is necessary for the protonation of the *p*-benzoquinone produced and its activation as a Michael acceptor [31]. Owing to this requirement, the optimum pH for nucleophilic addition of sulfinate ion to the *p*-benzoquinone ring was indicated to be lower than 3.1 [27]. The acidity constants, (pK_A), of benzenesulfinic and *p*-toluenesulfinic acids were reported as 1.45 and 1.55, respectively [32]. Accordingly, when sodium acetate (0.15 M) was used as the supporting electrolyte, the pH of the anodic compartment, containing 0.025 M *o*-hydroquinone and 0.05 M arylsulfinate ion, is about 8.9 at the beginning of the coulometry and decreases slowly in the course of electrolysis. The measured pH at the end of the electrolysis was 5.4, whereas, in the case of *p*-hydroquinone, acetic acid (0.20 M) was used as the supporting electrolyte, and the solution pH was measured as about 2.9 and 1.6 at the beginning and at the end of the coulometry, respectively. The use of two different supporting electrolytes with different pHs relates to the fact that *o*-quinones are more active acceptors than *p*-quinones and the latter compounds need a lower pH than the former for protonation.

4. Conclusion

The results obtained here show that the *o*- and *p*-benzoquinones obtained from the oxidation of corresponding hydroquinones can easily be attacked in an aqueous solution by sulfinic acids in the sequence of a Michael addition reaction. A mechanism is proposed for the nucleophilic attack of these nucleophiles to electrochemically generated *o*- and *p*-benzoquinones. It is shown that the presence of a methyl group with electron donating character has little effect on the reactivity of 4-metylcatechol in the presence of sulfinic acids.

Acknowledgements

The authors wish to express their gratitude to Tabriz University Research Council for the financial support of this work.

References

[1] D. Nematollahi, S.M. Golabi, J. Electroanal. Chem. 405 (1996) 133.
[2] D. Nematollahi, S.M. Golabi, J. Electroanal. Chem. 481 (2000) 208.
[3] S.M. Golabi, D. Nematollahi, Bull. Electrochem. 13 (1997) 156.
[4] S.M. Golabi, D. Nematollahi, J. Electroanal. Chem. 420 (1997) 127.
[5] S.M. Golabi, D. Nematollahi, J.Electroanal. Chem. 430 (1997) 141.
[6] D. Nematollahi, S.M. Golabi, Bull. Electrochem. 14 (1998) 97.
[7] I. Tabakovic, Z. Grujic, Z. Bejtovic, J. Heterocycl. Chem. 20 (1983) 635.
[8] M.A. Azzem, M. Zahran, E. Haggag, Bull. Chem. Soc. Jpn. 67 (1994) 1390.
[9] D. Nematollahi, S.M. Golabi, Iranian J. Sci. Technol., Trans. A 21 (1997) 121.
[10] L. Papouchado, G. Petrie, J.H. Sharp, N. Adams, J. Am. Chem. Soc. 90 (1968) 5620.
[11] F. Caturla, C. Najera, Tetrahedron 53 (1997) 11449.
[12] V.K. Aggarwal, A. Ali, M.P. Coogan, Tetrahedron 55 (1999) 293.

[13] N.E. Prilezhaeva, Russ. Chem. Rev. 69 (2000) 367.

[14] N.S. Simpkins, Sulfones in Organic Synthesis, Pergamon Press, Oxford, 1993.

[15] N.S. Simpkins, Tetrahedron 46 (1990) 6951.

[16] P.E. Reddy, R.M.V. Reddy, PCT Int. Appl. WO9918068 (1999) (Chem. Abstr. 1999 130: P 281870).

[17] J.K. Konopa, M.T. Konieczny, B.J. Horowska, A.J. Kunikowski, T. Asao, H. Nishino Y. Yamada, Jpn. Patent JP 9003037 (1997) (Chem. Abstr., 1997, 126:P 185889).

[18] D. Pathak, K. Pathak, A.K. Singla, Fitoterapia 62 (1991) 371.

[19] A. Das, J.H. Wang, E.J. Lien, Prog. Drug Res. 42 (1994) 134.

[20] D.N. Dhar, The Chemistry of Chalcones and Related Compounds, Wiley, New York, 1981.

[21] H.W. Wanzlik, M.L. Horchler, S. Mohmann, R. Gritzky, H. Heiderpriem, P. Pankow, Angew. Chem. Int. Ed. 3 (1964) 401.

[22] H.J. Barber, S. Smiles, J. Chem. Soc. (1928) 1141.

[23] C. Pauly, R. Otto, Chem. Ber. 10 (1877) 2181.

[24] J.L. Kice, B.R. Toth, D.C. Hampton, J.F. Barbour, J. Org. Chem. 31 (1966) 848.

[25] M. Kobayashi, H. Minato, Y. Ogi, Bull. Chem. Soc. Jpn. 45 (1972) 1224.

[26] Y. Ogata, Y. Sawaki, M. Isono, Tetrahedron 25 (1969) 2715.

[27] Y. Ogata, Y. Sawaki, M. Isono, Tetrahedron 26 (1970) 731.

[28] Z. Grujic, I. Tabakovic, M. Trokovnik, Tetrahedron Lett. (1976) 4823.

[29] A.J. Bard, L.R. Faulkner, Electrochemical Methods, Fundamentals and Applications, second ed., Wiley, New York, 2001, p. 496.

[30] J.M. Bruce, P.L. Williams, J. Chem. Soc., Perkin Trans. 1 (1992) 2877.

[31] J.D. Bu'Lock, J. Harley-Mason, J. Chem. Soc. (London) (1951) 703.

[32] S. Patai (Ed.), The Chemistry of Sulfinic Acids, Esters and their Derivatives, Wiley, New York, 1990, p. 276.

Appendix IV:

Electrosynthesis of organic compounds: II. Electrooxidative amination of 1,4-dihydroxybenzene using some aliphatic amines.

S. M. Golabi, F. Nourmohammadi, A. Saadnia.

J. Electroanal Chem., 548, 2003, 41.

Available online at www.sciencedirect.com

SCIENCE DIRECT

Journal of Electroanalytical Chemistry 548 (2003) 41–47

Journal of Electroanalytical Chemistry

www.elsevier.com/locate/jelechem

Electrosynthesis of organic compounds. Part II: Electrooxidative amination of 1,4-dihydroxybenzene using some aliphatic amines

S.M. Golabi[a,*], F. Nourmohammadi[a], A. Saadnia[b]

[a] *Electroanalytical Chemistry Laboratory, Faculty of Chemistry, University of Tabriz, Tabriz, Iran*
[b] *Organic Synthesis Laboratory, Faculty of Chemistry, University of Tabriz, Tabriz, Iran*

Received 2 September 2002; received in revised form 17 February 2003; accepted 8 March 2003

Abstract

The electrooxidative amination of 1,4-dihydroxybenzene (**1**) to give 2,5-disubstituted benzoquinones, using dimethylamine, piperidine and morpholine, as nucleophiles has been studied using cyclic voltammetry and controlled potential coulometry. The results indicate that the above-mentioned amines react with electrochemically generated *p*-benzoquinone via a Michael-addition reaction leading to 2,5-diamino-substituted benzoquinones. Products were obtained in good yield and purity, and were characterized by spectroscopic methods and elemental analysis.

Keywords: Electrooxidative amination; Cyclic voltammetry; Michael addition; *p*-Benzoquinone; Dimethylamine; Piperidine; Morpholine

1. Introduction

The addition of amines to 1,4-benzoquinone to yield 2,5-bis-(dialkylamino)-benzoquinones is one of the earliest reported instances of the addition of an amine nucleophile to a quinone [1,2]. Literature investigations show that in the usual procedure for the preparation of bis-(dialkylamino)-quinones from *p*-benzoquinone, two-thirds of the quinone is employed as an oxidizing agent so that, at the best, only around 30% of the starting material can be isolated as the product, i.e. the disubstituted quinone. It has been claimed that re-oxidation of the intermediates can be accomplished by a stoichiometric amount of cupric salt or by a smaller quantity when the reaction mixture is stirred with oxygen, and this procedure is preferable since the product crystallizes in virtually pure form from solution and uncontaminated by cuprous salts [3]. However, to the best of our knowledge, the electrosynthesis of aminoquinones has not yet been reported in the literature. A series of aminoquinones was desired for testing as possible antimalarial or antitumoral agents [4], and because of the advantages of synthesis by electrochemical methods it was of interest to study the applicability of electrochemical procedures for the preparation of this kind of disubstituted benzoquinone.

In this work, we investigated first the electrochemical behavior of 1,4-dihydroxybenzene in the presence of dimethylamine, piperidine and morpholine, and then we report the reactions involving the addition of these amines to the electrochemically generated *p*-benzoquinone to yield 2,5-disubstituted benzoquinones (**2**), (**3**) and (**4**), respectively. IR, ^{1}H-NMR, ^{13}C-NMR, mass spectrometry and elemental analysis were used to characterize the products.

2. Experimental

2.1. Chemicals

All chemicals (1,4-dihydroxybenzene, dimethylamine, piperidine and morpholine) were reagent grade materials obtained from Aldrich. Amines were distilled before

---

* Corresponding author. Fax: +98-411-3340191.
E-mail address: golabi@tabrizu.ac.ir (S.M. Golabi).

0022-0728/03/$ - see front matter
doi:10.1016/S0022-0728(03)00218-3

use. Supporting electrolyte solutions were made up from CH_3COOK that was pro-analysis grade from E. Merck. All experiments were carried out at room temperature using methanol and ethanol (p.a. grade) as the solvents of choice.

2.2. Apparatus and procedure

Cyclic voltammograms were obtained with a 746 VA Trace analyzer electrochemical system from Metrohm using a three-electrode electrochemical cell. The working electrode used in voltammetry was a glassy carbon disc (2 mm diameter) from Metrohm, and a platinum wire (Metrohm) was used as a counterelectrode. All potentials in voltammetry are quoted vs. Ag | AgCl (sat.) | KCl (sat.) reference electrode, whereas the reference electrode used in macroscale electrolysis and coulometry was the saturated calomel electrode (SCE). A personal computer was used for data storage and processing. Controlled potential coulometry and preparative electrolysis were performed using an Autolab PGSTAT 30 computer controlled potentiostat. The working electrode used in controlled potential macroscale electrolysis was an assembly consisting of two carbon rods (6 mm diameter and 5 cm length) and a large platinum sheet ($A \sim 4$ cm^2) constituted the counterelectrode. The working electrode potential was adjusted vs. SCE and at a value appropriate to the transformation of (**1**) to the anticipated diamino products.

2.3. Electroorganic synthesis of 2,5-bis(dimethylamino)- (2) and 2,5-dipiperidino- (3) benzoquinones

In a typical procedure, 40 ml of a methanolic solution containing 0.15 M potassium acetate as supporting electrolyte was pre-electrolyzed at 0.8 V vs. SCE in an undivided cell. Then, 1 mmol of (**1**) and 6 mmol of dimethylamine or piperidine were added to the cell. After a charge consumption of about 6 electrons per mole of hydroquinone, (the coulombs required for total transformation of starting material to the products), the electrolysis was considered as terminated. The electrolyzed solutions were evaporated under reduced pressure. In the case of the product (**2**), an aliquot of water (about 15 ml) was added to the residue. The mixture was extracted three times with toluene (about 60 ml) and was dried over anhydrous sodium sulfate. The extract was evaporated under reduced pressure and the remaining solid was purified by flash chromatography over silica gel (230–400 mesh) using a toluene+acetone (4:1) mixture as the solvent. The pure solid obtained from column chromatography was recrystallized in toluene giving dark purple needle crystals. In the case of product (**3**), the evaporated solution was extracted several times with toluene and then chromatographed as above, but a (3:1) mixture of toluene+acetone was used as eluent. The pure product obtained was recrystallized in toluene to yield black colored crystals. The calculated yield of the electrosynthesis was 50 and 73% for (**2**) and (**3**), respectively.

2.4. Electroorganic synthesis of 2,5-dimorpholinobenzoquinone (4)

Controlled potential macroelectrolysis of 1 mmol of (**1**) and 6 mmol of morpholine in ethanol containing 0.15 M CH_3COOK as supporting electrolyte was performed at 1.0 V vs. SCE in order to synthesize (**4**). At the end of the electrolysis (i.e. after a charge consumption of about 6 electrons per mole of the starting hydroquinone), the sparingly soluble product was filtered and washed several times with boiling ethanol. The brick-red solid was dissolved in boiling toluene. The red solution was kept at room temperature and the product (**4**) was recrystallized as red needle crystals.

2.5. Characteristics of the products

2.5.1. 2,5-Bis(dimethylamino)-p-benzoquinone (2)

M.p. 172.5–174.5 °C (literature: 173 °C [2]). IR (CCl_4): v_{max} 1630, 1555, 1275 and 1140 cm^{-1}. ^{1}H-NMR (400 MHz, $CDCl_3$), δ ppm: 5.36 (s, 2H, quinone ring); 3.20 (s, 12H, CH_3). ^{13}C-NMR (100 MHz, $CDCl_3$), δ ppm: 42.5 (CH_3), 101.8 (C3, =CH–), 152.2 (C2, C=N–), 181.5 (C1, C=O). MS: m/z 194. Anal. Found for $C_{10}H_{14}N_2O_2$: C, 61.92; H, 7.18; N, 14.38. Calc.: C, 61.86; H, 7.22; N, 14.43%.

2.5.2. 2,5-Dipiperidino-p-benzoquinone (3)

M.p. 178.4–180.4 °C (literature: 179–180 °C [1]). IR (CCl_4): v_{max} 2935, 1625, 1550, 1225, 1180 and 1120 cm^{-1}. ^{1}H-NMR (400 MHz, $CDCl_3$), δ ppm: 1.64–1.71 (m, 12H, $-CH_2CH_2CH_2-$), 3.51–3.57 (m, 8H, $-CH_2NCH_2-$), 5.53 (s, 2H, quinone ring); ^{13}C-NMR (100 MHz, $CDCl_3$), δ ppm: 24.2 (C4′, piperidine), 25.8 (C3′, pip.), 50.3 (C2′, pip.), 105.4 (C3, quinone), 153.1 (C2, qui.), 182.4 (C1, C=O). MS: m/z 274. Anal. Found for $C_{16}H_{22}N_2O_2$: C, 70.13; H, 8.01; N, 10.18. Calc.: C, 70.07; H, 8.03; N, 10.22%.

2.5.3. 2,5-Dimorpholino-p-benzoquinone (4)

M.p. 238–243 °C (literature: 232–238 °C [1]). IR (KBr): v_{max} 2900, 1635, 1565, 1440, 1295, 1205, 1115 and 935 cm^{-1}. ^{1}H-NMR (400 MHz, $CDCl_3$), δ ppm: 3.54 (t, $J = 4.8$, 8H, $-CH_2N-$), 3.81 (t, $J = 4.8$, 8H, $-CH_2O-$), 5.54 (s, 2H, quinone ring). ^{13}C-NMR (100 MHz, $CDCl_3$), δ ppm: 49 ($N-CH_2$), 6.65 ($-CH_2O-$), 107 (C3, quinone), 152.2 (C2, qui.), 182.7 (C1, C=O). MS: m/z 278. Anal. Found for $C_{14}H_{18}N_2O_4$: C, 60.50; H, 6.49; N, 10.04. Calc.: C, 60.44; H, 6.47; N, 10.07%.

3. Results and discussion

3.1. Electrooxidation of 1,4-dihydroxybenzene in the absence and presence of dimethylamine

Fig. 1 shows the cyclic voltammograms of a 1 mM solution of 1,4-dihydroxybenzene (**1**) in methanol containing 0.1 M CH_3COOK as supporting electrolyte and at different scan rates. As can be seen, at a low-enough scan rate there is one positive peak at about 0.34 V vs. Ag | AgCl | KCl (sat.) and no negative counterpart is observed. We assign this positive peak to the oxidation of (**1**) to *p*-benzoquinone (curve 1). With increasing scan rate, however, one negative peak appears at about −0.14 V and grows gradually. This peak can be related to the reduction of positively generated *p*-benzoquinone. Such a situation is indicative of a coupled chemical reaction that follows the two-electron oxidation of (**1**) and is observed when the time scale of the experiment and the rate of the chemical reaction are comparable. This behavior is fully confirmed by plotting the variation of peak current function, $I_{pa}/v^{1/2}$, and also that of the peak current ratio, I_{pa}/I_{pc}, vs. the scan rate, $\log v$, (insets A and B of Fig. 1). The following chemical reaction can be related to the methoxylation of the electrochemically generated *p*-benzoquinone under the experimental conditions, producing methoxyhydroquinones [5,6]. However, the peak current ratio is nearly constant at higher scan rates, particularly during the repetitive cycling of potential, which shows that any methoxylation or dimerization reactions are too slow to be observed on the time scale of the cyclic voltammetry. The oxidation of methoxylated hydroquinones is somewhat easier than the oxidation of the parent starting molecule (**1**) due to the presence of the electron-rich methoxy group on the quinone ring. Thus, it may be possible that the oxidation of these methoxyhydroquinones takes place also through a solution electron transfer reaction producing the methoxylated quinone and parent hydroquinone (**1**). Moreover, because of the poor electron-withdrawing character of *p*-benzoquinone in comparison with *o*-benzoquinone, the concentration of methoxy-*p*-quinone produced during the voltammetric experiment will be lower than that of methoxy-*o*-quinone, and this may be the reason why the reduction peak of this product could not be seen even at lower sweep rates on the reverse scan, contrary to that reported for methoxy-*o*-quinone [5].

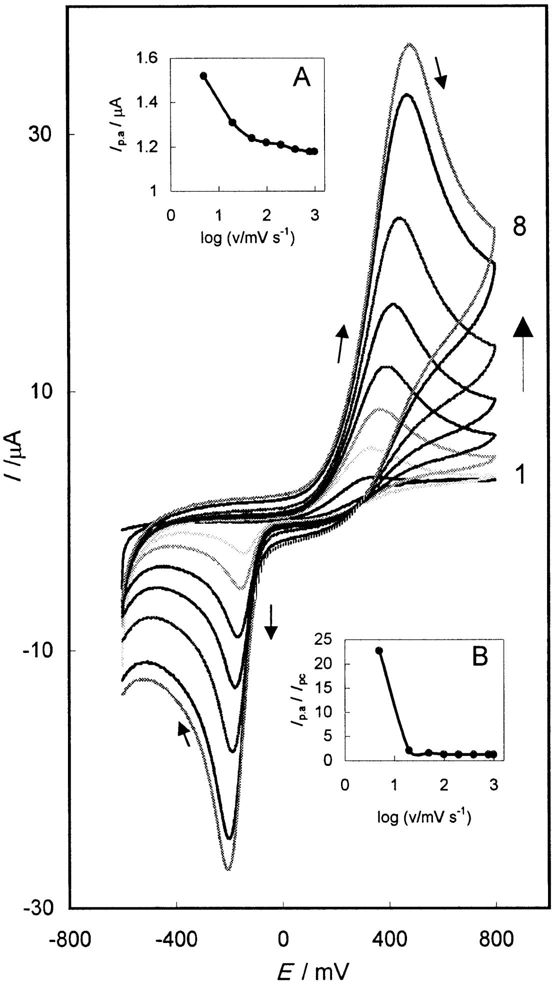

Fig. 1. Cyclic voltammograms of a 1 mM solution of 1,4-dihydroxybenzene in methanol containing 0.10 M CH_3COOK as supporting electrolyte and at scan rates: (1) 5, (2) 20, (3) 50, (4) 100, (5) 200, (6) 400, (7) 800 and (8) 1000 mV s^{-1}. Initial potential: −600 mV vs. ref. Inset A: variation of positive peak current, I_{pa}, vs. scan rate, $\log v$. Inset B: variation of peak current ratio, I_{pa}/I_{pc}, vs. scan rate.

Fig. 2 shows the cyclic voltammograms of a 1 mM solution of (**1**) in methanol containing 0.1 M CH_3COOK as supporting electrolyte in the presence of three different concentrations of dimethylamine. Dimethylamine is not electroactive under experimental conditions. At a scan rate of 20 mV s^{-1} and in the presence of dimethylamine, the positive oxidation peak of (**1**) is broadened and shifted a little toward less positive potentials with increasing concentrations of dimethylamine (curves b–d). On the reverse scan, three negative cathodic peaks (c_1, c_2 and c_3) appear at E_p values of −0.140, −0.395 and −0.535 V, respectively. With increase of the amine concentration, the height of peak c_1 decreases with a concomitant increase in the c_2 and c_3 peak heights. Furthermore, with increasing potential scan rates, the height of the negative peak c_1 increases, while that of peaks c_2 and c_3 decreases. Fig. 3 also shows the cyclic voltammograms of 1 mM of (**1**) in the presence of 6 mM of dimethylamine at different scan rates. Here, it is seen that, with increasing scan rate the c_1/c_2 peak ratio increases. These observations indicate that *p*-benzoquinone formed via two-electron oxidation of (**1**) participates in a following chemical reaction with dimethylamine. This behavior is fully confirmed by plotting the variation of positive peak current function, $I_{pa}/v^{1/2}$, vs. the scan rate, $\log v$, corresponding to the

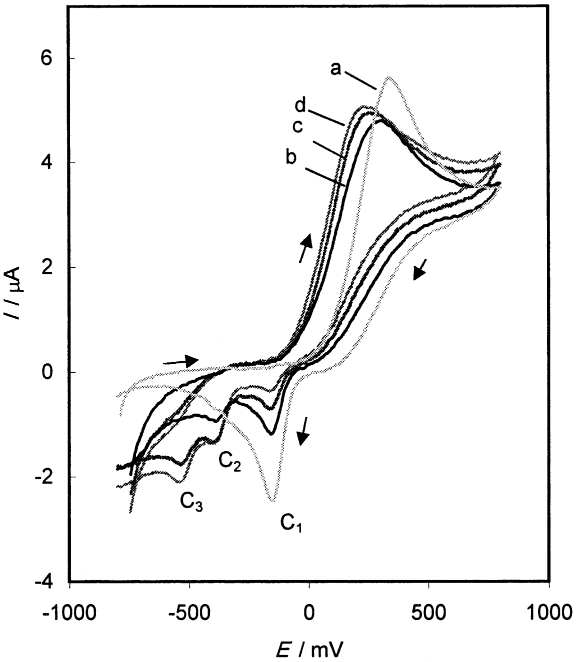

Fig. 2. Cyclic voltammograms of 1 mM 1,4-dihydroxybenzene (a) in the absence and in the presence of (b) 2 mM, (c) 4 mM and (d) 6 mM dimethylamine in methanol containing 0.10 M CH_3COOK as supporting electrolyte. Scan rate: 20 mV s^{-1}. Initial potential: −750 mV vs. ref.

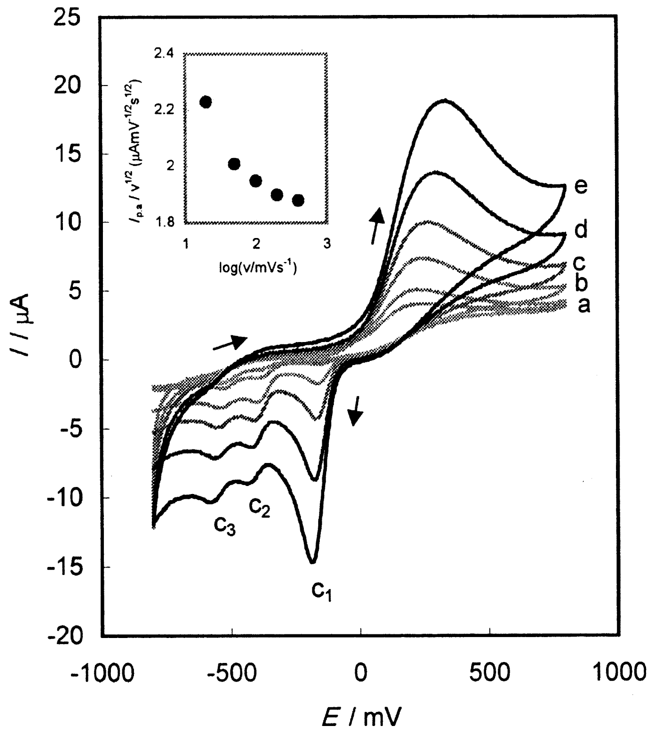

Fig. 3. Cyclic voltammograms of 1 mM 1,4-dihydroxybenzene in the

diagnostic criteria for an ECE mechanism (inset of Fig. 3) [7]. On the other hand, controlled potential coulometry of (**1**) in the presence of an adequate concentration of dimethylamine and at the potential of 0.8 V vs. SCE gave *n* value of about 6. Moreover, the comparison of voltammograms recorded at the beginning and at the end of the coulometry indicates that the final product of electrolysis can reduce at about −0.690 V (peak c_3) and the corresponding positive peak appears at about −0.130 V in reverse scan (peak a_3). Under these conditions, the positive peak a_3 (Fig. 4, curve 2) should appear as a shoulder of peak a_1 on the voltammogram recorded at the beginning of the coulometry (Fig. 4, curve 1); while the positive counterpart of peak c_2 (i.e. a_2) will be covered by peak a_1. Such behavior suggests that the reactions between dimethylamine and electrochemically produced *p*-quinones are slow enough. Cyclic voltammograms recorded during the electrolysis show clearly the progressive decrease of the a_1 peak height and the growth of the new peak a_3. These observations allow us to propose the following ECECE mechanism for electrochemical oxidation of 1,4-dihydroxybenzene in methanol and in the presence of dimethylamine:

E: $H_2Q \longrightarrow Q + 2H^+ + 2e^-$

C: $Q + A \longrightarrow H_2Q\text{-}A$

E: $H_2Q\text{-}A \longrightarrow Q\text{-}A + 2H^+ + 2e^-$

C: $Q\text{-}A + A \longrightarrow H_2Q\text{-}A_2$

E: $H_2Q\text{-}A_2 \longrightarrow Q\text{-}A_2 + 2H^+ + 2e^-$

(A denote amines).

Scheme 1.

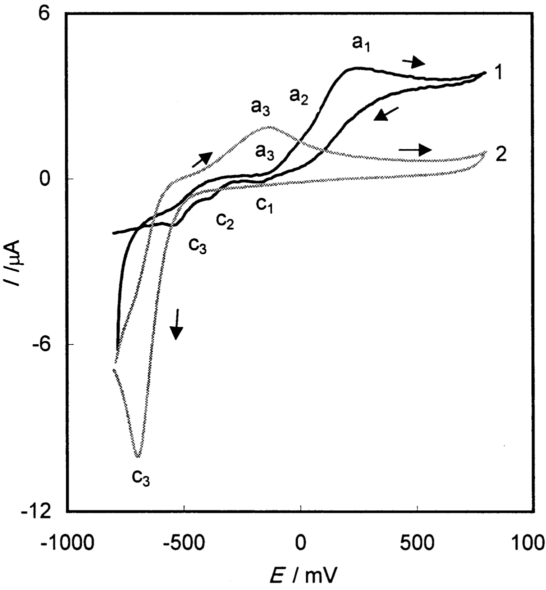

Fig. 4. Cyclic voltammograms of a 1 mM solution of 1,4-dihydroxybenzene in methanol containing 6 mM dimethlamine as the nucleophile and 0.10 M CH_3COOK as supporting electrolyte, (1) at the beginning and (2) at the end of coulometry at 800 mV vs. SCE. Scan rates: 20 mV s^{-1}. Initial potential: −800 mV vs. ref.

As mentioned above, the following chemical reactions (2) and (4) are sufficiently slow, resulting in a very low concentration of the product (**2**) (i.e. H_2Q-A_2) during cyclic voltammetry. So, at very low scan rates, it diffuses away from the electrode surface and the corresponding negative peak (i.e. c_3) is not observed in the reverse scan. This is also true for the product of the reaction (3) at low scan rates. With an increase of the scan rate, peak c_2, due to the reduction of Q−A, appeared at more negative potentials, but the peak c_3 which is due to the reduction of product (**2**), again disappears. This is because, with increasing potential sweep rate, the progress of the reaction (4) becomes more and more difficult and so the concentration of (**2**) decreases significantly.

*3.2. Electrooxidation of 1,4-dihydroxybenzene (**1**) in the presence of piperidine*

Fig. 5 shows the cyclic voltammograms representative of the behavior of 1,4-dihydroxybenzene (1 mM) in the absence and in the presence of three different concentrations of piperidine in methanol containing 0.1 M CH_3COOK as supporting electrolyte.

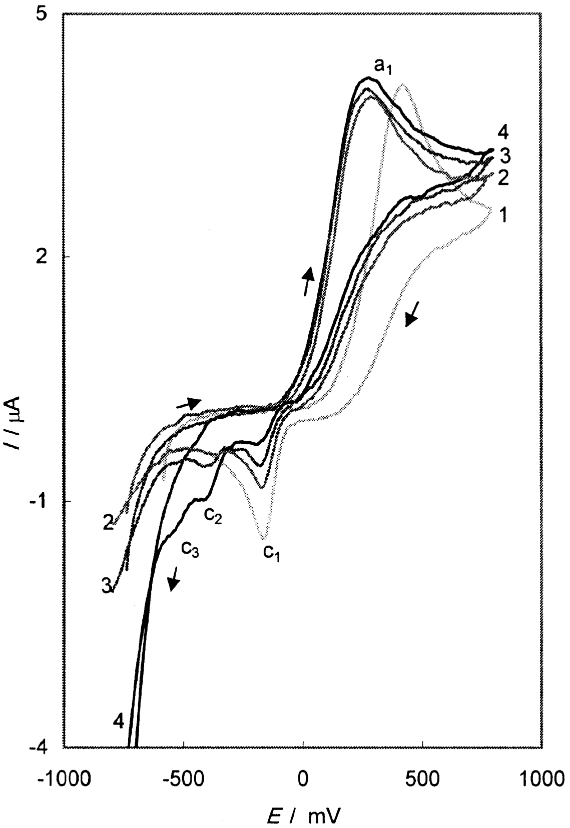

Fig. 5. Cyclic voltammograms of a 1 mM solution of 1,4-dihydroxybenzene in methanol containing 0.10 M CH_3COOK as supporting electrolyte, (1) in the absence and in the presence of (2) 2 mM, (3) 4 mM and (4) 6 mM piperidine as the nucleophile. Scan rate: 20 mV s^{-1}. Initial potential: −800 mV vs. ref.

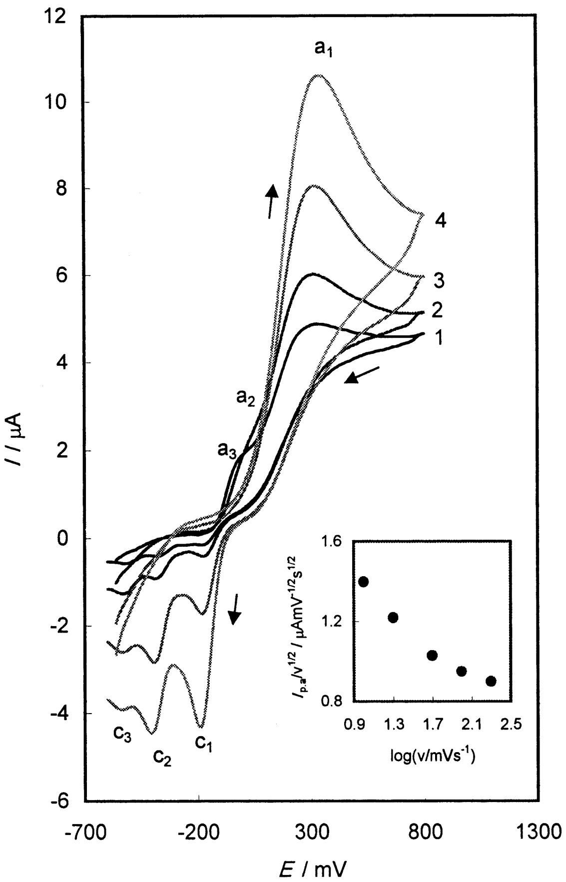

Fig. 6. Cyclic voltammograms of 1 mM 1,4-dihydroxybenzene in the presence of 6 mM piperidine in methanol containing 0.10 M CH_3COOK as supporting electrolyte and at scan rates: (1) 10, (2) 20, (3) 50 and (4) 100 mV s^{-1}. Initial potential: −600 mV vs. ref. Inset shows the variation of positive peak current, $I_{pa}/v^{1/2}$, vs. scan rate, $\log v$.

Similarly to the previous case, the c_1 negative peak height, which is due to the reduction of *p*-benzoquinone formed during the anodic oxidation of 1,4-dihydroxybenzene, decreases in the presence of piperidine, parallel with the appearance of two new negative peaks c_2 and c_3. With the increase of the concentration of piperidine, c_1 disappears at lower scan rates while the c_2 and c_3 peak heights increase. Furthermore, in the presence of a given concentration of piperidine, with increasing potential scan rate, the c_1 peak height increases with a concomitant decrease in the c_2 negative peak height and the disappearance of peak c_3 (Fig. 6). The inset of Fig. 6 shows the variation of the a_1 peak current function, $I_{pa}/v^{1/2}$, as a function of scan rate ($\log v$). The decrease of peak current function with the scan rate increase suggests clearly the involvement of an ECE mechanism in the electrode process. Moreover, the peak a_3, which corresponds to the oxidation of (**1**)–(**3**), appears only at low scan rates indicating the slow kinetics of the following chemical reactions. Based on these observations and considering the results obtained from the analysis of spectroscopic data, we can propose a mechanism similar to that shown in Scheme 1 for the electrooxidation of (**1**) in the presence of piperidine.

On the basis of the cyclic voltammetric data and owing to the low nucleophilicity of piperidine in comparison with that of dimethylamine, we conclude that the second chemical reaction (i.e. the addition of the second piperidine molecule to the *p*-benzoquinone produced) is sufficiently slow, leading to the formation of a very low concentration of dipiperidino-*p*-benzoquinone at the electrode surface. This brings about the appearance of the c_3 peak only at very low scan rates and in the presence of higher concentrations of piperidine. However, on the longer time scale of macroscale electrolysis, the conditions are favorable for the completion of the second chemical reaction and the dipiperidino product is obtained.

3.3. Electrooxidation of 1,4-dihydroxybenzene (1) in the presence of morpholine

Fig. 7 shows the cyclic voltammograms obtained for 1 mM of 1,4-dihydroxybenzene in ethanol in the absence and in the presence of three different concentrations of morpholine and 0.15 M CH_3COOK as supporting electrolyte. The effect of scan rate on the electrode process is also illustrated in Fig. 8. Similarly to the previous cases, the voltammograms indicate clearly that the oxidation product of 1,4-dihydroxybenzene undergoes a coupled chemical reaction to produce mono- and dimorpholino products. The inset of Fig. 8 confirms also the involvement of an ECE mechanism during the oxidation of (**1**) in the presence of morpholine. These observations and the results obtained from spectroscopic analyses allow us to propose the mechanism proposed in Scheme 1 for the electrooxidation of 1,4-dihydroxybenzene in the presence of morpholine. However, it is noteworthy that even in the presence of an excess of morpholine and at low scan rates, no negative peak showing the formation of the dimorpholino product is discernable, while peak c_2, which is indicative of the monomorpholino product is observed. These findings indicate that the second following chemical reaction is so much slower that it cannot proceed in the limited time scale of cyclic voltammetry. In other words, morpholine behaves as the weaker nucleophile amongst those employed in this work. Therefore, this can be considered as the main reason for the low yield of product (**4**) during the macroscale electrolysis.

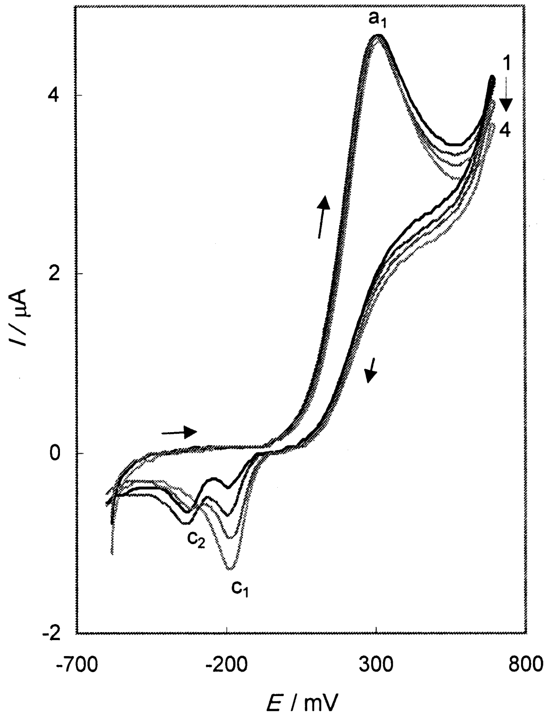

Fig. 7. Cyclic voltammograms of 1 mM 1,4-dihydroxybenzene in the presence of 8 mM morpholine in methanol containing 0.15 M CH_3COOK as supporting electrolyte and at scan rates: (1) 10, (2) 20, (3) 50, (4) 100, (5) 200 and (6) 400 mV s^{-1}. Initial potential: −600 mV vs. ref. Inset shows the variation of the positive peak current, $I_{pa}/v^{1/2}$, vs. scan rate, $\log v$.

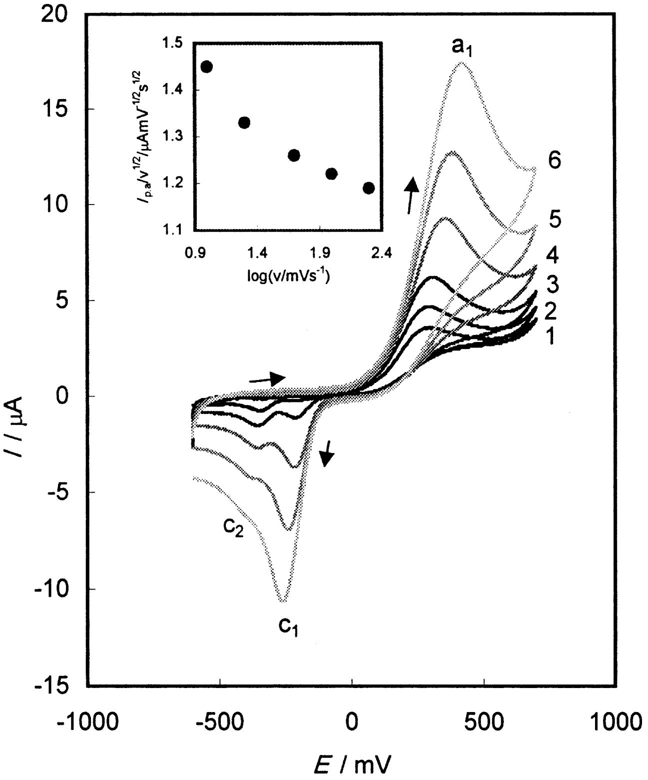

Finally, considering the above-mentioned results, it may be concluded that in the presence of the amines used as nucleophiles in this work, we are confronted always with two series of competitive Michael-addition reactions, i.e. methoxylation or ethoxylation (depending the nature of solvent used) and amination reactions. The high concentration of amines used in each electrosynthesis experiment can enhance remarkably the progress of the Michael-addition reaction in favor of the formation of amino products. The optimal concentrations of amines fulfilling this goal were determined using cyclic voltammetric experiments (see Figs. 3, 5 and 8).

On the other hand, since the anodic reactions (1), (3) and (5) are protogenic processes, the solution pH will decreases gradually in parallel with the progress of the electrode reaction leading to the formation of a buffered medium. Obviously, such a pH decrease will affects the methoxylation or ethoxylation reactions rather than those of amination, because of the high basicity of the methoxy or ethoxy groups with respect to that of the amines used in this study.

4. Conclusion

The results of this work show that 1,4-dihydroxybenzene is oxidized in methanol or ethanol to its corresponding *p*-benzoquinone. In the absence of any other nucleophiles, the *p*-benzoquinone formed can be attacked by the solvent molecules to yield methoxy or ethoxyquinones. But in the presence of some secondary amines (i.e. dimethylamine, piperidine and morpholine) as nucleophiles, the *p*-benzoquinone formed can be attacked favorably by these amines to produce diamino products. The cyclic voltammetric results and the results obtained from spectroscopic analyses of macroelectrolysis products indicate that the reaction between (**1**) and the mentioned amines as nucleophiles is fast enough to prevent the reaction between *p*-benzoquinone and solvent molecules to a considerable extent, so that the major products are diaminoquinones.

Acknowledgements

The authors wish to acknowledge the financial support of this work by the Research Council of Tabriz University.

References

[1] A.H. Crosby, R.E. Lutz, J. Am. Chem. Soc. 78 (1956) 1233.

[2] J.V. Shurman, E.I. Becker, J. Org. Chem. 18 (1953) 211.

[3] R. Bultzyl, E. Lorz, J. Am. Chem. Soc. 70 (1948) 861.

[4] R.E. Lutz, T.A. Martin, J.F. Codington, T.M. Amaker, R.K. Allison, N.H. Leake, R.J. Rowlett, Jr., J.D. Smith, J.W. Wilson, J. Org. Chem. 14 (1949) 982.

[5] D. Nematollahi, S.M. Golabi, J. Electroanal. Chem. 405 (1996) 133.

[6] D. Nematollahi, S.M. Golabi, J. Electroanal. Chem. 481 (2000) 208.

[7] A.J. Bard, L.R. Faulkner, Electrochemical Methods, Fundamentals and Applications, 2nd ed., Wiley, New York, 2001, p. 512.